FINAL REPORT

Application of Magnetic and Geotechnical Methods for Archaeological Site Investigations

SERDP Project RC-1697

JULY 2011

Bradley G. Fritz
Douglas McFarland
William Hertz
Jeffrey Gamey
Pacific Northwest National Laboratory

SERDP
DOD ▪ EPA ▪ DOE

Report Documentation Page

Form Approved
OMB No. 0704-0188

1. REPORT DATE	2. REPORT TYPE	3. DATES COVERED
JUL 2011	**Final**	**-**

4. TITLE AND SUBTITLE	5a. CONTRACT NUMBER
Application of Magnetic and Geotechnical Methods for Archaeological Site Investigations	5b. GRANT NUMBER
	5c. PROGRAM ELEMENT NUMBER
6. AUTHOR(S)	5d. PROJECT NUMBER
	5e. TASK NUMBER
	5f. WORK UNIT NUMBER
7. PERFORMING ORGANIZATION NAME(S) AND ADDRESS(ES) **Pacific Northwest National Laboratory**	8. PERFORMING ORGANIZATION REPORT NUMBER
9. SPONSORING/MONITORING AGENCY NAME(S) AND ADDRESS(ES)	10. SPONSOR/MONITOR'S ACRONYM(S)
	11. SPONSOR/MONITOR'S REPORT NUMBER(S)

12. DISTRIBUTION/AVAILABILITY STATEMENT
Approved for public release, distribution unlimited

13. SUPPLEMENTARY NOTES
SERDP Project RC-1697, The original document contains color images.

14. ABSTRACT
The overall objective of this research was to develop and use methods to measure and assess vehicle impacts on buried archaeological deposits. The need for this stems from the large number of archeological resources located on U.S. Department of Defense (DOD) sites where training includes vehicular activities. Specifically, the objectives of this research were to verify the quantitative relationship between soil compaction and changes in magnetic susceptibility, to develop a geotechnical model of subsurface compaction under a vehicle rut, to evaluate various compaction and deformation measurement methods in a controlled setting, to apply these measurements at the field scale, and to use magnetic modeling to interpret results. Multiple experiments were conducted, with each experiment building on the results of the previous ones. The first experiment was a core compaction test that verified the relationship between bulk density and magnetic susceptibility. Then a geotechnical model was developed, which provided a tool for estimating the compaction profile under a rut based on stress curves under footings with static loading. The accuracy and shortcomings of the geotechnical model were demonstrated in later tests. The first series of tests provided a detailed investigation of compaction of uniform soil within a large wooden box. These experiments were used to refine the measurement techniques, to verify the geotechnical model, and to develop a better understanding of the depth and distance that a surface impact could propagate into the subsurface. Overall, the results of the experiments demonstrated that cone penetrometer and down-hole volumetric magnetic susceptibility measurements could be used to accurately determine the magnitude of compaction, and that the geotechnical model accurately predicted compaction in the homogeneous soil.

15. SUBJECT TERMS

16. SECURITY CLASSIFICATION OF:			17. LIMITATION OF ABSTRACT	18. NUMBER OF PAGES	19a. NAME OF RESPONSIBLE PERSON
a. REPORT **unclassified**	b. ABSTRACT **unclassified**	c. THIS PAGE **unclassified**	**SAR**	**114**	

Standard Form 298 (Rev. 8-98)
Prescribed by ANSI Std Z39-18

Acknowledgments

The authors thank Dr. Bernie Housen of Western Washington University for his support with soil sample analysis, and Randy Korgel and Ryan Bowlin for providing access and assistance at the Yakima Training Center.

Acronyms

AF	alternating field
AMR	anisotropy of magnetic remanence
AMS	anisotropy of magnetic susceptibility
DOD	U.S. Department of Defense
DRM	depositional remnant magnetism
EW	east-west
g/cm^3	gram(s) per cubic centimeter
GPS	global positioning system
M	meter(s)
MC	moisture content
mT	milli Tesla
NHPA	national historic preservation act
NRM	natural remnant magnetism
NS	north-south
nT	nano Tesla
ID	inside diameter
OSB	oriented strand board
psi	pounds per square inch
PVC	polyvinyl chloride
RMS	root-mean-square

Contents

Figures

Tables

Abstract

The overall objective of this research was to develop and use methods to measure and assess vehicle impacts on buried archaeological deposits. The need for this stems from the large number of archeological resources located on U.S. Department of Defense (DOD) sites where training includes vehicular activities. Specifically, the objectives of this research were to verify the quantitative relationship between soil compaction and changes in magnetic susceptibility, to develop a geotechnical model of subsurface compaction under a vehicle rut, to evaluate various compaction and deformation measurement methods in a controlled setting, to apply these measurements at the field scale, and to use magnetic modeling to interpret results.

Multiple experiments were conducted, with each experiment building on the results of the previous ones. The first experiment was a core compaction test that verified the relationship between bulk density and magnetic susceptibility. Then a geotechnical model was developed, which provided a tool for estimating the compaction profile under a rut based on stress curves under footings with static loading. The accuracy and shortcomings of the geotechnical model were demonstrated in later tests. The first series of tests provided a detailed investigation of compaction of uniform soil within a large wooden box. These experiments were used to refine the measurement techniques, to verify the geotechnical model, and to develop a better understanding of the depth and distance that a surface impact could propagate into the subsurface. Overall, the results of the experiments demonstrated that cone penetrometer and down-hole volumetric magnetic susceptibility measurements could be used to accurately determine the magnitude of compaction, and that the geotechnical model accurately predicted compaction in the homogeneous soil.

After the success of the box tests, the same rut formation methodology and measurement techniques were applied in the field at the Yakima Training Center (Washington). These experiments also indicated that cone penetrometer and down-hole volumetric magnetic susceptibility measurement techniques were capable of identifying the depth and width of compaction under a rut. Unfortunately, these experiments also indicated that the geotechnical model was less accurate in the heterogeneous sediment; the model did not have the functionality to account for the change in soil type limiting the depth of soil compaction. Finally, the results of the magnetometer measurements made as part of the field compaction experiments indicated that the change in the magnetic signature created by the ruts was easily identifiable. Although magnetometer surveys with subsequent modeling did not appear to be a viable option for identifying depth of sediment compaction at existing vehicle impact sites, analysis of the anisotropy of magnetic susceptibility did. Overall, this project validated tools and methods that could be used to conduct archaeological site assessments cheaper and faster. This could enable site operations managers to make decisions about when it would or would not be acceptable to allow military vehicles to drive over areas with known or suspected archaeological materials in the subsurface, and what type of archaeological materials would be affected if a drive-over occurred.

1 Objectives

The overall objective of this research was to develop and use methods to measure and assess the impacts of vehicles on buried archaeological deposits. The need for this is driven by the large number of archeological resources located on U.S. Department of Defense (DOD) sites where training includes vehicular activities. The DOD Statement of Need focused on the need to explain and quantify the manner and extent to which specific impacts diminish the potential for recovering scientifically useful information from archeological sites. The scientific value of an archaeological site is often dependent on the depositional integrity of the site and the information it provides (Little et al. 2000). The integrity of an archaeological deposit in turn is dependent on its depth below surface, horizontal extent, and physical nature (size and structure), as well as the nature of the impact. Sites where vehicles have driven over known or suspected archeological deposits require assessments under Section 106 of the National Historic Preservation Act (NHPA). In addition, methods for predicting when sites would or would not be adversely impacted by a drive-over would be beneficial for coordinating training activities to reduce the number of future assessments. With this project, we used minimally invasive or non-invasive geophysical techniques (magnetic) and other more invasive measurements of soil properties to assess compaction, deformation, and the potential impacts on archaeological materials that result from vehicle disturbance of the soil surface.

Specifically, the objectives of this research were to verify the quantitative relationship between soil compaction and changes in magnetic susceptibility, to develop a geotechnical model of subsurface compaction under a vehicle rut, to evaluate various compaction and deformation measurement methods in a controlled setting, to apply these measurements at the field scale, and to use magnetic modeling to interpret the results. It was hypothesized that after applying this step-wise approach, guidelines for conducting archeological site assessments using magnetic techniques could be developed; the objective of these guidelines would be to provide tools and guidance that would reduce the time and cost necessary to conduct required site assessments of vehicle impacts on archeological resources, and could potentially lead to the ability to predict when training activities would or would not result in impacts to archeological resources.

2 Background

2.1 Archaeological Context

Impacts that change the spatial relationships of objects or sediment in archaeological deposits can reduce the integrity of the archaeological resource (Little et al. 2000; McPherron et al. 2005). These disturbances can include soil compaction, soil mixing, and erosion. Depositional integrity can be a critical determinant of an archaeological site's significance, and therefore protective status (NHPA Section 106). If a site is eligible for listing on the National Register of Historic Places (NRHP or National Register) then an impact on data or information that makes that site significant is considered an adverse effect on the site. Typically both a determination of National Register eligibility and a determination of adverse effect use excavation-based techniques in the

assessment to determine depositional integrity, whether there is any loss of integrity, and the loss of archaeological data that resulted from the loss of depositional integrity. Excavation can be time consuming and expensive. If there is loss of depositional integrity and associated archaeological data, then the loss must be mitigated. Mitigation is often accomplished through data recovery in the form of controlled excavation.

When vehicles create ruts, the depth of the rut is the *visible* disturbance. The subsurface depth of impact, and its influence on the depositional integrity is an unknown. Archaeological resources are non-renewable so a non-destructive evaluation approach is preferred (Nickens 1991). Three questions should be considered when determining whether a site has suffered an adverse effect:

1. Can the surface and subsurface disturbance be indentified and characterized (size, depth, and degree of disturbance)?
2. Does the depth of disturbance meet or exceed the depth of archaeological materials? Sites that are significant (eligible for NRHP listing) have most likely been evaluated through excavation, and depths of archaeological deposits are known.
3. Did the disturbance actually result in a loss of the important scientific information that made the site eligible for the National Register in the first place?

Sites are determined eligible by having specific data that can answer questions "important to history or prehistory" (Little et al. 2000). If the specific material that holds these data is not impacted by an activity, then the information that made it eligible for listing has not been affected.

2.2 Geophysics Background

When geophysical archaeologists investigate a site to identify features, noise from vehicle impacts and other disturbance may be visible in the data. Evidence of vehicle impacts in magnetic survey data is not uncommon, and is normally a problem to be avoided, ignored, or dealt with in processing (Somers et al. 2003). If the signal from the vehicle disturbance is the actual target of investigation it may be used for assessing impacts. Compaction of sediment and soils creates two types of soil conditions: increased density (and subsequent increased soil strength) and ruts. Measurement of these two parameters provides a means for identifying the location and magnitude of subsurface compaction. Increased soil density causes an increase in volumetric magnetism. This magnetism can be measured directly or indirectly. Magnetics has the benefit of being independent from the effects of moisture, and is very sensitive to sedimentary disturbance (Maier et al. 2006; Mathé et al. 2006), making it an ideal tool for long-term comparative studies. Soil magnetism can be changed by vehicle traffic in multiple ways; the list below identifies some of the soil magnetic properties that were key to this research. A more detailed description of key magnetic and geophysics terms is provided in Appendix A.

- Magnetic susceptibility. Topsoil has a higher magnetic susceptibility than underlying sediments as a result of weathering (Dalan 2006). Magnetic susceptibility (induced magnetism) contributes to the total field reading measured by magnetometers (Dalan 2006). Stripping this topsoil away will leave areas of lower magnetism. Magnetic susceptibility can be measured on a volumetric basis (magnetic susceptibility per unit volume, S_v) or on a mass

basis (magnetic susceptibility of the individual particles, S_m). This is important because the mass susceptibility is constant, while the volumetric susceptibility increases as the bulk density (ρ_b) increases.

- Depositional remanant magnetism (DRM) results from natural depositional processes and creates weak background magnetism (Parkes 1986). Disturbance of sediments will create areas of lower remanant magnetism because the magnetic soil particles will no longer be oriented in the same direction.
- Compaction increases the magnetic signal. Compression of magnetic soils and sediments creates a stronger magnetic susceptibility by having a higher density of magnetic material present per unit volume (Dalan 2006).
- Rutting and changes in surface elevation result in materials being farther from magnetic sensors. Because the strength of the magnetic field decreases with distance, this creates areas of lower apparent magnetism (Mathé and Lévêque 2003).
- Sediments and soils that have a directional intensity of magnetization have magnetic anisotropy (Taux et al. 2006). This is true whether the magnetism is induced (magnetic susceptibility) or remanent. Two kinds of magnetic anisotropy, which can be changed by sediment disturbance, include:
  - Anisotropy of magnetic susceptibility (AMS) – in which directional magnetism is a function of direction of the applied field and physical iron oxide crystal geometry and orientation (Lagroix and Banerjee 2004). Depending on the AMS of a given soil, disturbance from off-road vehicle impacts could increase or decrease this measurement.
  - Anisotropy of magnetic remanence (AMR) – in which directional magnetism is a function of the orientation of permanent magnetic domains within individual magnetic particles. This type of anisotropy is also referred to as paleomagnetic orientation, when found in old earth materials. Disturbance of sediments will create areas of decreased AMR because the magnetic soil particles and the magnetic directional magnetic moments (magnetic fields) associated with them will no longer have the same degree of directional agreement (Butler 1992).

3 Methods

To meet the project objectives, a number of field methods were used. They included the use of various instruments and measurement techniques, as well as a combination of experimental approaches, as discussed in this section. Generally, the experimental approaches started small, and increased in size as the project progressed. The same measurement techniques were applied at each step, with some new techniques being added as the scale of the experiments allowed.

3.1 Core Compaction

Preliminary magnetic modeling indicated that the soil compaction and air space magnetic signal contributions could be separated from each other in magnetic data using geophysical modeling. To use increased magnetic susceptibility from soil compaction as a model parameter it was necessary to verify this relationship. Theory dictates that the relationship between

volumetric magnetic susceptibility and sediment compaction is proportional; an increase in bulk density results in an increase in volumetric magnetic susceptibility (Dearing 1996). This is the result of a reduction in pore space between magnetically susceptible mineral particles; in other words, a higher bulk density means that there are more magnetically susceptible particles squeezed into the same volume, resulting in a stronger magnetic signal. This relationship is expressed in Eq. 1.

$$S_v = S_m \rho_b \quad (1)$$

To verify Eq. 1, the bulk density of a fixed mass of soil was incrementally increased by compaction. Test soil was hand mixed and then packed into a 30 cm long polyvinyl chloride (PVC) pipe (2.7 cm inside diameter [ID]). The volumetric magnetic susceptibility (S_v) of the core was then measured with a magnetic susceptibility core reading instrument (MS2C, Bartington Instruments, Oxfordshire, United Kingdom) at three locations along the pipe (Figure 1). The soil column was then packed tighter by tamping the soil in the pipe. Bulk density was calculated using the mass of the soil sample and the known volumes after each successive compaction. The mass magnetic susceptibility (S_m) was calculated for the soil based on the initial bulk density using Eq. 1. The magnetic susceptibility measurements were repeated for six different bulk densities.

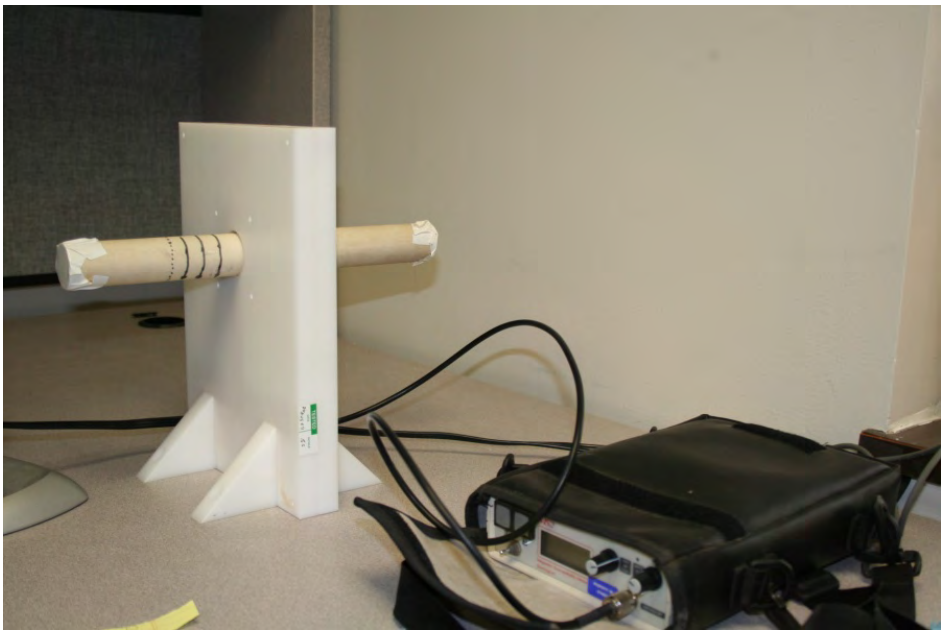

Figure 1. Packed Soil Core Used in Compaction Test with Bartington Magnetic Susceptibility System with MS2C Sensor Shown

3.2 Geotechnical Model

To estimate compaction under a rut, a geotechnical model of compaction at depth was developed. This model is two-dimensional and estimates density increase vs. depth beneath square or infinite strips of compacted soil. The constitutive relationship between volume change and stress change is very complex, especially for unsaturated soils, and would be difficult to

address even with extensive soil property knowledge. Volume change is thought to be a function of net mean stress and soil suction change, and is influenced by stress path, soil characteristics (e.g., grain size distribution and moisture content), and previous loading history, as well as other factors. For the initial modeling, very little soil information was available. However, it was judged that for the intended purpose the simplified approach described below would provide an adequate range of possible post-loading density distributions. Some of the main simplifying assumptions explicit and implicit in the approach are as follows:

- The density increase beneath the wheel ruts was assumed to be proportional to the vertical stress increase that would be predicted using a Boussinesq analysis. The Boussinesq analysis assumes the subsurface is a semi-infinite homogeneous half space. Use of Boussinesq analysis of stress increase below a surface load with its many simplifying assumptions is a common geotechnical engineering practice where detailed subsurface information is lacking. The assumption that density increase will be proportional to vertical stress increase is certainly not rigorous, but was considered adequate for this purpose.
- Stress increases were estimated only for the boundary cases of narrow infinitely long strip and square loadings. These are reasonable approximations of the wheel and track loadings from the assumed army vehicles and the square hand tamp.
- Only the stress increase from a single wheel rut is considered. The very small added stress increase due to the vehicle's adjacent wheel track is ignored.
- The vehicles were assumed to input sufficient energy to compact the soil and increase the dry density at the bottom of the wheel ruts to a maximum level for the soil type; this is the density determined using a modified Proctor compaction test for similar soil (Figure 2). The Proctor tests is a standard laboratory test for controlling engineered compacted fill at construction sites (ASTM 2007). Maximum density is a function of both compactive energy and moisture content. The maximum density initially chosen was the same as published values for similar soils compacted at low moisture content (7%), but other densities can be used in the model.
- Initially, the post-loading density distributions were developed assuming a uniform pre-loading density for the soil taken from published literature for similar soil, but the model facilitates changing initial conditions so that a range of boundary conditions can be investigated.
- The effects of vibration on compaction were ignored. Engineering experience shows that vibration can increase compaction of granular soils; however there was no reasonable way to estimate the vibration of the assumed vehicles.

The model is a simple spreadsheet that implements published Boussinesq stress increase influence factors (Figure 3) to predict the distribution of post-loading density (from its highest value at the rut base to the assumed pre-loading density where the stress increase was insignificant based on the assumption that the density increase would be proportional to stress increase. The post-loading density distribution was computed for vertical columns beneath the center, edge, and one rut width (measured from the center) to the side of the rut.

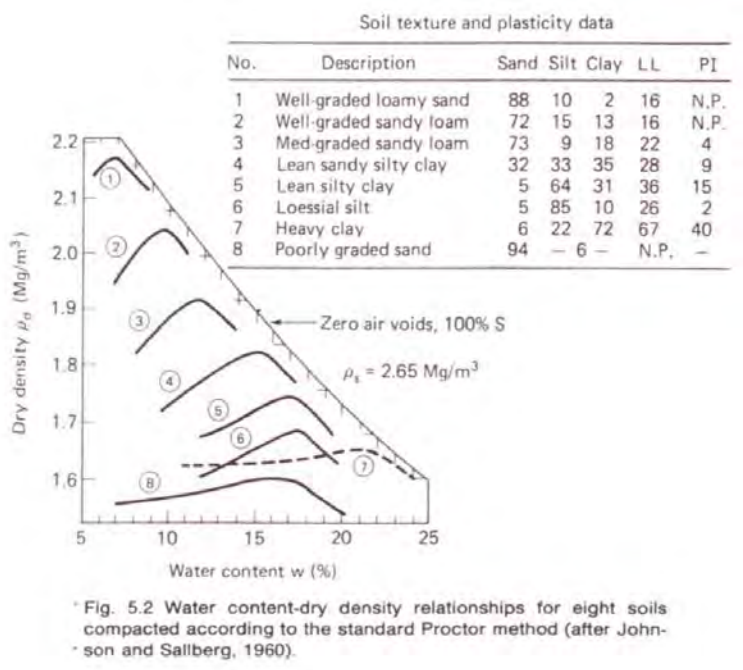

Figure 2. Maximum Bulk Density Achieved in Eight Soil Types Using the Standard Proctor Method (from Holtz and Kovacs 1981)

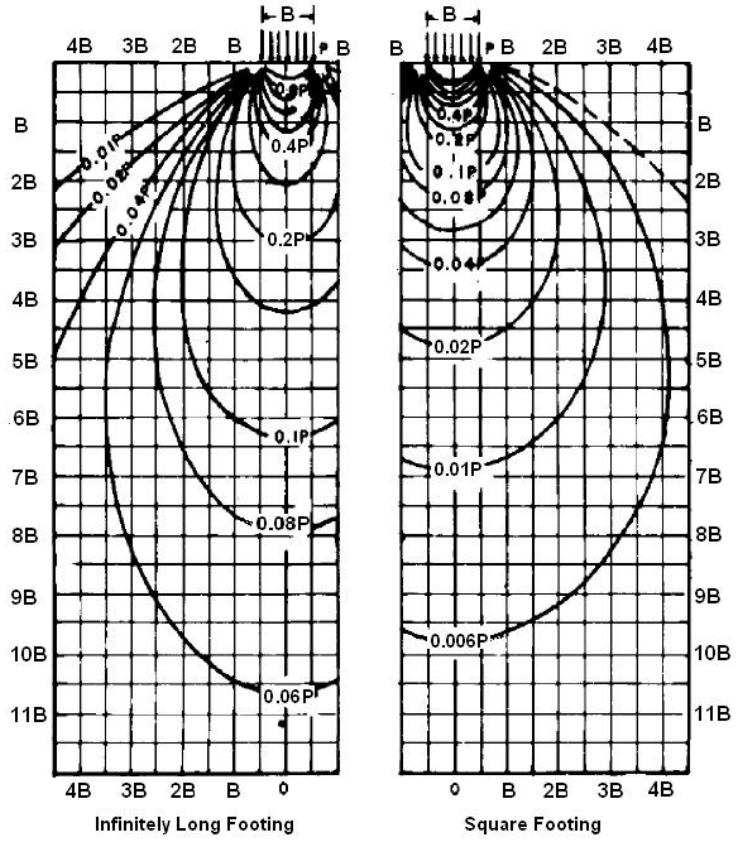

Figure 3. Boussinesq Stress Contours Under Strip and Square Footings (from NAVFAC Design Manual DM-7.1, p. 7.1-167)

3.3 Proof-of-Principle Testing

A proof-of-principle test was conducted to provide assurance that the magnetic instrumentation intended for use in field experiments would have adequate sensitivity to detect the changes in bulk density created by vehicle ruts. The geotechnical model (Section 3.2) was used to predict the compaction profiles under various compaction scenarios. The moderate case was a rut where the bulk density increased from 1.1 to 1.34 g/cm^3. This scenario was built into the software and a forward model was run to estimate the resulting magnetic signature (see Section 3.9). The modeled scenario was also run with no compaction under the rut footprint, and with compaction but no rut, to provide an estimate of how the two components contribute to the net change magnetic field.

3.4 Soil Box Experiments

Compaction tests were conducted by loading soil into a wooden box (1 m^3) constructed of oriented strand board (OSB) and structural lumber. This was intended to provide a soil column of uniform bulk density and uniform magnetic susceptibility, thereby allowing for experimental results to be analyzed without having to compensate for natural variability in sediment properties. The soil was collected from the Yakima Training Center (U.S. Army training site located in eastern Washington State). The soil was sieved to remove plant material and rocks larger than 1 cm. The soil was loaded into the box in lifts of either 10 or 20 cm. For each lift, the mass of soil at the measured moisture content necessary to achieve a bulk density of 1.4 g/cm^3 was weighed out. This soil was then loaded into a standard cement mixer, and water was added to bring the moisture content up to the desired level. The mixed and wetted soil was then put into the box and tamped down to the appropriate thickness (such that the bulk density was 1.4 g/cm^3). These steps were repeated for the next layer, but with one addition—a small portion of the wetted soil was removed, dyed with shrimp dye (used to dye fishing bait), and then spread in a thin layer over top of the previous soil lift. This provided a visual marker between each soil lift. These steps were continued until the box was filled to 81 cm deep.

After loading, a "rut" was created in the center of the soil surface by manual compaction (Figure 4). This was accomplished by pounding a 30- × 30-cm steel plate with a standard sledge hammer. After rut compaction, measurements (cone penetrometer, magnetic susceptibility, bulk density) were made both within and adjacent to the rut (see other sections for measurement methods). After these measurements were completed, the front of the box was removed and half of the soil was removed. This left half of the soil intact, allowing for a visual inspection and quantification of the deformation created by the rut (because the dyed soil layers were readily visible [Figure 5]).

Figure 4. Manual Rut Formation for Box Tests. Note the hole left from the density sample collected prior to compaction and the PVC sleeves for down-hole magnetic susceptibility measurements.

Figure 5. Example of Visible Deformation Made Possible by the Addition of Dyed Soil Layers

3.5 Magnetic Susceptibility

Magnetic susceptibility was measured using a Bartington magnetic susceptibility instrument (Bartington Instruments, Oxfordshire, United Kingdom). This instrument includes multiple attachments that can be used to measure the susceptibility of a soil surface (vertical or horizontal) within a core hole or in discrete samples. For all magnetic susceptibility measurements, the manufactures procedures were followed. The surface instrument merely

required the sensor to be held flush with the soil surface; the instrument provided a reading of the volumetric magnetic susceptibility integrated about 2 mm deep. For down-hole measurements, the hole was made by advancing a thin-walled aluminum pipe (2.1 cm outside diameter) into the soil and removing it, thereby creating a hole only slightly larger than the 1.9-cm diameter of the down-hole magnetic susceptibility probe. The probe was typically advanced 2 cm between readings, although the probe provided an integrated result for a cylindrical volume nominally 1.2 cm tall with a 5 cm radius. Discrete samples could be measured for mass magnetic susceptibility; this was done by placing samples in small cups, measuring the weight of soil within the container, and measuring the volumetric mass susceptibility. Because the soil was disturbed, the volumetric susceptibility was inaccurate, but knowing the volume of the container and mass of soil, the mass susceptibility is calculated according to Eq. 1.

3.6 Cone Penetrometer

A cone penetrometer (Field Scout 900, Spectrum Technologies, Inc.) was used to evaluate vertical changes in soil compaction. The penetrometer was used according to the manufacturer's instructions; this included placing an aluminum plate on the soil surface for reflection of the ultrasonic depth sensor signal and pushing the penetrometer tip into the soil at a constant rate of approximately 2.5 cm/s (Figure 6). The instrument measures and records the resistance pressure per unit of area (pounds per square inch [PSI]) as the tip is pushed through the soil. Data were downloaded from the instruments internal logger and correlated to the location with field notes.

Figure 6. Cone Penetrometer Measurements Conducted in an Engineered Rut and in the Field.

3.7 Field Compaction Tests

After completing the box experiments, similar experiments were conducted in the field at the Yakima Training Center. For these experiments, a "rut" was created on natural, undisturbed soil using a compaction plate and a sledge hammer (Figure 7). Cone penetrometer and down-hole

volumetric mass susceptibility measurements were made (Figure 7), and samples for bulk density and soil moisture analysis were collected. In addition to these invasive measurements, a non-invasive magnetometer was used to evaluate the change in magnetic signature caused by the compaction by taking readings before and after compaction.

Figure 7. Rut Formation and Down-Hole Magnetic Susceptibility Measurements as Part of the Field Compaction Tests

3.8 Drive-Over Tests

A large field-scale experiment was conducted to verify the geotechnical model, the geophysical model, and to determine whether impact from compaction also resulted in damage to buried archaeological deposits. This experiment consisted of constructing artificial buried archaeological sites, driving over them with military vehicles, and then conducting field measurements to determine the compaction signature and changes in the archeological deposits. The drive-over test site was constructed with a small bulldozer. Three 10-m × 40-m test beds were constructed for the drive-over tests (Figure 8). In addition, three 5-m × 5-m practice beds were excavated to develop a backfilling protocol that would not over- or under-compact the soils. Each of the 10-m × 40-m test beds was excavated to a different depth (25, 51, and 76 cm). Six magnetic targets were created in each bed by inducing a thermo-remnant signature into the soil by burning at high temperature (Figure 9). In addition to being magnetically distinct and detectable, these signatures mimic several different types of archaeological features (hearths, earth ovens, roasting pits, etc. [Abbott and Frederick 1990; Somers et al, 2003]). The features were created in sets of two in each bed. One was burned soil only, and the other was burned soil overlain by burned rock. This would provide two extremes for tensile strength. Altering or disturbing the spatial relationships of these burned earth materials would change their magnetic signatures. The test pits were then backfilled with the previously excavated material. Two sets of drive-over tests were completed with three different military vehicles: an M1A1 tank, a HEMMET tanker truck, and a Humvee (Figure 9). Baseline magnetometer data were collected prior to vehicles driving over the plots. After baseline data collection, each vehicle made two passes over the assigned route, and magnetometer data collection was repeated. A second set of two passes for each vehicle was conducted, and was followed by a final set of magnetometer data collection.

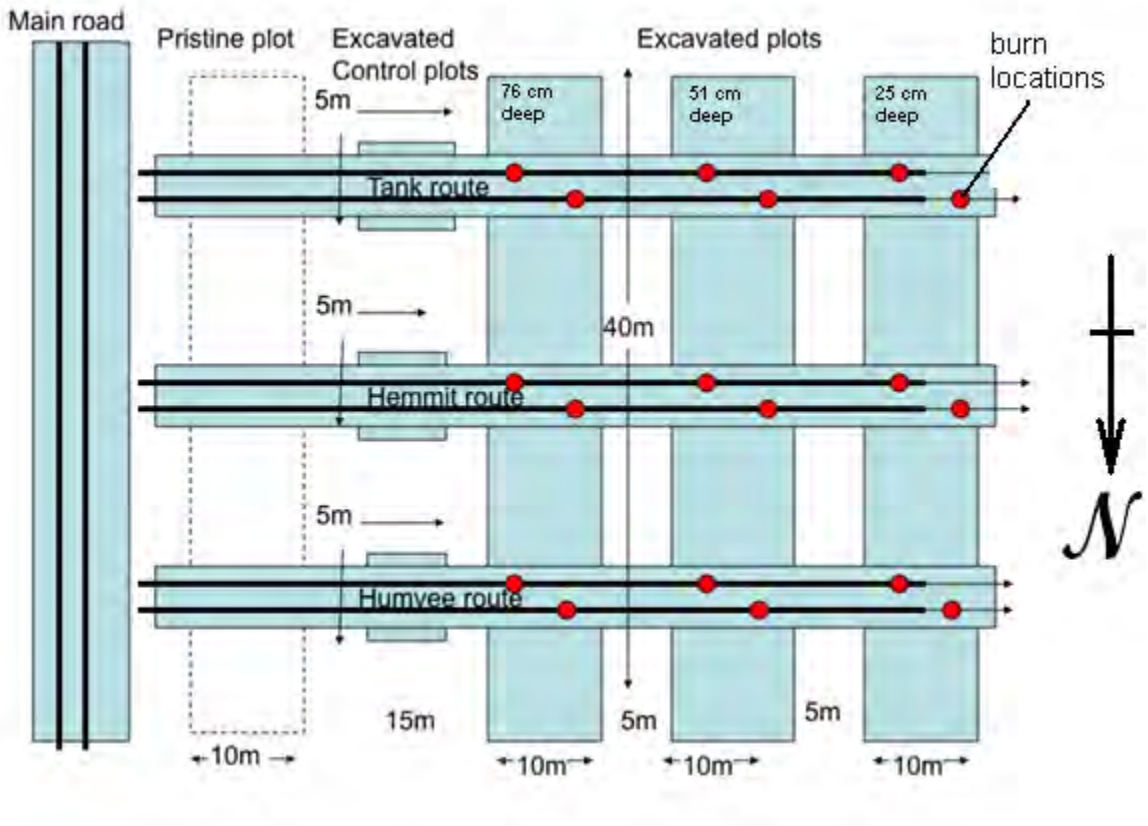

Figure 8. Schematic of Drive-Over Test Pits (not to scale)

Figure 9. Fire Feature at the Bottom of an Excavated Pit and the M1A1 Tank Driving over the Backfilled Test Pits

3.9 Magnetometer

Indirect measurement of soil magnetism is measured passively by non-invasive readings of the local magnetic field with a magnetometer. The local magnetic field can be affected by variations in surface relief (Foss 2003) and by the increased magnetism of soil (resulting from compaction). Compaction creates a positive magnetic response, while a rut creates a negative

magnetic response. Magnetometer measurements were conducted as part of the field compaction tests and the drive-over tests, and were used to conduct a remanence test.

3.9.1 Field Compaction Tests

Measurement of the magnetic field with all its contributing components was accomplished using a Geometrics (San Jose, California) 858G cesium magnetometer with gradiometer option. This instrument is capable of detecting magnetic anomalies greater than 0.05 nT. For the field compaction tests the baseline magnetic signature was measured and subtracted from the magnetic signature measured after manual compaction, leaving only the magnetic signature that resulted from compaction. This was done so that modeling results could be evaluated; obviously, no baseline magnetic data could be collected at a site already driven over by vehicles.

Due to the small expected anomaly strength caused by soil compaction, very sensitive magnetometers were used for the surveys, and a closely spaced grid system was implemented. The grid had three 1-m transects spaced 4 cm apart with data points in each transect spaced 2.5 cm apart. A sampling grid template was constructed so that the surveys could be replicated easily (Figure 10).

Figure 10. Magnetometer Data Collection Field Compaction Test

3.9.2 Remanence Testing

Preliminary data collection activities indicated that the background soils at the Yakima Training Center had a strong remanence magnetic signature. To test this hypothesis, a plug of soil was subjected to rotation in place with geophysical measurements before and after each

rotation (Figure 11). The magnetometer readings using the procedure described above were taken, then a shovel was used to remove a cylindrical plug of soil (nominally 25 cm diameter × 25 cm deep). The soil was replaced but at an orientation 90° to the original alignment, readings were repeated, then the soil was rotated to 180°, etc. In this manner, the Q-ratio could be calculated by determining the best fit of the measured magnetic signature to the results obtained using the forward modeling procedure. The Q-ratio is a measure of remanence strength relative to the susceptibility (Foss and McKenzie 2006).

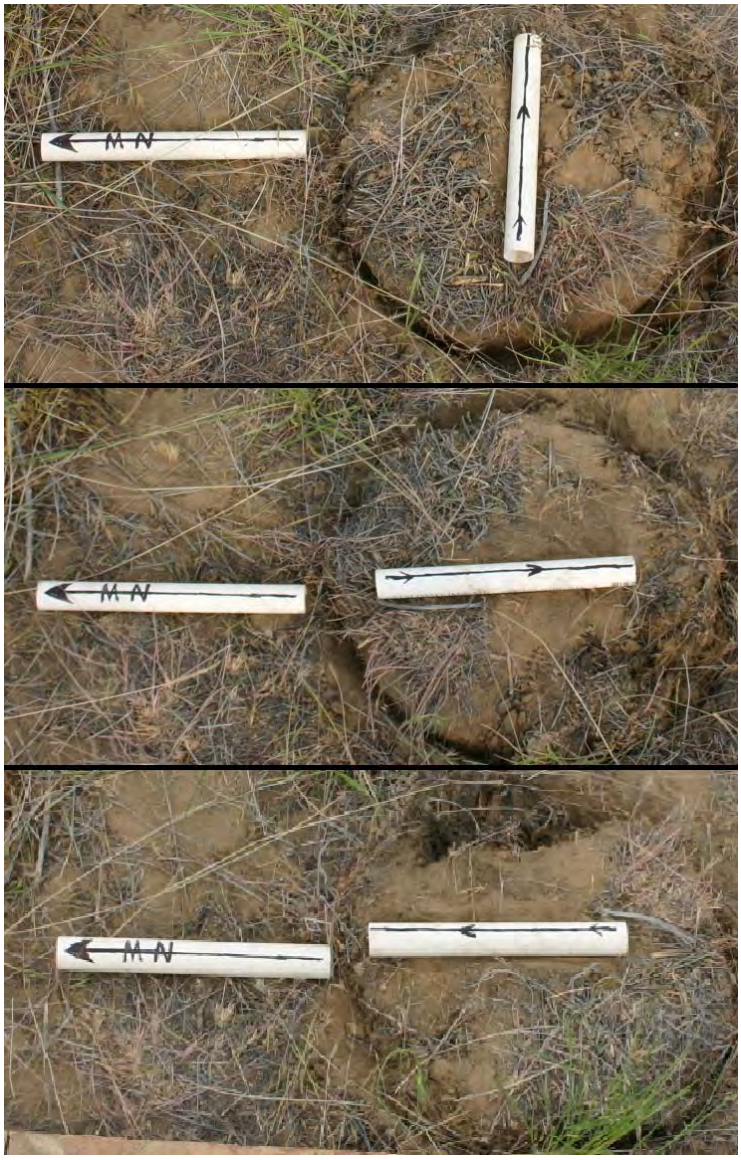

Figure 11. Remanence Testing. Soil plug rotated in-between sets of magnetometer measurements.

3.9.3 Drive-Over Tests

Magnetometer data were collected using a custom-built cart to pull a magnetometer array over the soil surface (Figure 12). The locations of the cart and sensors were tracked using a

global positioning system (GPS), as well as marked transects. Data were collected with a Scintrex (Ontario, Canada) system with 14 sensors set up as 7 gradient pairs. Bottom sensor height was 10 cm and top sensor height was 50 cm. The transect routes were established such that there was a minimum of 20 cm separation between the individual passes.

Figure 12. Magnetometer Data Collection Cart Used at the Drive-Over Test Site

Unfortunately, the project ended before any of the planned data analysis methods could be implemented. The intention had been to use the previously developed magnetic model as a filter, removing the signal from rut formation and compaction. With that noise filtered out, the change to the buried features would be discernable in the magnetic signal. Each thermo-remanant signature was to have been analyzed for change, providing 18 data sets to evaluate.

3.10 Magnetic Modeling

Modeling can be used to separate the magnetic signal resulting from compacted soil and the signal created by the air gap of the rut. If the shape and magnetic properties of a buried body are known, the resulting magnetic anomaly can be calculated. This is called forward modeling. Inverse modeling is a process where the shape and magnetic properties of a buried body are reconstructed from the measured magnetic anomaly, and is dependent on the uniqueness of the magnetic problem and the shape and heterogeneous composition of the magnetic body. With inverse modeling, there are many possible solutions that will fit the measured magnetic anomaly.

Forward magnetic modeling was done as a proof-of-principle experiment and to assess field compaction test results. Forward modeling was used to determine whether the magnetic signature generated by rut formation and compaction would be detectable with the magnetometer instrument. In addition, forward modeling was done in an iterative fashion to compare the measured magnetic signal to the modeled signal. In this fashion, the shape of the magnetic body that resulted in the best agreement between the measured and modeled magnetic signature could be compared to the shape of the compaction determined by other methods.

For the proof-of-principle test, the geotechnical model was used to calculate the vertical profile of bulk density. These bulk densities were converted to magnetic susceptibility models based on the assumption that a relative increase in density would lead to a corresponding increase in volumetric susceptibility (Eq. 1). It was also assumed that compaction resulted in the development of a rut in the ground equivalent to the change in bulk density, and that no compaction occurred below the 500-cm level. Each layer was compacted in thickness according to the relative change in bulk density, and then stacked from a depth of 500 cm. Magnetic models were constructed using horizontal tabular bodies oriented north-south and east-west NS and EW. Each layer was 10-m long. Width was determined by the expected rut width. The thickness of each layer was determined by the original layer thickness divided by the relative density increase. The depth was determined by the sum of the compacted layers below. Ruts were simulated by adding a tabular body of zero susceptibility at the top of each column. Compaction levels were constructed by linearly interpolating the susceptibility of each layer in the 100% model down to the background of 0.0004 cgs. This assumes that the compaction occurs uniformly across the entire model. The ModelVision Pro software (Encom, North Sydney, Australia) was used to generate total field profiles across the center of each model. Sensor height was set at 35 cm above the level ground surface, with measurements recorded at 10 cm intervals across the track. The background field applied was equivalent to the International Geomagnetic Reference Field at the test site (intensity 53480nT, inclination 67.7º, declination 16.4º). This declination produced a slight asymmetry in the NS track results. The EW track was modeled with the field at 90º declination, or exactly perpendicular to the track.

For the assessment of the field compaction tests, an approach similar to that used for the proof-of-principle testing was used for constructing the forward models.. The differences included varying the sensor heights to match the heights used in actual field data collection; adjusting the directional alignment to match actual field conditions; and iteratively varying the rut depth, maximum bulk density, and bulk density profile to provide the best agreement between measured and modeled magnetic signal.

3.11 Pilot-Scale Test

In situ sediments and soils have a pedofabric. This results in directionally dependent magnetic intensity, which can be changed by disturbances. Changes in the magnetic pedofabric can be used to identify changes in sediment and stratigraphic integrity (Lagroix and Banerjee 2004). Disturbance is a result of reorienting and/or changing particle size distribution of magnetic mineral crystals in soils and sediments (Butler 1992; Lagroix and Banerjee 2004; Tauxe et al. 2006). Changes in magnetic pedofabric properties can be measured in soil samples using paleomagnetic analysis techniques to determine AMR and AMS.

Ferrimagnetic minerals can dictate both the AMR and AMS of unconsolidated sediments. Magnetite is the most common and most magnetic of the ferrimagnetic iron oxides found in soils and sediments (Marwick 2005). It can be deposited from parent material and/or created in situ through both chemical weathering and biogenic microbial processes in sediment and soil environments. The orientation of magnetic domains (individual magnetic fields) in this magnetite is primarily determined by the directional strength of the local geomagnetic field at the time of crystal formation. This magnetite can dictate directional magnetism in very small

percentages. For example, AMS is dictated by the 0.01 to 0.1 percent of magnetite in a sediment matrix (Marwick 2005). This is similar to AMR, except domain agreement and the strength of the magnetizing geomagnetic field during the mineral creation are more important than particle alignment for the remnant directional intensity. This means that highly magnetic soils are not necessary to measure AMR and AMS.

3.11.1 Anisotropy of Magnetic Remanence

The pilot study for application of the AMR measurement techniques took place on a recorded archaeological site at the Yakima Training Center. This location was chosen for the definitive presence of vehicle impact and the near-surface proximity of archaeological material (Figure 13). Two locations within this site were chosen for comparative study: a control location and a location within a visible military vehicle rut. The age of the rut was unknown, but much rounding and the presence of vegetation within the rut indicated it was not made recently. The locations were separated by about 15 m, and were both located on the same terrace along a creek with the same soil, vegetation, and environmental conditions. Archaeological excavation units were set up at both locations with the long-term goal of using both locations to compare magnetic fabric differences to differences in the conditions of archaeological materials.

Figure 13. Pilot Site for Anisotropy of Magnetic Remanence Testing

Topsoil organic matter was removed to a depth of 5 cm to reduce root mass in order to simplify the sampling process, and to set the first of 10 incremental depth intervals for the analytical comparison mentioned above. Eight specimens were taken from both the control and pilot locations using archaeomagnetic sampling techniques. Each set of eight specimens is considered a sample. Specimens were collected by cutting pedestals of sediment, and then casting the pedestals in plaster (Figure 14). The plaster casts had to be leveled, and the magnetic orientation recorded. The number of specimens required for acceptable statistical analysis between samples using archaeomagnetic analysis is six. Samples were then sent to Dr. Bernie Housen at the Western Washington University (WWU) Pacific NW Paleomagnetism Lab for sample analysis.

Figure 14. Collecting Archaeomagnetic Cast Samples from the Control Unit. Specimen casts must be leveled and their directional orientation measured and recorded.

To determine whether there were any magnetic overprints, and to better characterize the geomagnetic field recorded by the sediment samples, a step-wise alternating field demagnetization was used. Specimens were subjected to a 0.05-mT field during alternating field (AF) decay from 100 mT using a Dtech 2000 alternating field demagnetizer, and the AMR was measured using a 2-G Enterprises Model 755 magnetometer after each treatment. An oblate fabric with the minimum axis oriented perpendicular to horizontal was assumed, so specimens were magnetized and measured along the Z axis (horizontal) and the X axis (vertical). The ratio Z/X was calculated for each specimen and mean values were calculated for each site.

Principal component analysis was used to determine the directions of the characteristic magnetization observed between 20 and 80 mT. The direction was determined using a bootstrap-resampling technique. Samples were also compared for natural remnant magnetism (NRM) intensity (normalized by susceptibility).

To evaluate possible differences in remanence intensity, a “pseudo-Thellier” analysis was performed (Tauxe et al. 1995). An artificial anhysteretic remanence was applied using the same set of AF steps as was used in the AF demagnetization experiments. Plotting the decay of NRM during AF demagnetization vs. ARM gain on an Arai-type plot yields a relationship between the NRM and ARM whose slope will be proportional to the geomagnetic field intensity present when the sediment samples were originally magnetized.

3.11.2 Anisotropy of Magnetic Susceptibility

The pilot study for application of the AMS measurement techniques took place at the drive-over test site at the Yakima Training Center. This location was chosen for the definitive and known vehicle impact and timeline for impact. The M1A1 tank track rut in the previously undisturbed sediment was bisected for comparative study; the control was located outside of the rut and the pilot test location was within the vehicle rut.

Topsoil organic matter was removed to a depth of 5 cm to reduce root mass in order to simplify the sampling process. Eight specimens were taken from both the control and test

location using archaeomagnetic push container sampling techniques. Each set of eight specimens is considered a sample. Specimens were collected by wetting the exposed soil surface with a spray bottle and pushing the cylindrical sampling containers into the soil until they were flush with the surface (Figure 15). The directional orientation of the arrow on the bottom of each sample container was then measured and recorded. The number of specimens required for acceptable statistical analysis between samples using archaeomagnetic analysis is six. Samples were then sent to Dr. Bernie Housen at the WWU Paleomagnetics Laboratory for sample analysis. All measurements were made with an Agico KLY-3S Kappabridge housed in the WWU Pacific NW Paleomagnetism Lab, using standard software and analytical methods. The AMS susceptibility axes orientations were plotted on stereonets, and average axes orientations calculated using procedures described by Tauxe (1998).

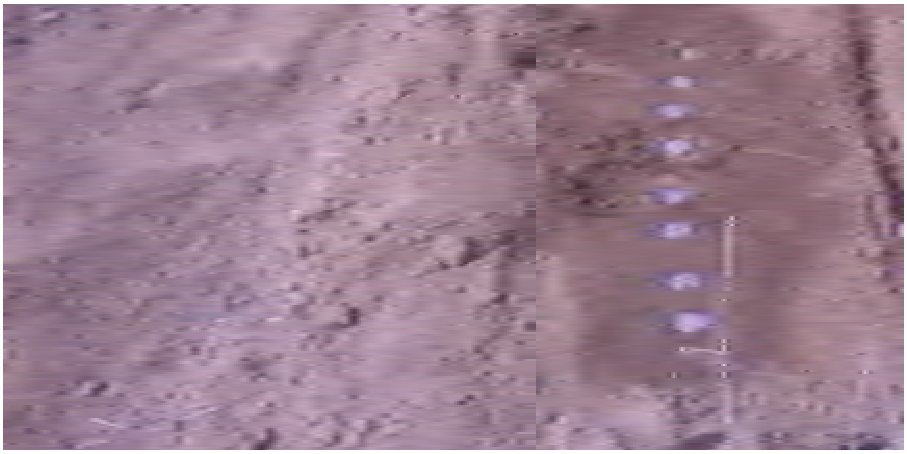

Figure 15. Collection of Push-Container Samples for AMS Analysis

4 Results and Discussion

4.1 Core Compaction Test

The results of the core compaction test verified the theoretical relationship between bulk density and magnetic susceptibility shown in Eq. 1 (Figure 16). A regression plot between the measured and calculated volumetric magnetic susceptibility indicates that if two of the three parameters in Eq. 1 are known, then the third can be calculated with less than a 10% error in the estimated result. Confirming this relationship provides a basis for converting between bulk density, volumetric magnetic susceptibility, and mass magnetic susceptibility.

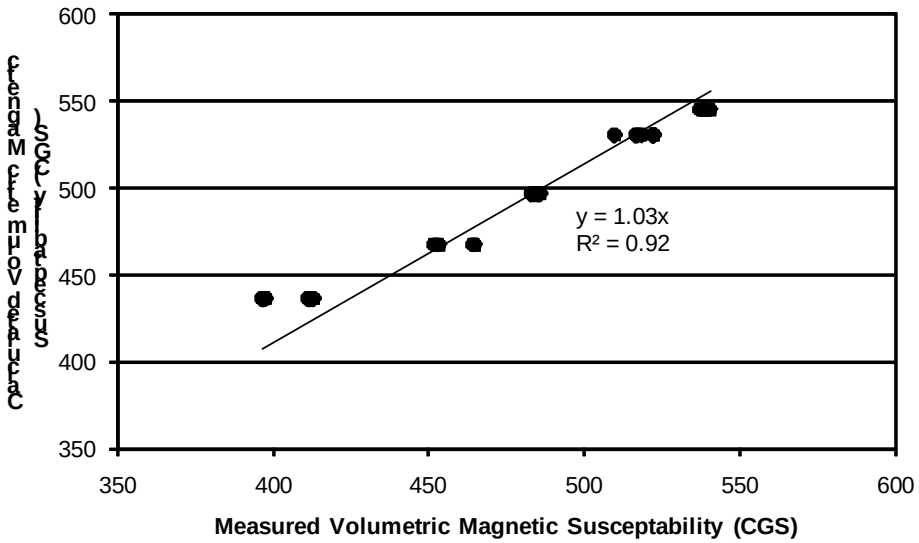

Figure 16. Results of the Core Compaction Test Illustrating a Linear Relationship Between the Measured Magnetic Susceptibility and the Magnetic Susceptibility Calculated with Equation 1

4.2 Geotechnical Model

The geotechnical model was implemented as a simple MSExcel™ spreadsheet, with user inputs of rut width (B), initial bulk density (assumed uniform), and final bulk density at the top of the rut. The final bulk density can be estimated using Proctor Method compaction curves, or it can be measured directly. The modeled bulk densities are provided in both tabular and graphical output (Figure 17). Comparisons of the geotechnical model results to measured results are provided in subsequent sections.

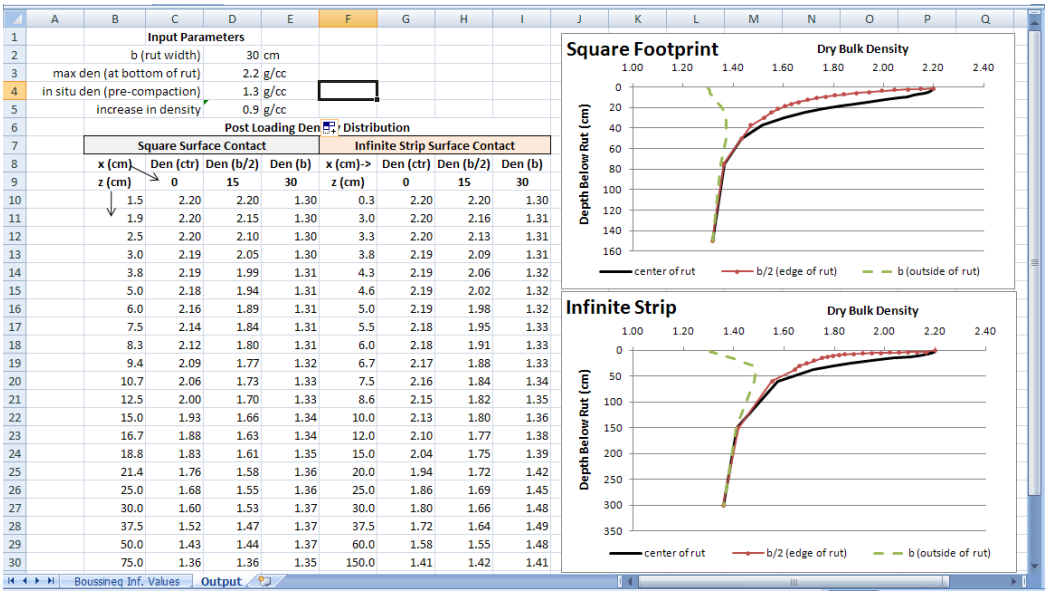

Figure 17. Example of Geotechnical Model Output for a 30-cm Wide Rut with a 0.9-g/cc Increase in Bulk Density

4.3 Proof-of-Principle Testing

The proof-of-principle testing indicated that the anticipated compaction would result in a readily detectable magnetic signal (Figure 18). The total change in magnetic signal for a moderate compaction scenario (bulk density increase from 1.1 to 1.34 g/cm^3) resulted in signal amplitude of approximately 15 nT. This is about 300 times stronger than the nominal detection limit of the magnetometer (0.05 nT). Additional modeling evaluated the change in total magnetic field caused by a rut with no compaction and by a compacted rut that was backfilled. This analysis revealed that the majority of the change in magnetic field resulted from the formation of the rut, not the compaction (Figure 19). However, the contribution from compaction alone was still several nano-Teslas, or much larger than the sensitivity of the magnetometer.

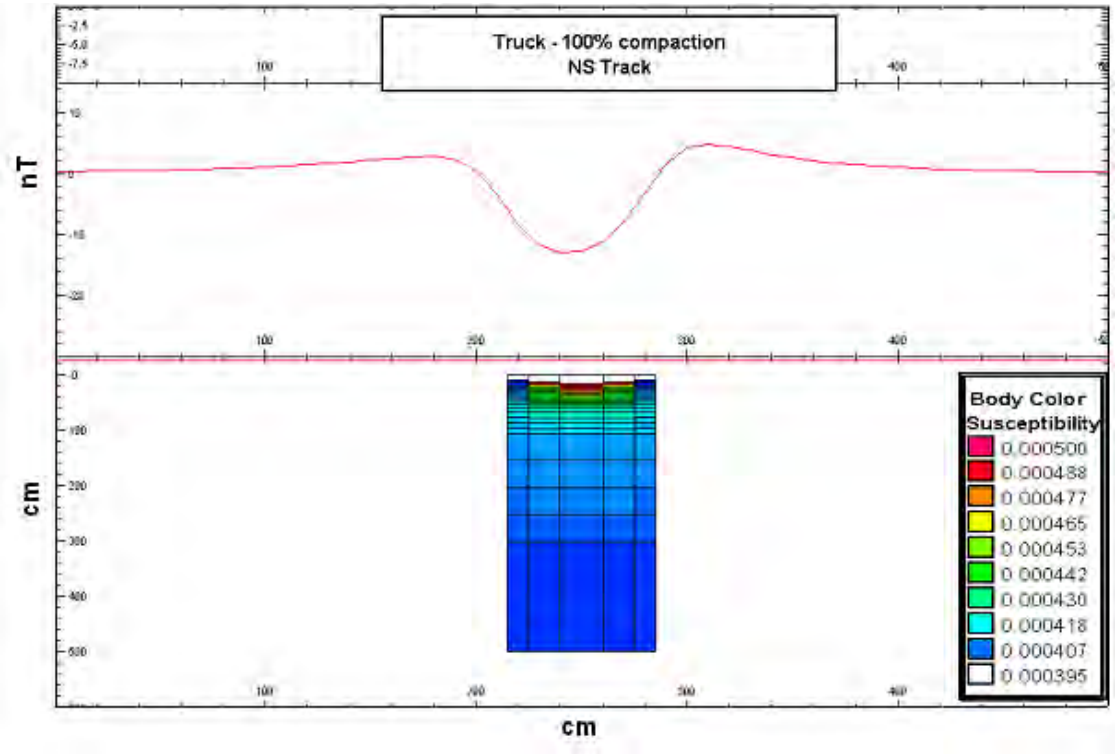

Figure 18. Total Magnetic Field Response over the Compacted Soils and Rut Caused by Compaction Increasing Bulk Density from 1.10 to 1.34 g/cm^3

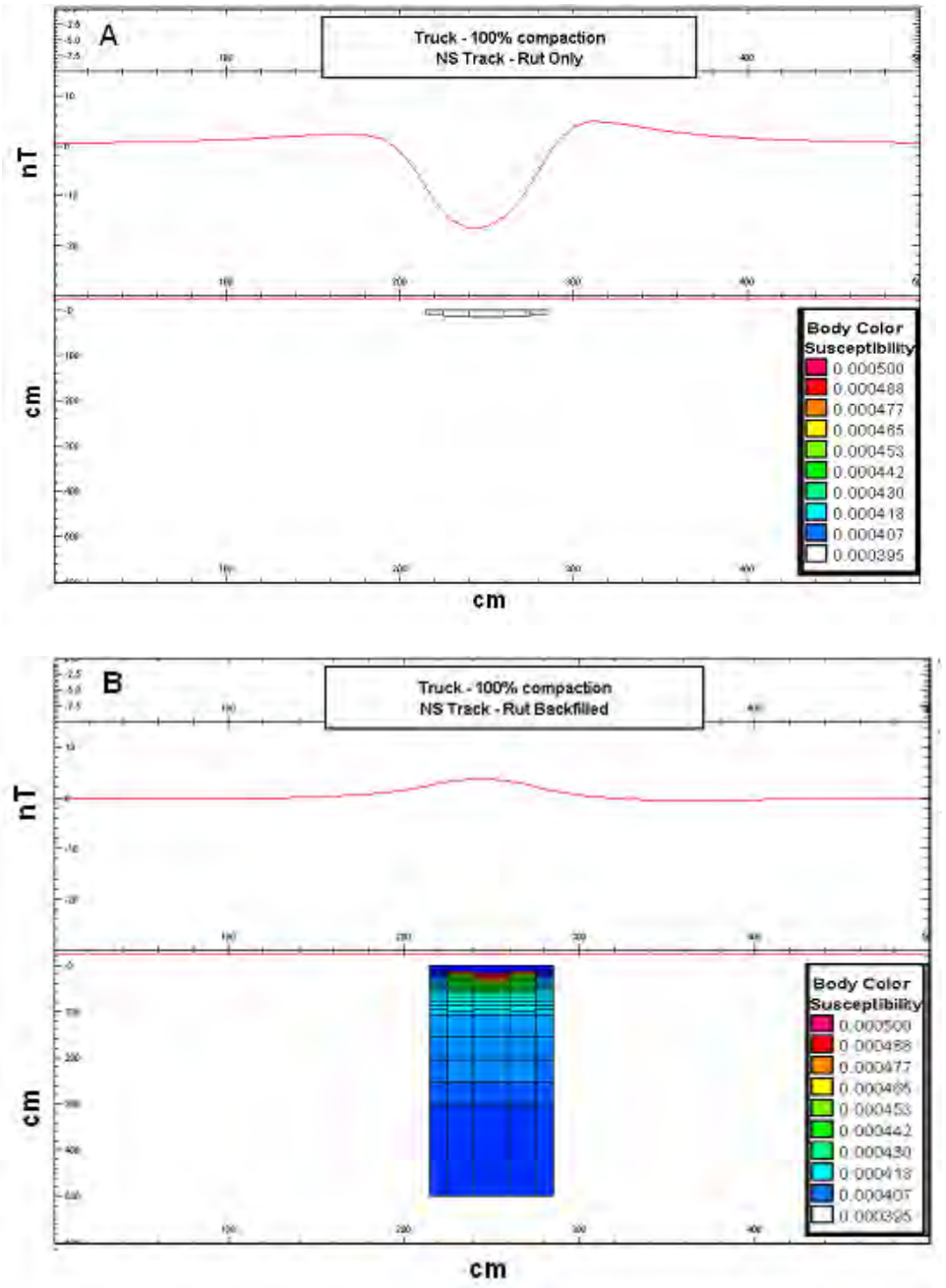

Figure 19. Changes in Total Magnetic Field Caused by a Rut with no Compaction (A) and by Compaction with No Rut Formation (B)

4.4 Box Tests

Three separate controlled compaction tests were conducted in a wooden box. Compaction under ruts with depths of 10 cm, 15 cm, and 20 cm was evaluated. Experiments were conducted at two nominal moisture contents (MCs): 10% for the 10-cm experiment and 15% for the other two. The results of the individual tests for all measurement techniques are included in the following subsections.

4.4.1 Box Test 1 – 10% MC, 10-cm Rut

Eleven samples from four core locations were collected for bulk density and soil moisture measurements (Figure 20, Table 1). Two of these samples were collected from larger diameter coring tools in the non-compacted portion of the box. The other nine samples were collected using a 2-cm coring tool. The average soil moisture of these 11 samples was 9.4% (Table 1). The bulk density in the non-compacted areas ranged from 1.27 to 1.48 g/cm^3. A maximum bulk density of 2.02 g/cm^{3}was measured under the rut footprint (Table 1). Note that these measurements are for core samples ranging in length from 10 to 30 cm, so the measured bulk density is the average over the vertical interval at that location.

Table 1. Soil Moisture, Bulk Density, and Position of Core Samples Collected and Analyzed for Box Test 1

x (cm)	y (cm)	z* (cm)	Bulk Density (g/cm^3)	Soil Moisture (%)
10.2	10.2	15.2	1.32	9.0
10.2	36	41.3	1.37	9.3
45.7	36	18.4	2.02	9.4
45.7	36	37.6	1.48	10.0
45.7	36	56.7	1.41	10.0
45.7	36	73.9	1.45	9.5
5	30	8.3	1.27	8.7
5	30	23.7	1.48	9.4
5	30	39.5	1.45	9.5
5	30	55.2	1.29	9.3
5	30	72.4	1.29	9.5

* Depth below undisturbed soil surface to center of core sample.

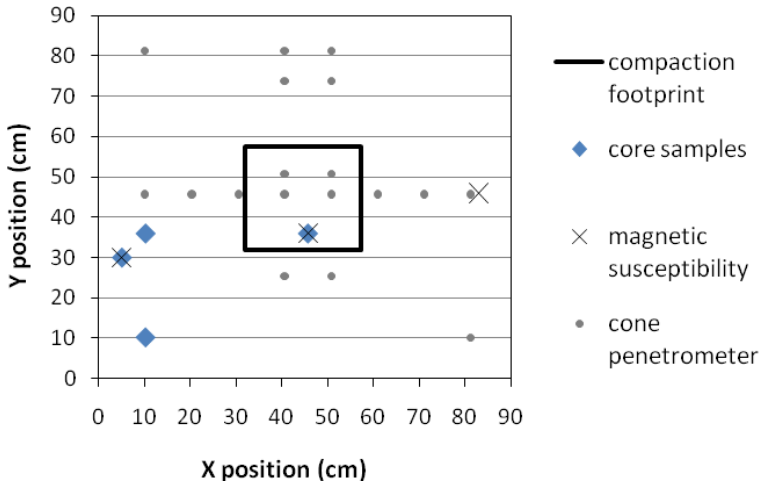

Figure 20. Positions of Data Collection Locations for Box Test 1. View is looking down on the top of the soil surface, with east to the left and west to the right.

The down-hole magnetic susceptibility measurements indicated that the compaction extended down to about 40 cm below the original soil surface (Figure 21). It should be noted that with this technique some collection inefficiencies were observed near the top of soil. This was attributed to disturbance of the soil at the surface during the coring and the need for the the sensor to be completely below the soil for valid measurements. These volumetric magnetic susceptibility measurements were coupled with bulk density measurements to calculate the mass susceptibility of the soil using Eq. 1. Equation 1 could then in turn be used to calculate the bulk density at a 2-cm vertical resolution using the vertical volumetric susceptibility measurements. For the compaction footprint, this calculated bulk density was compared with the bulk density distribution predicted using the geotechnical model (Figure 22). The geotechnical model also estimated the increase in bulk density to be less than 5% at the 40-cm depth, which is consistent with the magnetic susceptibility measurements. Assuming that the compaction occurred entirely in the vertical direction, a 10-cm rut would have compacted the 20- × 20- × 40-cm soil volume directly under the rut footprint into a 20- × 20- × 30-cm volume, resulting in an increase in bulk density from the measured undisturbed bulk density in the top 40 cm (1.4) to an average bulk density of 1.8. This is consistent with the average bulk density measured in the top 30 cm under the compaction footprint (Table 1).

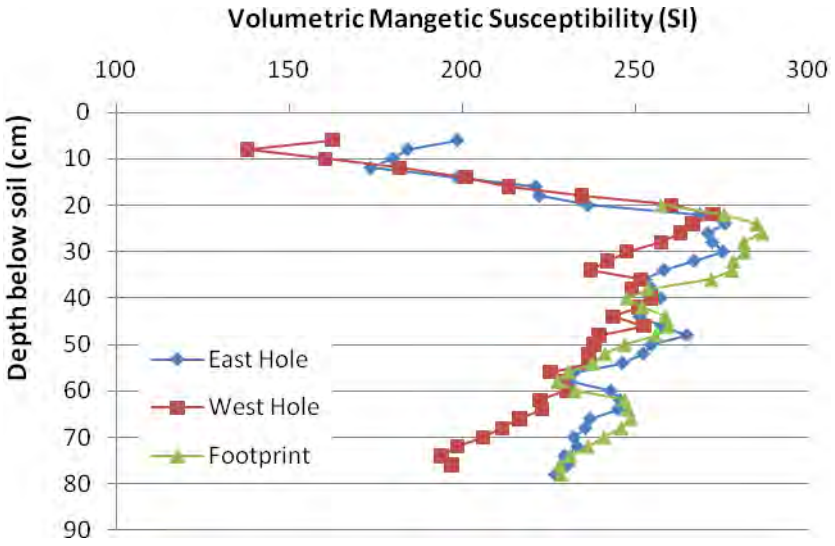

Figure 21. Down-Hole Measurements of Volumetric Magnetic Susceptibility –Box Test 1

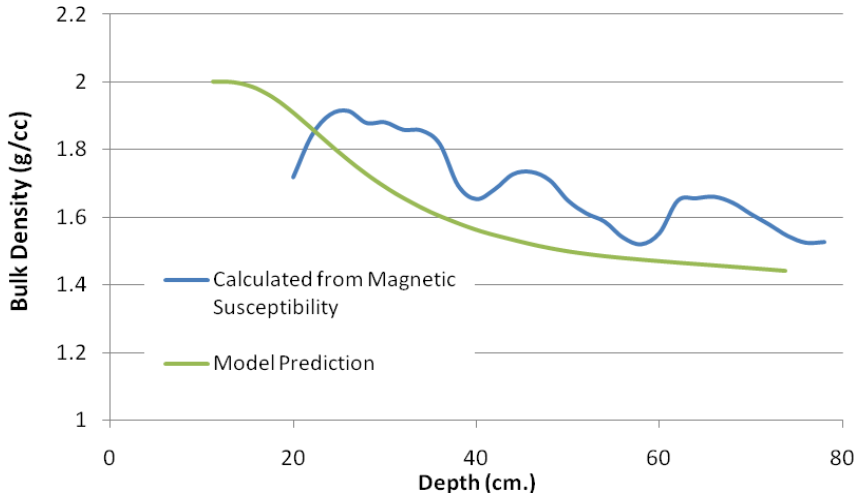

Figure 22. Comparison of the Bulk Density Directly Under the Compaction Footprint Predicted by the Geotechnical Model and Calculated Using Equation 1 and Volumetric Magnetic Susceptibility Measurements

Eighteen cone penetrometer pushes were made during box test 1. Eleven of them were well outside of the compaction footprint, four were inside of the footprint, and three were close to the footprint (less than 10 cm). The measurements made with the cone penetrometer indicate that there was significant compaction down to the 40-cm depth (Figure 23). The data also indicate that there may have been some compaction down to 46 cm, but this is likely an artifact of limited data below 40 cm; only one of the four cone penetrometer pushes within the rut footprint reached below 40 cm.

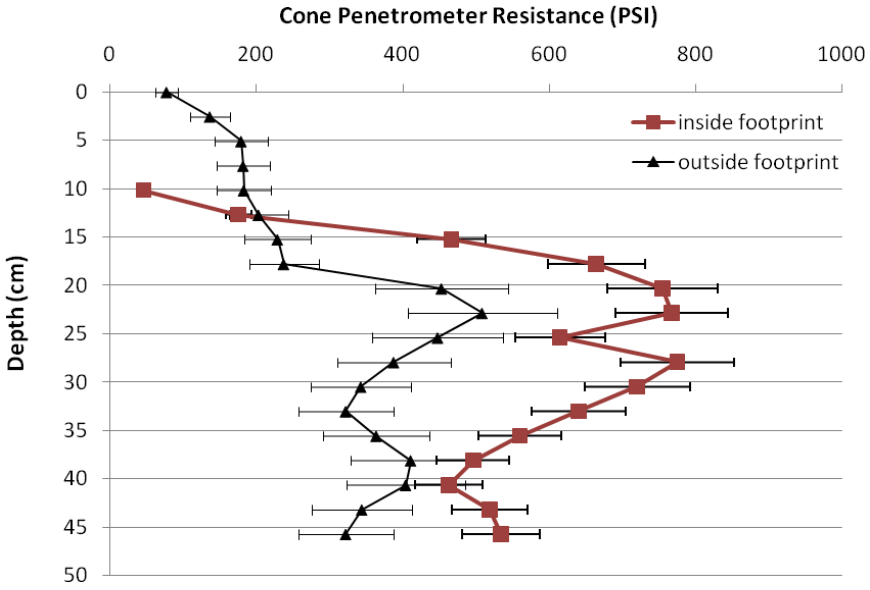

Figure 23. Average Cone Penetrometer Measurements Made Within the Rut Footprint and Outside of the Rut Footprint. Error bars represent typical standard deviation of the measurements.

For the first box test, there were dyed soil layers at 20 cm and 40 cm (nominal depth). The layer at the 40-cm depth had no visible deformation, which is consistent with other measurements. The layer at the 20-cm depth had a maximum deformation of 1.5 cm (Figure 24). It is interesting to note that the shape of the deformation pattern was consistent with the ellipsoid shape predicted by the Boussinesq curves of the geotechnical model where compaction is greatest at the center of the load.

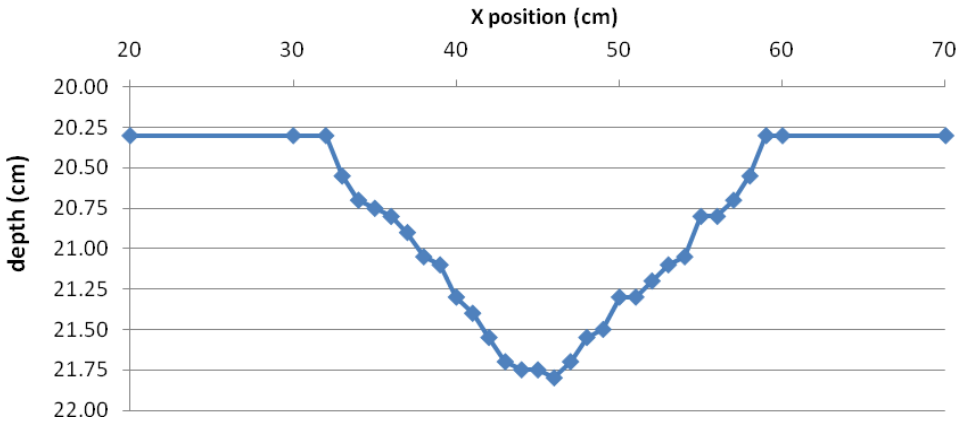

Figure 24. Deformation of Dyed Soil Layer at the 20-cm Depth Caused by Compaction. Note that x and y axis are not at the same scale.

Combining the multiple measurement methods provides a more comprehensive assessment of the data. Two normalization schemes were used. One was a simple technique where the results under the compaction footprint were normalized by subtracting the minimum value and dividing by the difference between the maximum and minimum. The other normalization technique involved estimating the initial values based on post-compaction measurements adjacent to the compaction area, subtracting them from measurements made under the compaction footprint, and then normalizing the results. The shape of these normalized curves provided mixed interpretation about where the maximum compaction occurred (Figure 25). While the expected maximum compaction is at the top of the soil surface within the compaction footprint, the down-hole magnetic susceptibility and cone penetrometer measurements indicate that the maximum compaction occurred below the surface of the rut. This is likely a combined result of the surface soils "un-compacting" some following compaction, inefficiencies in data collection methods near the surface, and variability (both vertical and lateral) of the soil bulk density during loading of the soil into the box. Neither normalization technique provides results particularly consistent with the results predicted by the geotechnical model, but they do follow the general trend.

For comparison of the horizontal data only the simple normalization technique was applied because there was insufficient data to subtract baseline measurements correctly (Figure 26). For this comparison, data from 20 cm below the initial soil surface were used (or 10 cm below the bottom of the compaction footprint). Results from measurements of the dyed soil layer indicated that vertical deformation was limited to the width of the footprint. However, results obtained with the cone penetrometer and magnetic susceptibility measurements indicate that some compaction occurred farther out than the compaction footprint, which is consistent with the

results of obtained from the geotechnical model. This agreement with the geotechnical model can be further evaluated by comparing normalized results of the cone penetrometer at various depths to the normalized increases in bulk density predicted with the geotechnical model (Figure 27). This comparison shows that the cone penetrometer results are reasonably consistent with model predictions at the edge of the footprint (B/2) and one half of a footprint width beyond the edge of the footprint (B).

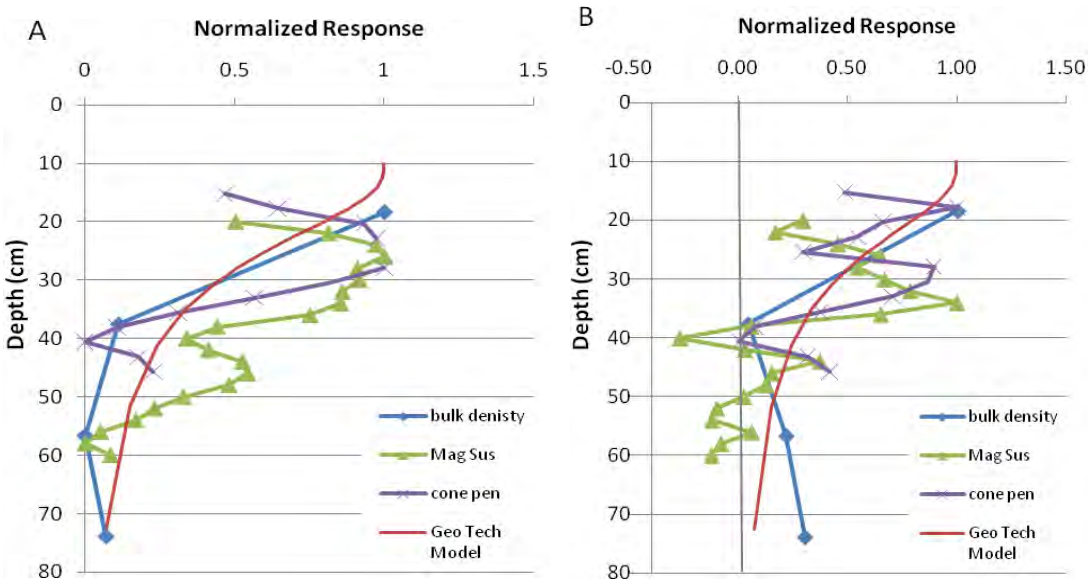

Figure 25. Normalized Results Under Compaction Footprint for Box Test 1 Using a Simple Normalization Technique (A), and a Background Subtraction Scheme (B)

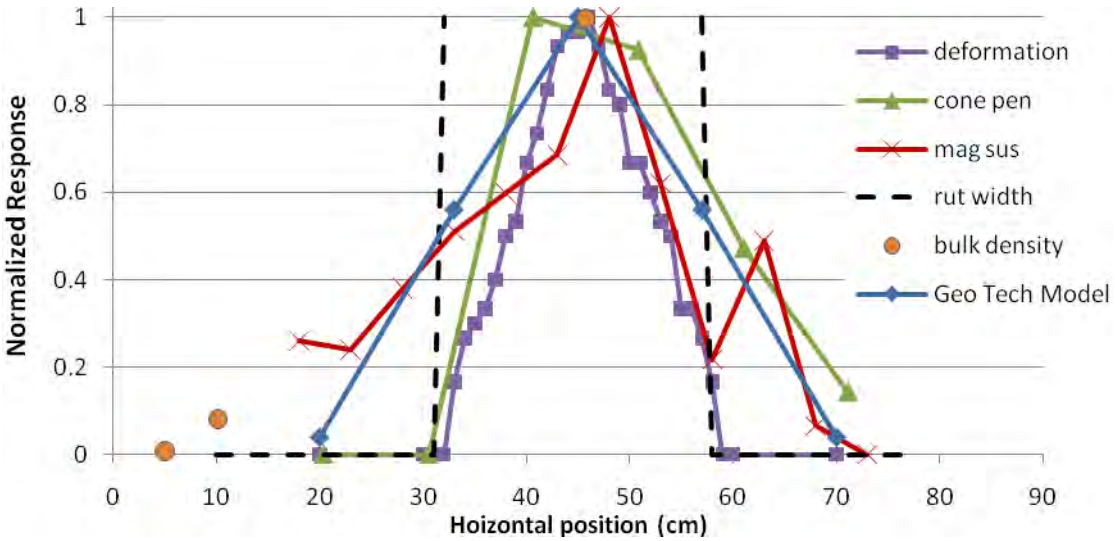

Figure 26. Normalized Results Laterally Across the Test Cell for Box Test 1. These data are from nominally 20 cm below the initial soil surface.

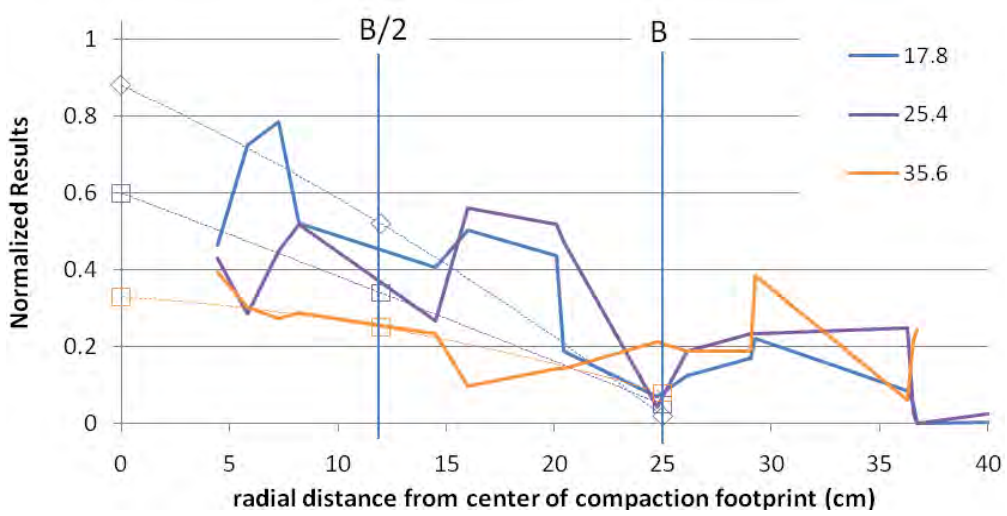

Figure 27. Normalized Cone Penetrometer Results (Solid Lines) Compared to the Geotechnical Model Predictions (hollow symbols). Results are shown at three depths. Dashed lines indicate a best-fit polynomial trend line.

4.4.2 Box Test 2 – 15% MC, 15-cm Rut

For the second box test, 18 core samples were collected for bulk density and soil moisture analysis (Figure 28). The average soil moisture for these samples (excluding the surface samples that had visibly dried) was 14% (Table 2). The bulk density measured in the non-compacted portions of the box ranged between 1.1 and 1.4, with an average of 1.25. The maximum bulk density measured just under the rut was 1.94. However, this measurement is a vertically integrated average of the top 6 inches, and was collected towards the edge of the rut footprint. The bulk density of the top centimeter at the center of the rut was likely larger than 1.94.

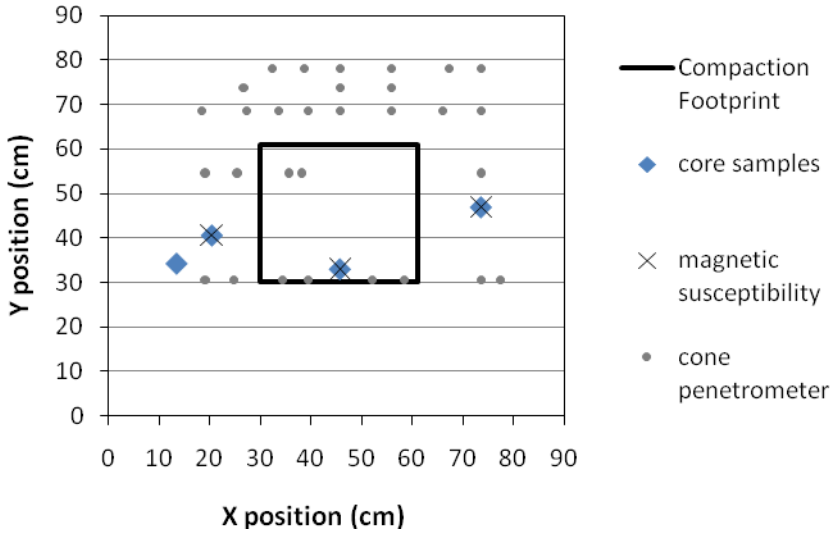

Figure 28. Positions of Data Collection Locations for Box Test 1. View is looking down on the top of the soil surface, with east to the left and west to the right.

Table 2. Soil Moisture, Bulk Density, and Position of Core Samples Collected and Analyzed for Box Test 2

x (cm)	y (cm)	z* (cm)	Bulk Density (g/cm^3)	Soil Moisture (%)
13.3	34.3	8.4	1.19	13.5
13.3	34.3	25.7	1.29	14.3
13.3	34.3	44.6	1.17	14.8
13.3	34.3	65.3	1.23	15.6
73.7	47.0	7.6	1.37	13.6
73.7	47.0	22.9	1.41	14.5
73.7	47.0	38.3	1.11	15.1
73.7	47.0	53.5	1.19	15.8
73.7	47.0	72.4	1.31	16.1
20.3	40.6	7.6	1.24	13.1
20.3	40.6	22.9	1.48	14.1
20.3	40.6	53.3	1.27	15.2
20.3	40.6	71.1	1.24	15.6
45.7	33.0	18.1	1.94	13.8
45.7	33.0	25.7	1.74	14.8
45.7	33.0	38.1	1.39	15.6
45.7	33.0	53.3	1.38	16.3
45.7	33.0	68.6	1.57	16.6

* Depth below undisturbed soil surface to center of core sample.

The magnetic susceptibility measured with the down-hole instrument indicated that compaction occurred down to about 65 or 70 cm below the initial soil surface (Figure 29). These results were coupled with the mass magnetic susceptibility of the soil by applying Eq. 1 and predicting the bulk density. These calculated bulk densities were then adjusted by subtracting the average initial bulk density measured with the down-hole instrument to provide a baseline corrected increase in bulk density. Normalizing these results allowed for a comparison with the changes in bulk density predicted by the geotechnical model (Figure 30). This comparison indicated that the geotechnical model was reasonably accurate in the prediction of changes in bulk density under the footprint caused by this compaction scenario.

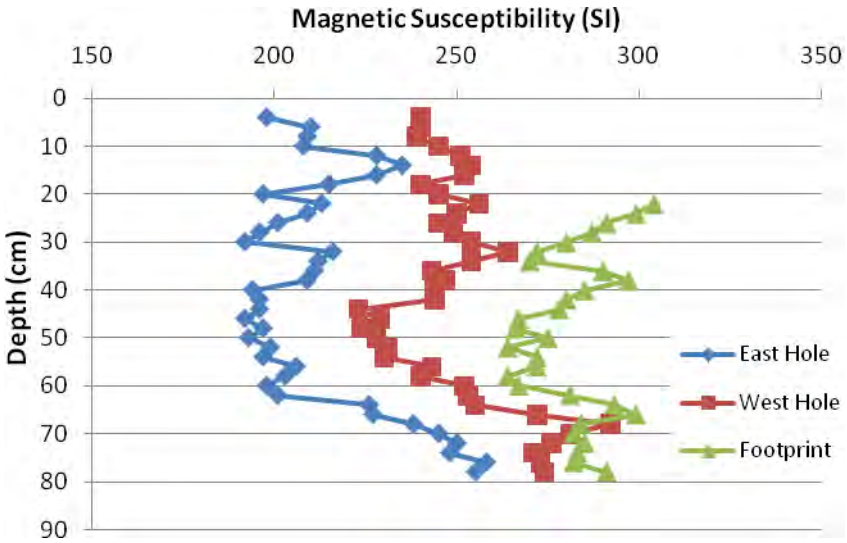

Figure 29. Down-Hole Measurements of Volumetric Magnetic Susceptibility –Box Test 2

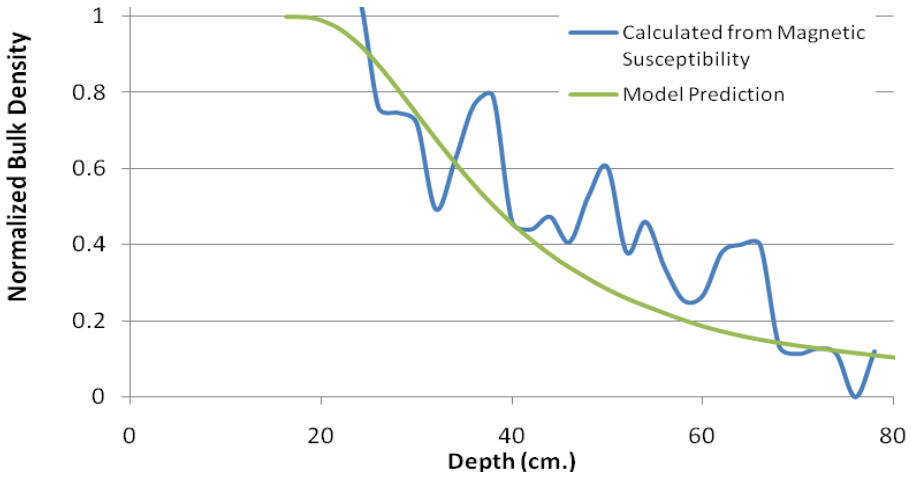

Figure 30. Comparison of the Normalized Bulk Density Directly Under the Compaction Footprint Predicted by the Geotechnical Model and Calculated Using Equation 1 and Volumetric Magnetic Susceptibility Measurements. Normalization used in conjunction with background subtraction to remove vertical variations in bulk density.

The results of the cone penetrometer tests indicated that the compaction continued deeper than 45 cm, which is the vertical extent of the cone penetrometer (Figure 31). This is consistent with the other measurements conducted during box test 2, including the manual deformation measurements (Figure 32). For the second box test, there were dyed layers at the 10-, 20-, 40-, and 60-cm depths. It is interesting to note that even though the compaction footprint extended deeper than the shallowest dyed layer, the dyed soil remained unbroken as a continuous strata across the width of the box (Figure 33). This indicates that for a rut deeper than a layer with

cultural significance there would be compaction of the sediment, but the possibility exists that all the lithologic information would be intact (although very compressed).

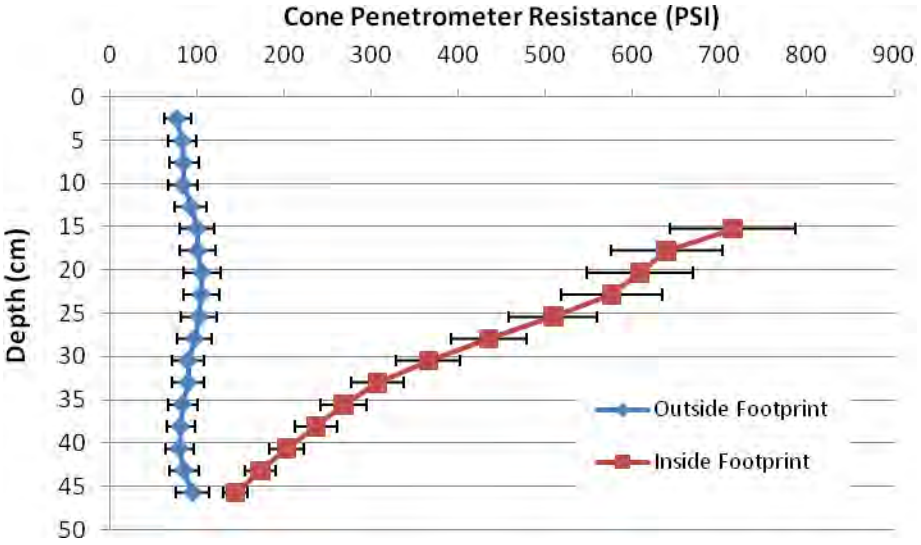

Figure 31. Average Cone Penetrometer Measurements Made Within the Rut Footprint and Outside of the Rut Footprint for Box Test 2. Error bars represent typical standard deviation of the measurements.

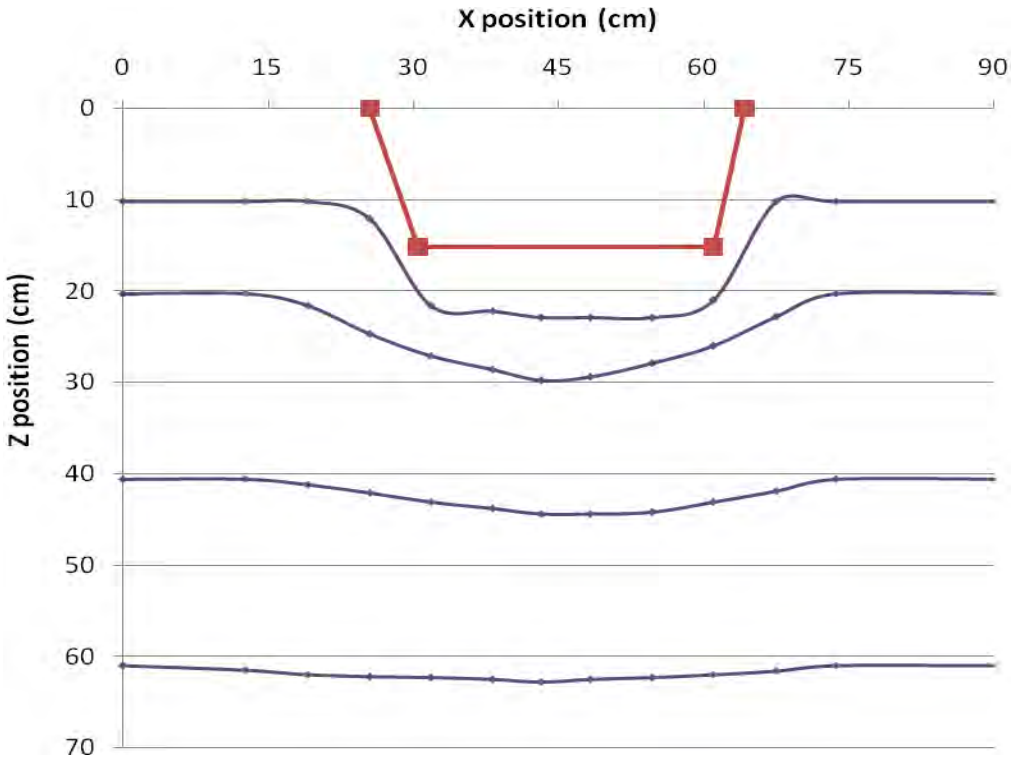

Figure 32. Deformation of Dyed Soil Layers at Four Depths Caused by Compaction During Box Test 2

Figure 33. Close-Up View of the Dyed Soil Layers, and the Deformation Caused by Compaction During the Second Box Test

Combination of the data sets provides a method of inter-comparison. In the vertical direction, both simple and background subtracted normalization techniques were used (Figure 34). Using the background subtraction provided a better interpretation of the results because it is apparent from the bulk density and magnetic susceptibility measurements that the soil layer between the 60- and 80-cm deep was more compacted than the shallower soil. This is likely due to the bottom layer continuing to undergo compaction as the subsequent layers were loaded into the box. An adjusted height scheme was used to minimize variation in the data; the background used for subtraction at a given height under the footprint was the background at the original starting height of that soil. Unfortunately, this background subtraction technique did not fully remove the effects of vertical variation in the soil bulk density; note the shift from low to high magnetic susceptibility that occurs around 40 cm. It is assumed that this anomaly occurred because the soil for the 40- to 60-cm layer was compacted from the top, creating a more compact layer around the 40-cm depth. Then the soil for the 0- to 40-cm-deep layer was added, resulting in a less compact portion just above the 40-cm depth. Although this created some anomalies in the data, it also highlights the outstanding vertical resolution that is provided by the down-hole volumetric magnetic susceptibility measurements.

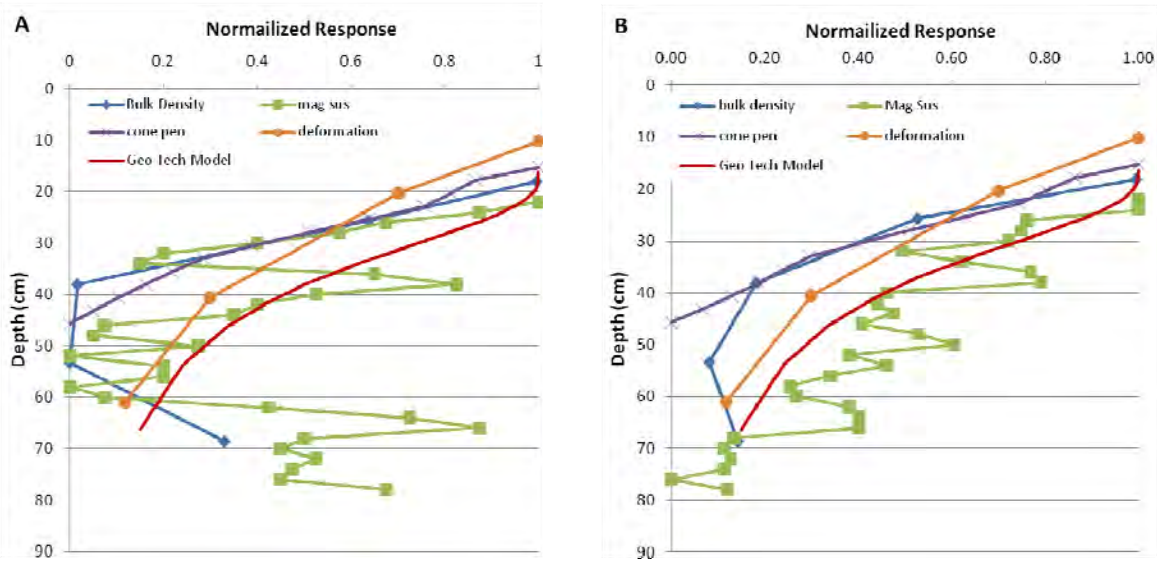

Figure 34. Normalized Results Under Compaction Footprint for Box Test 2 Using a Simple Normalization Technique (A), and a Background Subtraction Scheme (B)

Comparison of the horizontal data implemented a simple normalization technique, and was done at two depths: 20 and 30 cm (Figure 35). This comparison showed that there was generally very good agreement between the various data collection methods. The exception is the volumetric magnetic susceptibility at the 30-cm depth. These data indicate compaction farther outside of the footprint that any of the other methods. The reason for this is not readily apparent, but it is likely a result of non-uniform initial bulk density created during the box-loading procedure.

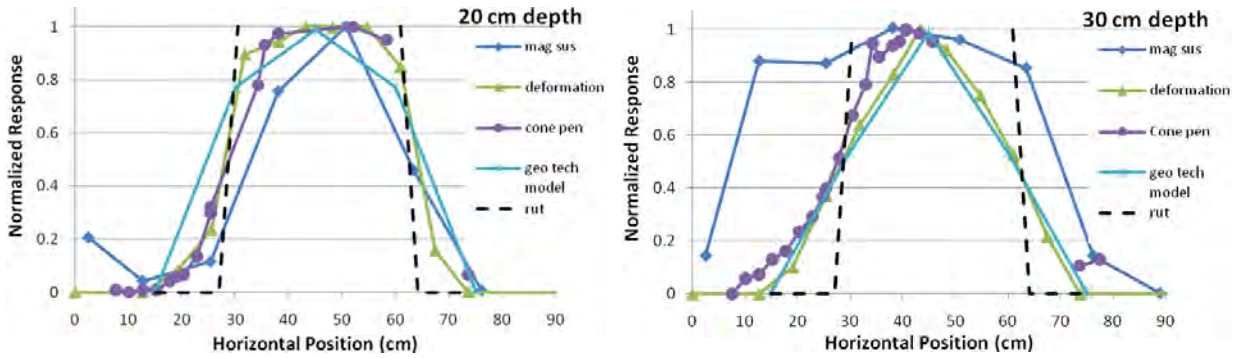

Figure 35. Normalized Results in the Horizontal Direction at the 20- and 30-cm Depths for Box Test 2

The agreement between the Geotechnical Model and the deformation measurements was particularly interesting, and prompted a more thorough analysis (Figure 36). The deformation predicted by the geotechnical model was calculated at the center, edge, and half-footprint width beyond the edge of the footprint (x distances of 15, 30, 45, 60, and 75 cm). To convert the

modeled change in bulk density at each level into a deformation, the soil at each interval was divided into 1-cm^2-wide columns with height equal to the distance between model output depths. The change in height at each interval was calculated from the ratio of the pre- and post-compaction bulk density, and deformation was determined as the sum of the change in heights of each interval from the bottom up. This analysis showed very good agreement between the modeled deformation and the measured deformation. One shortcoming is that the geotechnical model begins at the bottom of the impaction footprint, so there was no way to compare the shallowest deformation measurement marker.

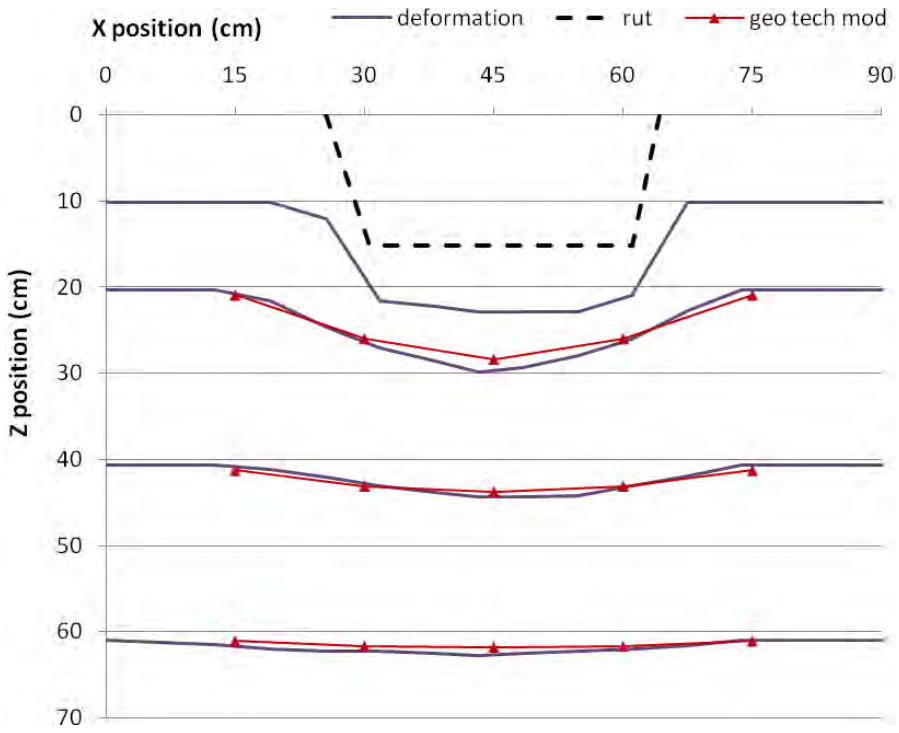

Figure 36. Comparison Between the Observed and Modeled Soil Deformation for Box Test 2

4.4.3 Box Test 3 – 15% MC, 20-cm Rut

The third and final box test was adversely affected by freezing conditions; an early frost resulted in no core samples being usable for bulk density measurements. However, results from the first two box tests indicated that the other measurement techniques were better for identification of the depth of compaction, and the test continued without the core sample results (Figure 37). The magnetic susceptibility measurements indicated that compaction occurred down to about 60 cm (Figure 38). This result was consistent with the predicted compaction depth; also the shape of the compaction curve was generally consistent with the predicted compaction profile, although there was a lot of noise in the magnetic susceptibility results (Figure 39). This may have been a result of the freeze-thaw cycle that the box was subjected to before the magnetic susceptibility measurements were conducted, or it may have been an artifact of the slightly modified box-loading procedure applied for this final test; the larger 20-cm layers were loaded and gently compacted in sub-layers of 5 cm.

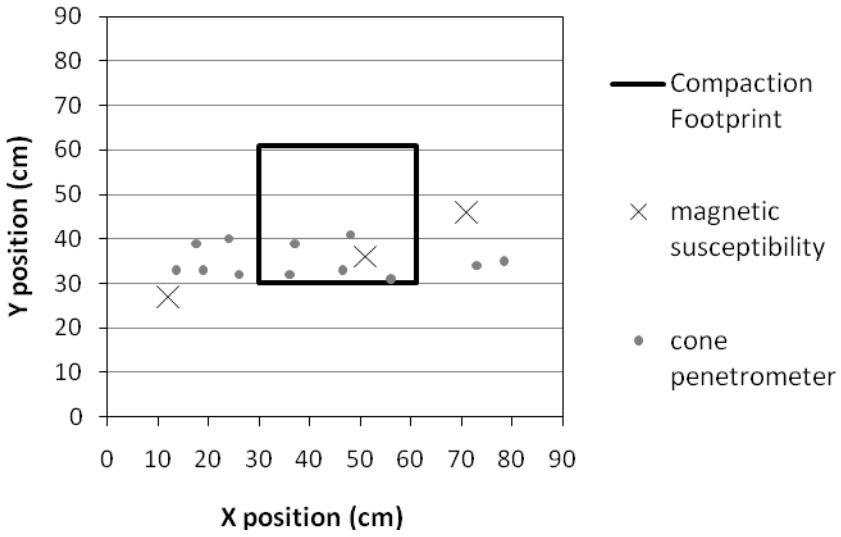

Figure 37. Positions of Data Collection Location for Box Test 3. View is looking down on the top of the soil surface, with east to the left and west to the right.

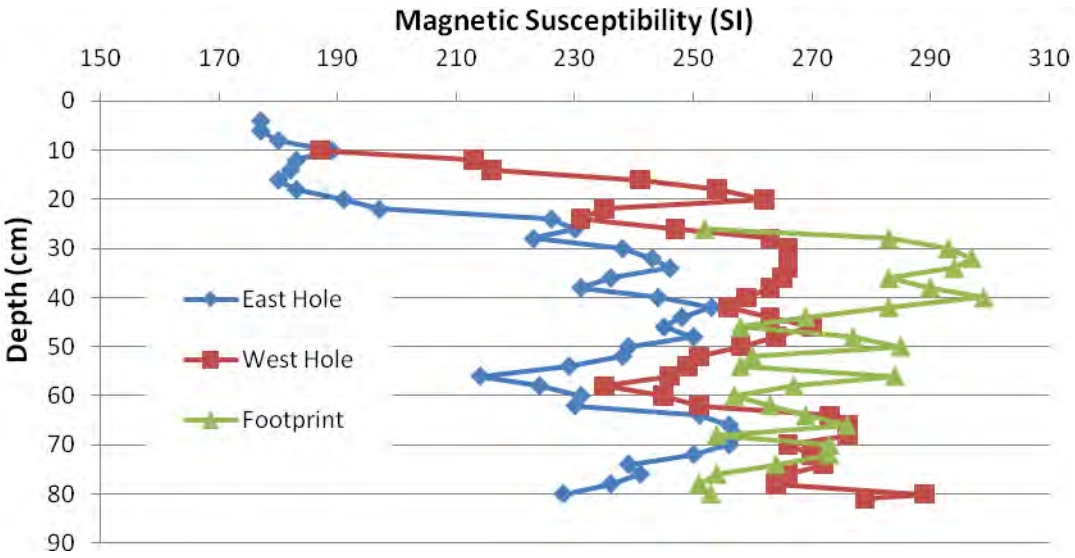

Figure 38. Down-Hole Measurements of Volumetric Magnetic Susceptibility – Box Test 3

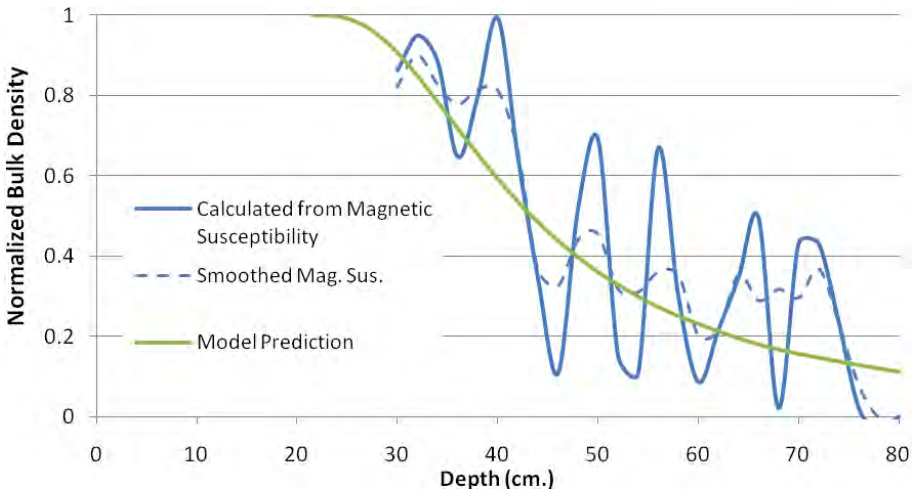

Figure 39. Comparison of the Normalized Compaction Directly Under the Compaction Footprint Predicted by the Geotechnical Model and Measured Using Volumetric Magnetic Susceptibility

The cone penetrometer results indicated that compaction occurred deeper than the penetration depth of the instrument (45 cm). Projection of the best fit curves indicate that the soil strength decreases to baseline conditions around 55 cm below the soil surface (Figure 40). This is different than the depth impact estimated from the magnetic susceptibility measurements; however, the magnetic susceptibility measurements show that the bulk density decreases between 45 and 60 cm, so the linear projection of the non-impacted cone penetrometer measurements is probably not appropriate. This example serves to highlight the benefits of the high spatial resolution measurements provided by the down-hole magnetic susceptibility instrument. Analysis of the combined normalized results indicated that all of the measurement techniques provided similar results (Figure 41). This is consistent with the other box tests.

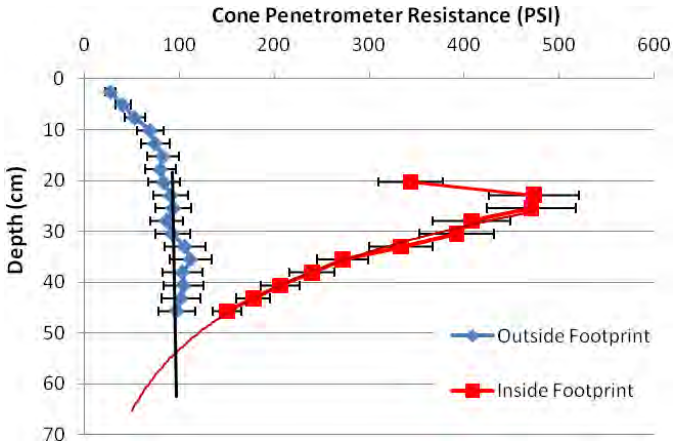

Figure 40. Average Cone Penetrometer Measurements Made Within the Rut Footprint and Outside of the Rut Footprint. Error bars represent typical standard deviation of the measurements. Solid lines represent projections of the best-fit curves beyond the depth range of the instrument.

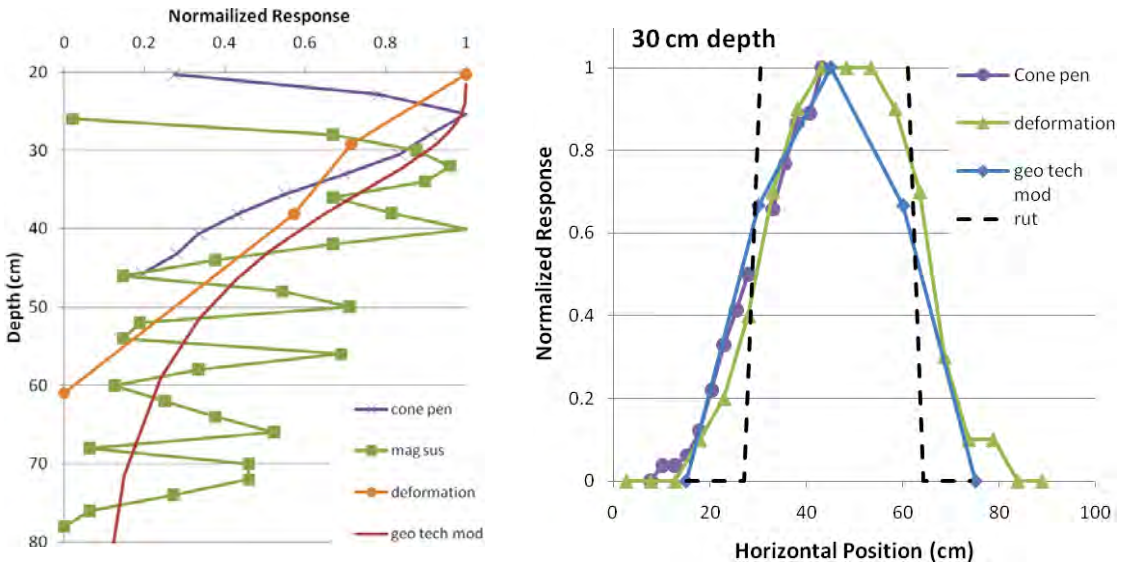

Figure 41. Combined Normalized Results in the Vertical and Horizontal Directions

Comparison of the measured deformation and the deformation predicted by the geotechnical model indicated that the geotechnical model accurately described the deformation (Figure 42). It is very encouraging that the geotechnical model appears capable of not only correctly predicting the deformation directly under the footprint, but also at the edges and outside of the footprint. This demonstrates the effectiveness of the geotechnical model to provide a tool for correct placement of measurement points outside of the impact footprint, as well as a method for estimating the total volume of soil that is disturbed by a surface rut without requiring any invasive measurements.

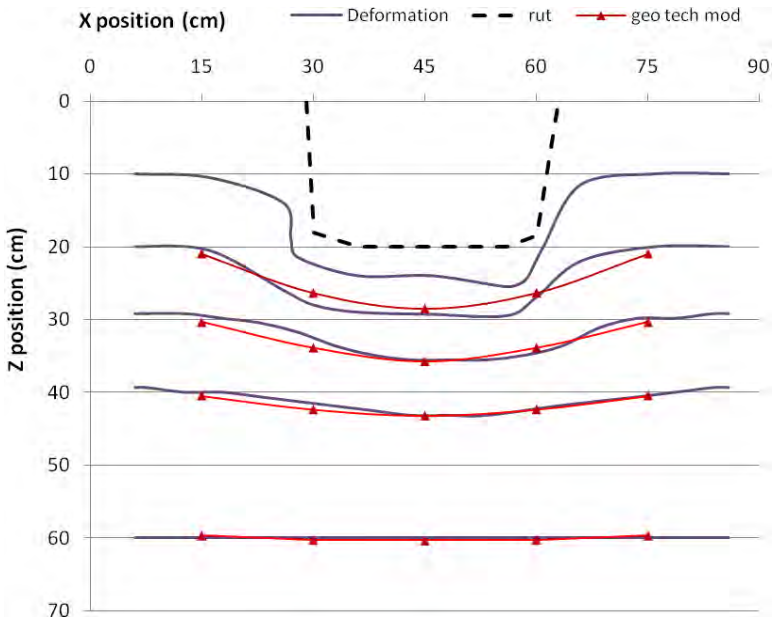

Figure 42. Comparison Between the Measured and Modeled Soil Deformation for Box Test 3

4.5 Field-Scale Compaction Tests

After completing the laboratory box tests, similar experiments were conducted in the field at the Yakima Training Center on natural, undisturbed soil. The measurement techniques used in the box tests were implemented for these field-scale tests. In addition, magnetometer measurements were made before and after compaction to evaluate the change in magnetic signature created by the rut formation. The magnetometer results for all three field compaction tests are discussed separately at the end of this section.

4.5.1 Test 1 – 13-cm Rut Depth

Samples for bulk density and soil moisture analysis were collected after rut formation inside and outside of the rut footprint (Figure 43). The results of these samples indicated that the compaction extended down to about 35 or 40 cm (Table 3). These bulk density results were combined with the down-hole volumetric magnetic susceptibility measurements (using Eq. 1), to calculate the mass susceptibility at each interval. This analysis indicated a distinct change in lithology between 40 and 50 cm below ground surface. This was reflected in the sharp decrease in the mass magnetic susceptibility of the sediments (Figure 44). Also note the linear change in soil moisture at depth—this is not surprising because these experiments were conducted early in the spring and reflect recent snowmelt and precipitation. However, the Proctor analysis curves (Figure 2) show the relationship between soil moisture and maximum potential compaction; less compaction would be expected at depth for this decreasing soil moisture profile than if the moisture content were uniform vertically throughout the soil column.

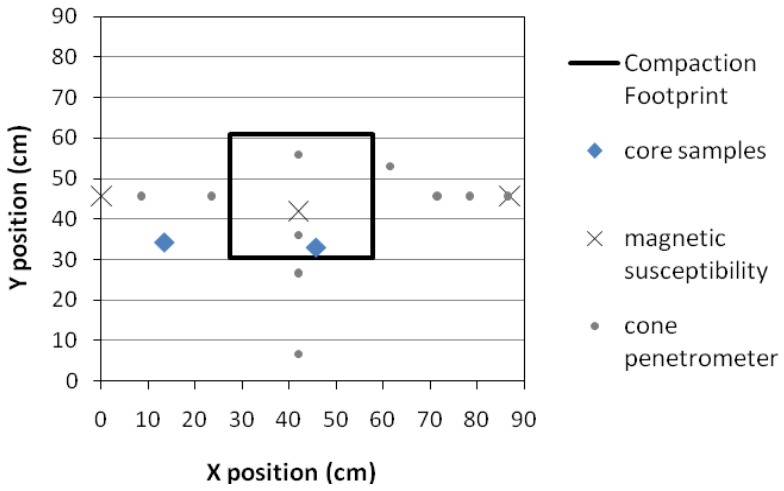

Figure 43. Relative Positions of Data Collection Locations for the Field Compaction Test 1. North is up.

Table 3. Locations of Core Samples, Measured Bulk Density and Soil Moisture, Average Measured Volumetric Magnetic Susceptibility, and Calculated Mass Magnetic Susceptibility, Test 1

x (cm)	y (cm)	z* (cm)	Bulk Density (g/cm^3)	Soil Moisture	Volumetric Magnetic Susceptibility	Mass Magnetic Susceptibility
13.3	34.3	8	1.11	20%	434	391
13.3	34.3	23	1.27	16%	429	339
13.3	34.3	38	1.05	14%	392	373
13.3	34.3	53	1.80	12%	284	157
45.7	33.0	20	1.63	16%	633	387
45.7	33.0	35	1.18	15%	506	429
45.7	33.0	50	1.50	8%	261	174
45.7	33.0	66	1.44	6%	208	144

* Depth below undisturbed soil surface to center of core sample.

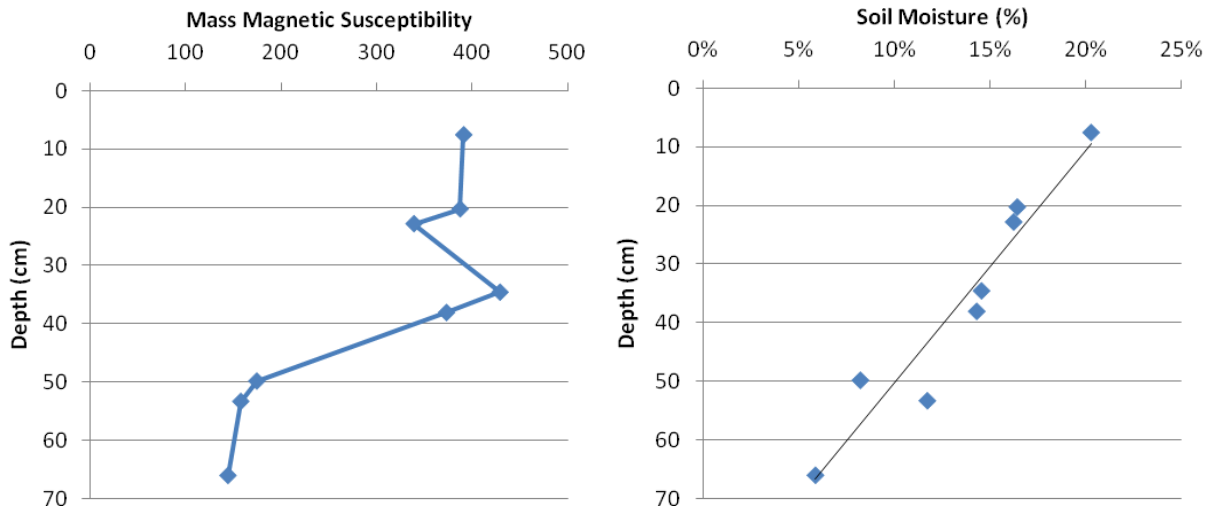

Figure 44. Profiles of the Mass Magnetic Susceptibility and the Soil Moisture Showing Vertical Properties of the Soil at the Time of the Experiment

Analysis of the down-hole volumetric magnetic susceptibility measurements illustrates that significant compaction occurred down to about 30 cm, with some compaction extending down to a depth of 40 cm (Figure 45). When the depth-specific mass magnetic susceptibility is used to convert the volumetric magnetic susceptibility measurements to bulk density, a similar compaction depth is estimated. When the lower mass susceptibility of the soil below 40 cm is taken into account, the increase in bulk density at the lower depths is readily visible. The data collected during the cone penetrometer testing differed from the magnetic susceptibility results; the cone penetrometer testing indicated that the compaction occurred below 45 cm (Figure 46).

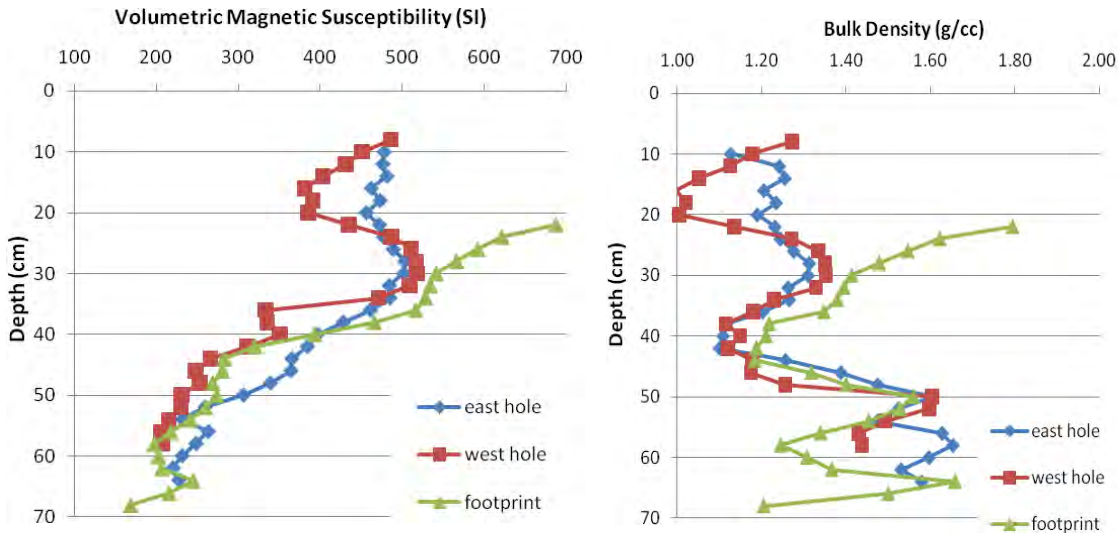

Figure 45. Down-Hole Volumetric Magnetic Susceptibility Measurements, and Calculated Bulk Density for Field Compaction Test 1

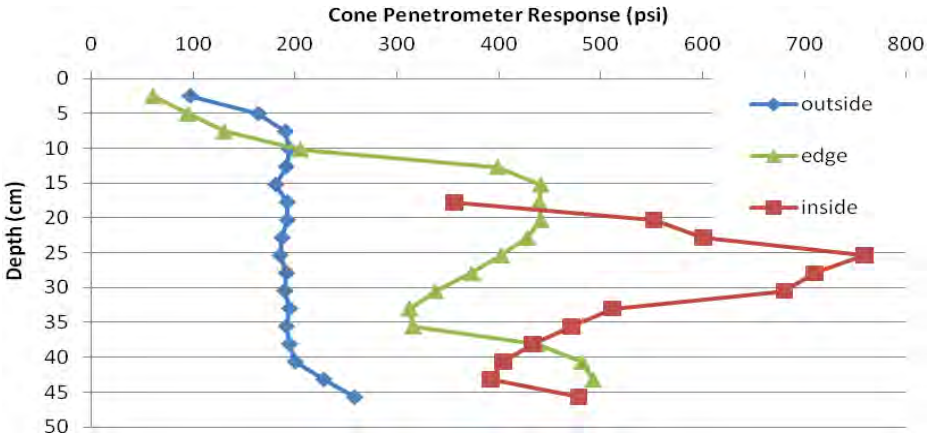

Figure 46. Average Cone Penetrometer Measurements Outside of, at the Edge of, and Within the Rut Footprint

Application of the background subtraction normalization technique provided some interesting results. The three measurement techniques all had similar responses, indicating a maximum depth of compaction of about 40 cm (Figure 47). However, the geotechnical model results led to an estimated depth of compaction deeper than 70 cm. When the bulk density predicted by the geotechnical model are compared with the undisturbed bulk density profile calculated from the magnetic susceptibility measurements, it can be seen that between 45 and 50 cm the bulk density of the in situ sediments exceeds the post compaction bulk density predicted by the geotechnical model (Figure 48). This would indicate that this harder, denser layer served to limit compaction to that portion of the soil column above the 45- or 50-cm depth.

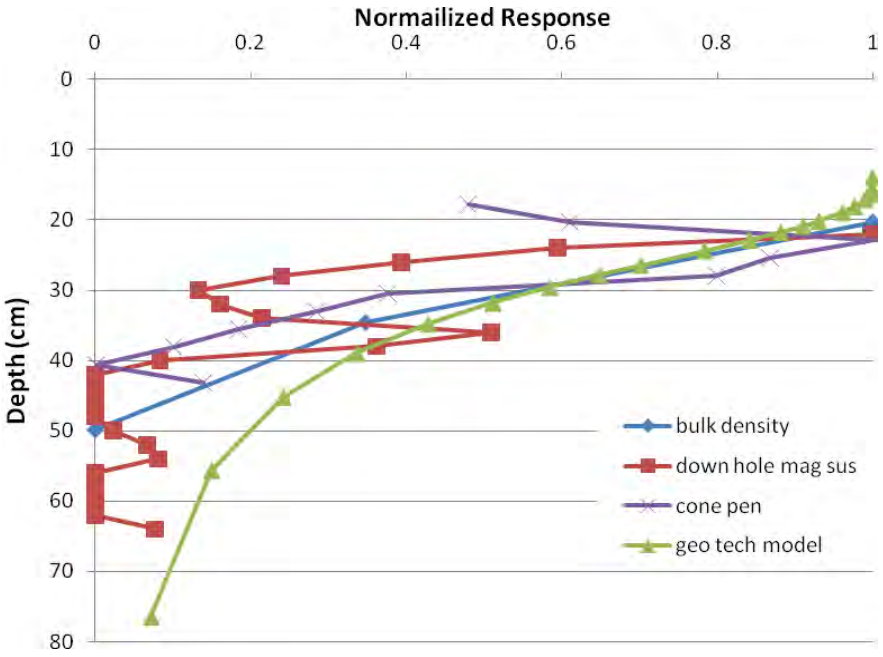

Figure 47. Normalized Vertical Profile Comparison of Results for Field Compaction Test 1 (with background subtraction)

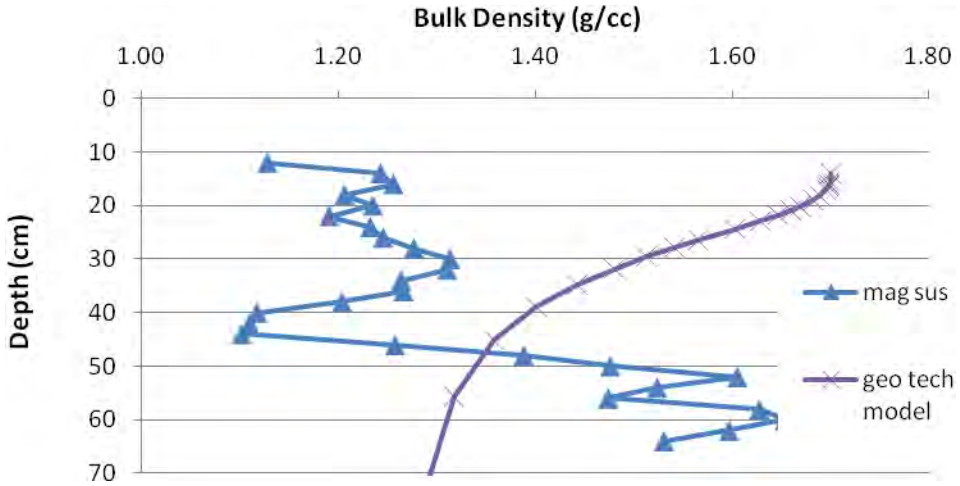

Figure 48. Comparison of the Bulk Density Predicted by the Geotechnical Model and the Bulk Density Calculated from the Down-Hole Magnetic Susceptibility Measurements

4.5.2 Test 2 – 15-cm Rut Depth

Samples for bulk density and soil moisture analysis were collected after rut formation inside and outside of the rut footprint (Figure 49). The results of the bulk density samples could not be used to estimate the depth of compaction because the two deepest samples under the rut footprint were lost during analysis (Table 4). Similar to the first test, integration of the bulk density and

volumetric magnetic susceptibility results revealed a sharp decrease in the mass susceptibility between 35 and 40 cm below ground surface (Table 4). Combining the depth-specific mass magnetic susceptibility with the down-hole volumetric susceptibility measurements (Eq. 1) provided an estimate of the vertical bulk density profile (Figure 50). This analysis indicated that the compaction extended down to about 35 cm (Figure 50), which is similar to the first test, and is also about the depth of the observed change in lithology. This is in contrast to the geotechnical model, which predicts compaction to extend deeper than 1 m (Figure 51), and slightly shallower than the depth of compaction indicated by the cone penetrometer testing (Figure 51). Again, it appears than the depth of compaction was limited by the denser sediments found below 40 cm. This is also supported by comparison of the cone penetrometer results on a horizontal profile (Figure 52). At the 40- and 43-cm depths, the cone penetrometer resistance on the left side of the rut is close to, or equal to, the resistance under the rut footprint.

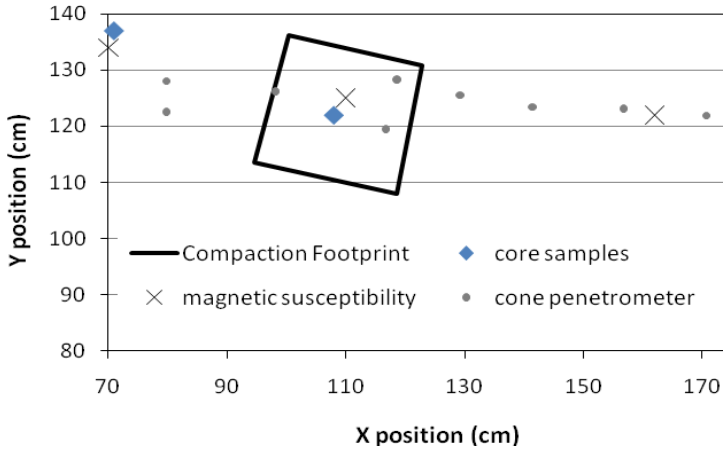

Figure 49. Relative Positions of Data Collection Locations for Field Compaction Test 2. North is up.

Table 4. Locations of Core Samples, Measured Bulk Density and Soil Moisture, Average Measured Volumetric Magnetic Susceptibility, and Calculated Mass Magnetic Susceptibility, Test 2.

x (cm)	y (cm)	z* (cm)	Bulk Density (g/cm^3)	Soil Moisture	Volumetric Magnetic Susceptibility	Mass Magnetic Susceptibility
71	137	8	1.35	16%	405	299
71	137	23	1.16	14%	438	376
71	137	38	1.18	16%	240	203
71	137	53	1.17	7%	150	128
108	122	23	1.62	16%	610	376
108	122	38	1.37	12%	373	273

* Depth below undisturbed soil surface to center of core sample.

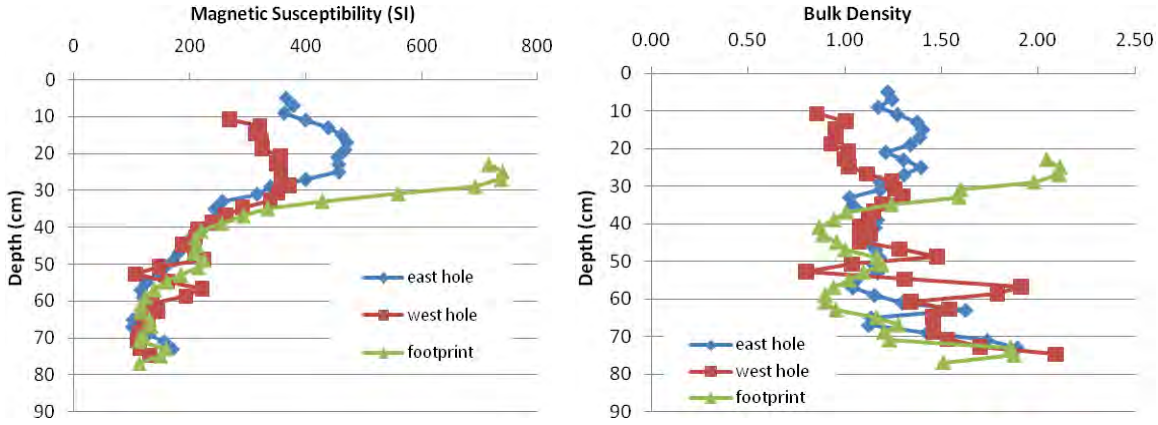

Figure 50. Down-Hole Volumetric Magnetic Susceptibility Measurements and the Bulk Density Profile Calculated from the Magnetic Susceptibility Measurements

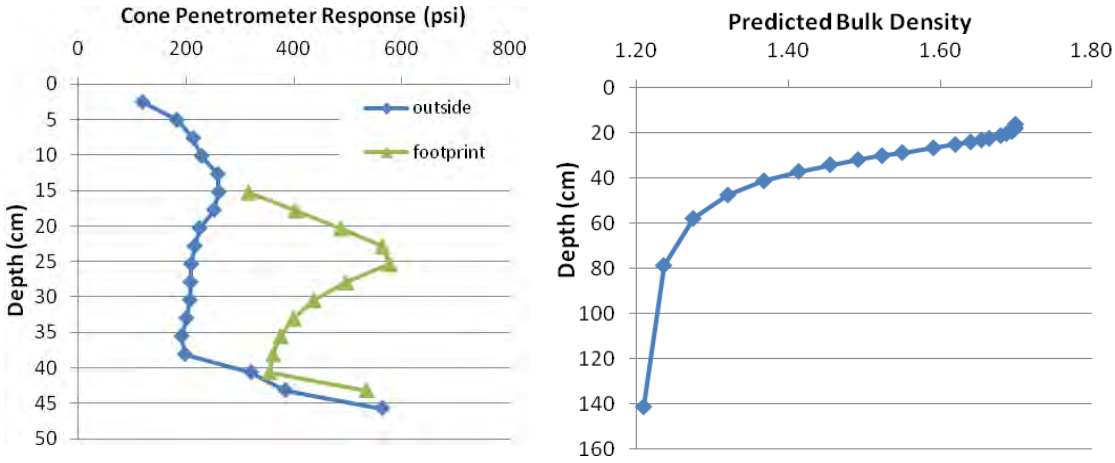

Figure 51. Measured Vertical Profile of Cone Penetrometer Resistance and the Profile of Bulk Density Predicted by the Geotechnical Model.

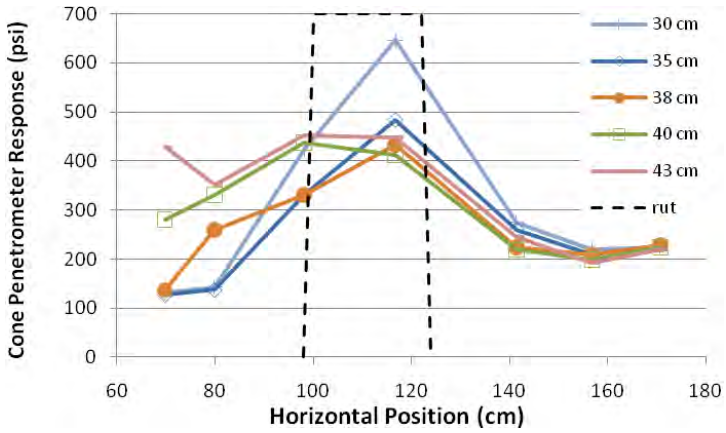

Figure 52. Horizontal Profiles of Cone Penetrometer Resistance Measured During Test 2.

4.5.3 Test 3 – 17-cm Rut Depth

The same general methodology applied to the first two field compaction tests was applied for the third test. Core samples, magnetic susceptibility measurements, and cone penetrometer measurements were made (Figure 53). The bulk density samples seemed to be systematically lower outside of the footprint and were not considered usable in determining depth of compaction (Table 5). It is interesting to note the distinct decrease in soil moisture at the lower depths. This is likely related to change in lithology. Based on the results of the volumetric magnetic susceptibility readings, as well as the calculated bulk densities, it appears that compaction occurred down to about 45 or 50 cm (Figure 54). This is consistent with the other two field tests conducted at this site. Again, it appears that a change in lithology around 50 cm (identified by the change in mass susceptibility, Table 5) resulted in limiting the compaction to the portion of the soil column above 50 cm (Figure 55). While the cone penetrometer did not reach deep enough to identify the vertical extent of compaction, the horizontal profiles were adequate to estimate the lateral extent of compaction outside of the footprint (Figure 56).

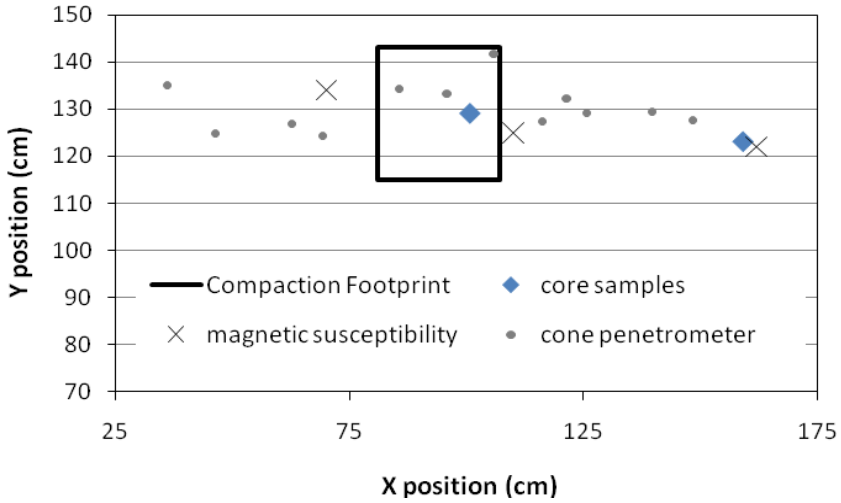

Figure 53. Relative Positions of Data Collection Locations for Field Compaction Test 3. North is up.

Table 5. Locations of Core Samples, Measured Bulk Density and Soil Moisture, Average Measured Volumetric Magnetic Susceptibility, and Calculated Mass Magnetic Susceptibility, Test 3

x (cm)	y (cm)	z* (cm)	Bulk Density (g/cm^3)	Soil Moisture	Volumetric Magnetic Susceptibility	Mass Magnetic Susceptibility
159.0	123.1	7.62	0.90	16%	355	396
159.0	123.1	22.86	0.97	15%	368	378
159.0	123.1	38.10	1.04	13%	394	377
159.0	123.1	53.34	1.07	7%	260	244
100.7	129.1	24.12	1.69	16%	626	370
100.7	129.1	39.36	1.57	15%	538	343
100.7	129.1	54.60	1.26	13%	313	249
100.7	129.1	69.84	1.24	7%	235	189

* Depth below undisturbed soil surface to center of core sample.

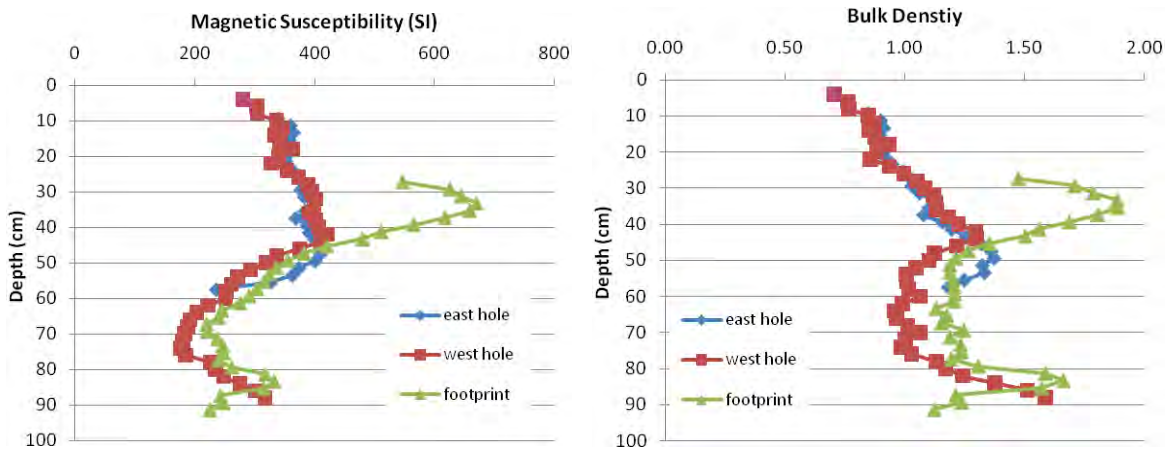

Figure 54. Down-Hole Volumetric Magnetic Susceptibility Measurements and the Bulk Density Profile Calculated from the Magnetic Susceptibility Measurements, Test 3

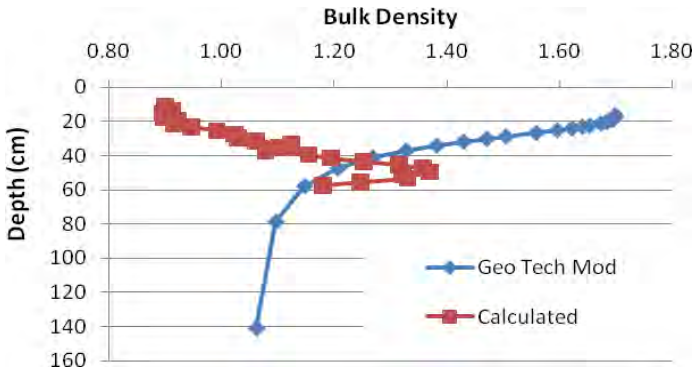

Figure 55. Comparison of the Bulk Density Predicted by the Geotechnical Model and the Bulk Density of the Undisturbed Sediment Calculated from the Magnetic Susceptibility Measurements

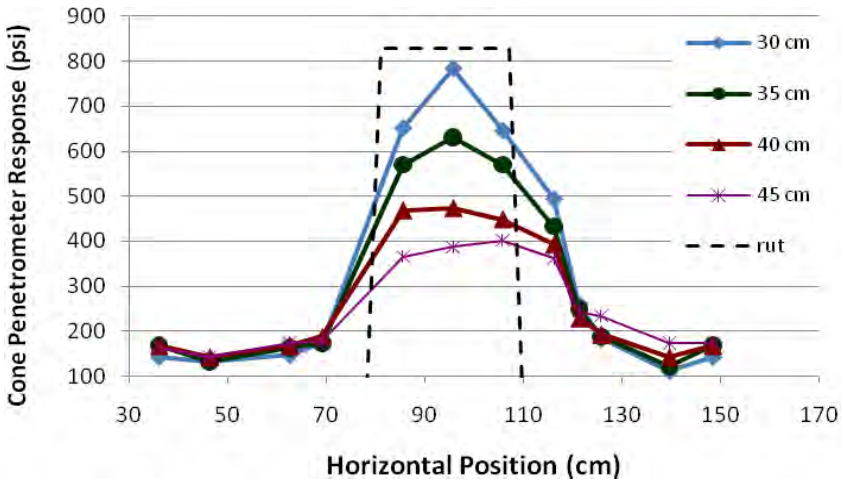

Figure 56. Horizontal Profiles of Cone Penetrometer Resistance Measured During Test 3

4.5.4 Magnetic Measurements and Modeling of Field Compaction Tests

The total magnetic field was measured before and after compaction using the magnetometer. The difference in the magnetic field gradient between the top and bottom sensors was calculated for each test. By comparing the difference in the gradient only the magnetic signal created by the compaction is evaluated; lateral variability in magnetic field is subtracted out between the pre- and post-compaction measurements. The results indicate that the compaction is readily discernable in the change in magnetic field measurements (Figure 57). Note that the shape of the measured magnetic gradient profile is very similar to the shape predicted by the proof-of-principle evaluation (Section 4.3). What is not as clear is what portion of the signal is created by the increase in bulk density and what part is created by the void space of the rut. The proof-of-principle evaluation revealed that the majority of the signal is typically caused by the rut formation, and that the magnitude of the decrease in magnetic field caused by the rut is only slightly offset by the increase in magnetic field caused by compaction.

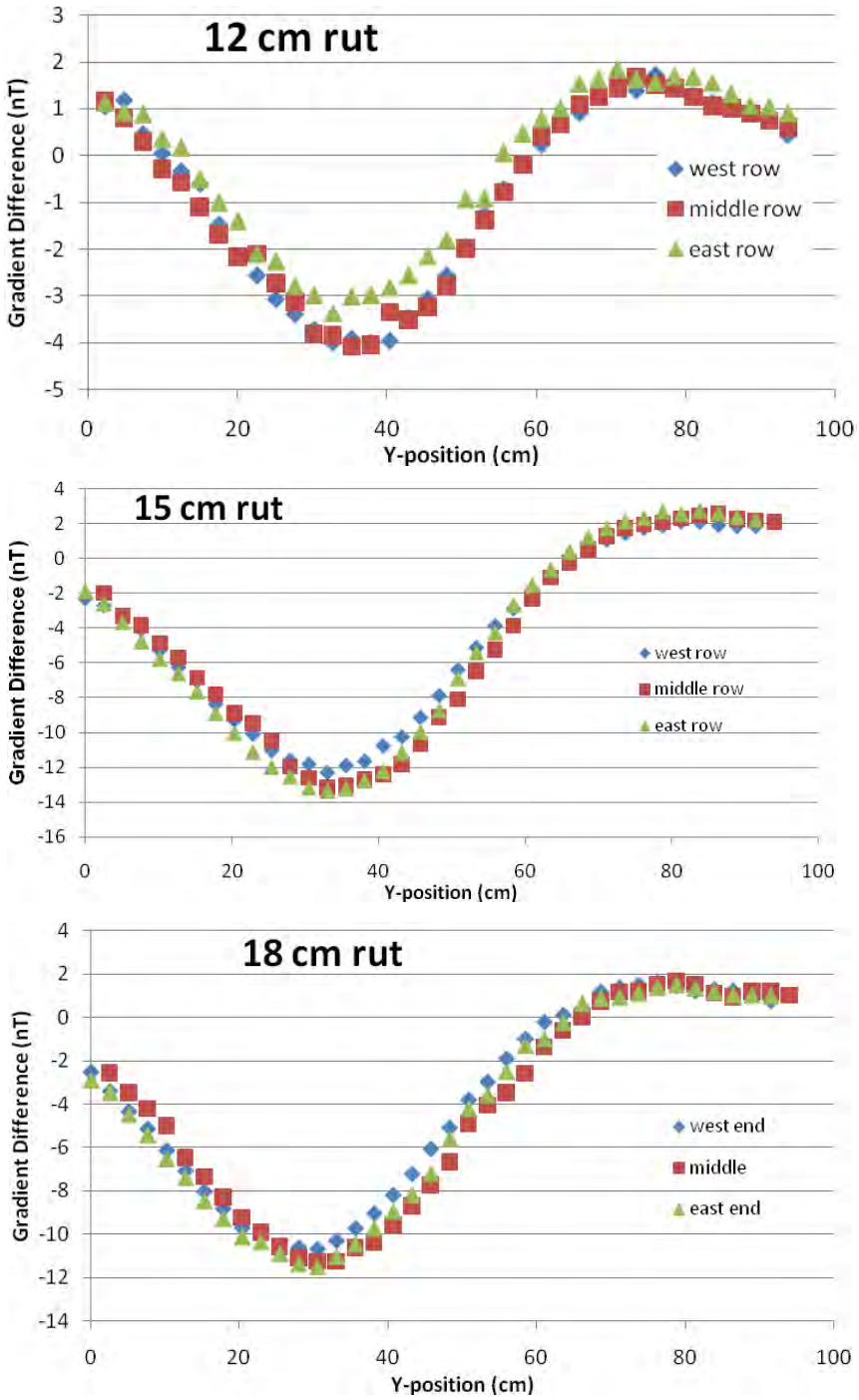

Figure 57. Measured Difference in Magnetic Gradient Measured for All Three Compaction Tests. Rut footprint between 20 and 50 cm.

Initial forward modeling of the field compaction tests required much deeper rut depths in the modeling domain than actually existed in order to achieve a reasonable fit with the measured data (Table 6). This was fixed by incorporation of remanent magnetism into the magnetic model (see Section 4.6). The introduction of remanence alone could not account for the differences between actual and modeled rut depth; however the progressive *elimination* of

remanence could. It was assumed that compaction could result in shock demagnetization of individual soil grains, or rotation of individual grains. Shock demagnetization eliminates remanence magnetism in each grain, while rotation of soil grains randomizes the direction of the remanence so that the cumulative effect is reduced or eliminated.

Table 6. Results of the Iterative Forward Modeling to Estimate Compaction Properties Based on Matching the Measured Change in Magnetic Signal

Model Scenario	Max Density (g/cm^3)	Rut Depth (cm)	Surface Susc. (µcgs)	RMS Fit w/o Demag.	RMS Fit w Demag.
12-cm test w/o remanence	1.28	9.4	448	6.6	NA
12-cm test w remanence	1.27	9.1	444	6.6	12.3
15-cm test w/o remanence	2.30	43.7	805	5.27	NA
15-cm test w remanence	1.42	14.1	497	18.4	5.9
18-cm test w/o remanence	1.95	31.9	68	4.8	NA
18-cm test w remanence	1.49	16.5	521	13.5	6.4

To match the geophysical data, the rate of demagnetization must include the following parameters: a starting remanence factor (Q-ratio), a minimum compaction level, a maximum compaction level, and a correlation factor that relates compaction to demagnetization. The starting remanence was estimated from the rotation test (Section 4.6). The minimum compaction level is the density at which demagnetization begins to take effect. Small amounts of compaction are assumed to be too light to induce demagnetization. The maximum compaction level is the density at which the remanence signal has been reduced to zero. Observation of the forward model results for the true rut depth shows that very little demagnetization is required to achieve a good fit between measured and modeled magnetic signal for the 12-cm test. On the other hand, demagnetization is required for both the 15- and 18-cm tests. The simplest approach for demagnetization that provides reasonable model results is a step function where remanence remains intact when the compacted surface volumetric susceptibility is below 480 µcgs but is completely destroyed above that.

This step-wise approach to demagnetization proved adequate for correctly modeling the magnetic signature measured after the three compaction tests. Using the densities required to duplicate the measured rut depth and assuming the remanence is destroyed above 480 µcgs, the best fit models occurred with demagnetization considered by applying a Q-ratio of 0.4. Because the total field response depends on both the susceptibility and remanence, variations in the background susceptibility model were tested. These sensitivity tests showed that the background model of 350 µcgs was accurate, with local minima at 350 and 360 µcgs. The effect of the introduction of remanence to the 12-cm compaction test was to slightly degrade the original

results. This test fell below the destruction threshold, and lowering the threshold to include this model resulted in a poorer fit, with an increase in the root-mean square RMS fit of 6.6 to 12.3 (Table 6). For the other two compaction tests, where compaction exceeded the remanence destruction threshold, incorporation of the Q-ratio increased the accuracy of the model significantly.

Evaluation of the modeled compaction profile indicates that the depth of compaction is overestimated. For example, with the 18-cm field compaction test, the depth of compaction is modeled to extend down to 80 cm (Figure 58). This can be seen by the change in color of the model output in the 60- to 80-cm depth layer under the compaction footprint relative to the color outside of the compaction footprint. Further analysis would need to be conducted to determine if reasonable agreement between the measured and modeled results could be found by fixing the depth of compaction at 40 cm (as observed with the magnetic susceptibility and cone penetrometer measurements, Section 4.5.3).

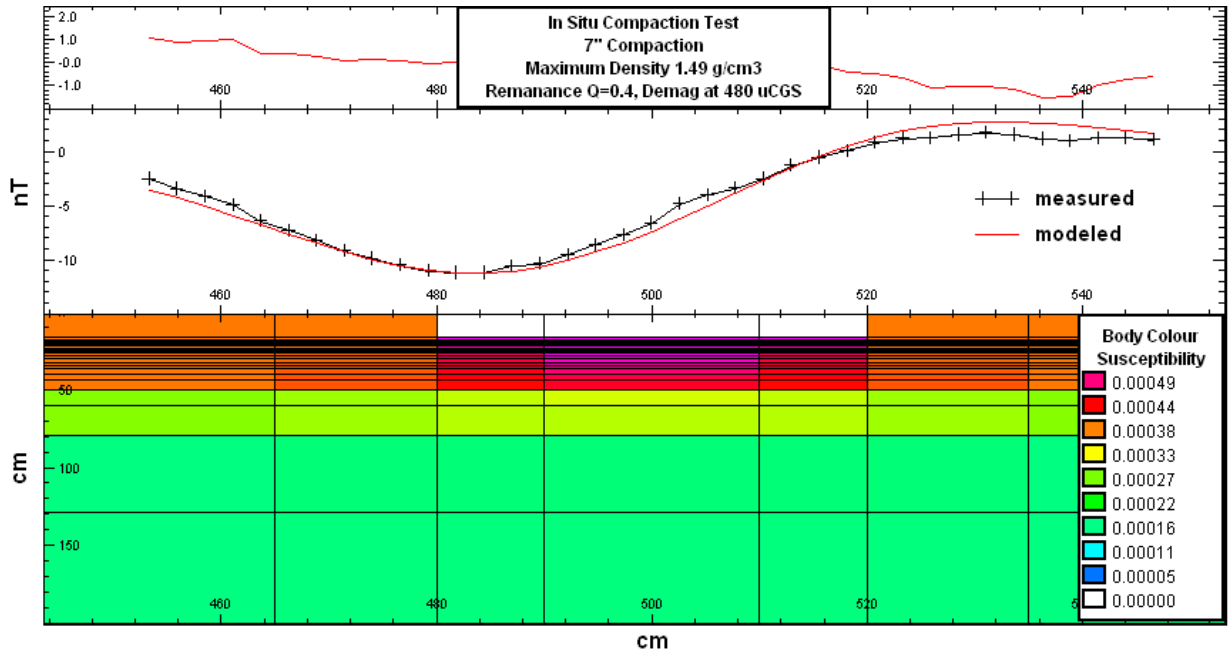

Figure 58. Forward Model of 18-cm Compaction Test

4.6 Remanence Test

The results of the remanence test indicated a strong remanence signature. The best fit of the measured and modeled magnetic signature was obtained with a Q-ratio of approximately 2.5 (Figure 59). The Q-ratio is a measure of remanence strength relative to the susceptibility. A Q-ratio of 2.5 implies that the remanent effect is 2.5 times stronger than the induced effect. This remanence is in addition to the susceptibility when considering surface-collected total field data. The optimal background susceptibility was 350 µcgs, which is consistent with the field susceptibility measurements and the other model tests.

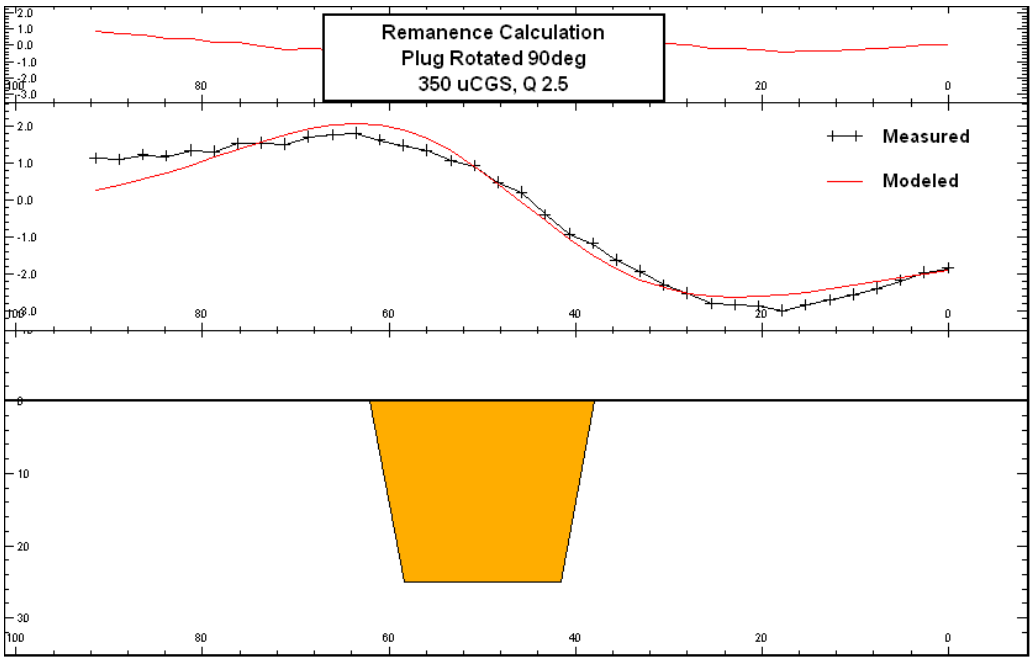

Figure 59. Remanence Calculation Results. Best fit for a background susceptibility of 350 µcgs obtained with a Q-ratio of 2.5 (RMS error of 6.7).

4.7 Drive-Over Tests

After a brief analysis of the magnetic data collected during the drive-over tests, it was determined that there was neither time nor money available to conduct the in-depth filtering and processing that was necessary to glean usable information from the collected data. However, the cursory analysis that was conducted indicated that the data were probably not of sufficient quality to provide much in the way of meaningful results. The background geology was considerably magnetic, and it had magnetic gradients on a spatial scale smaller than the spacing between the sensors on the data collection cart. This, coupled with some gaps in lateral coverage of the magnetometer data, made the likelihood of extracting usable information quite low.

Visual inspection of the ruts left by the three vehicles on the undisturbed ground during the drive-over tests indicated that the rut depths were 7 cm, 5 cm, and less than 1 cm, respectively, for the M1A1 tank, the HEMMET, and the Humvee (Figure 60).

Figure 60. Rut Left in Previously Undisturbed Area by M1A1 Tank After Four Passes

4.8 Pilot-Scale Rut Investigations

4.8.1 Anisotropy of Remanent Magnetism

The natural remanent magnetism for all of the samples collected from the pilot experiment unit and the control unit were very well defined. To determine whether there were any magnetic overprints, and to better characterize the geomagnetic field recorded by the sediment samples, a step-wise alternating field demagnetization was used. All samples had well-defined demagnetization results (Figure 61). For most, a steeply inclined overprint was removed between the NRM and 15 mT demagnetizations. Principal component analysis was used to determine the directions of the characteristic magnetization observed between 20 and 80 mT. These vector components were very well-defined and yielded site mean directions with very little scatter (Figure 62). The mean directions are very similar, and analyses of these directions, using a bootstrap re-sampling technique, indicates the two populations of data from the control and pilot sites are statistically indistinguishable.

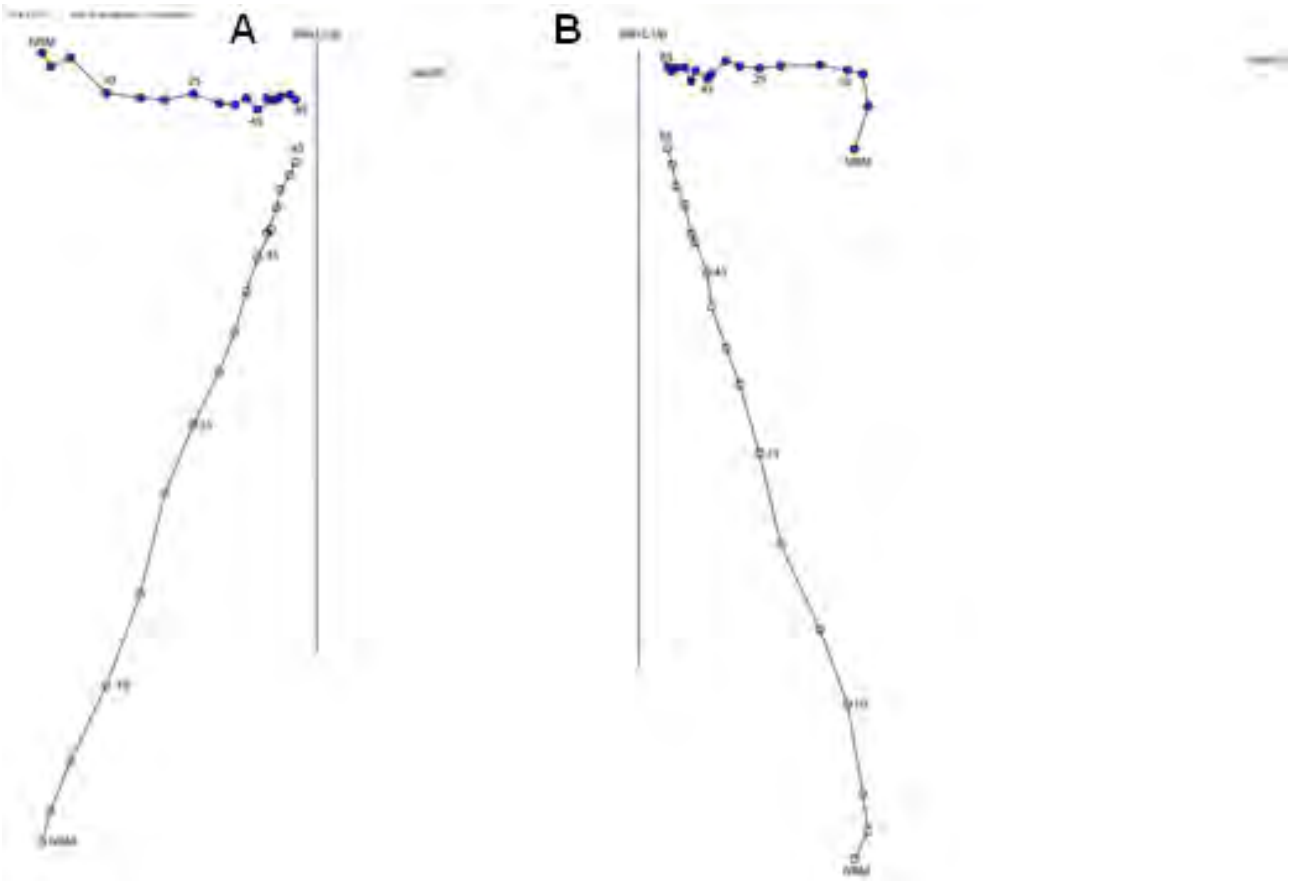

Figure 61. Demagnetization of a Control Unit Specimen (A) and a Pilot Experiment Unit Specimens (B)

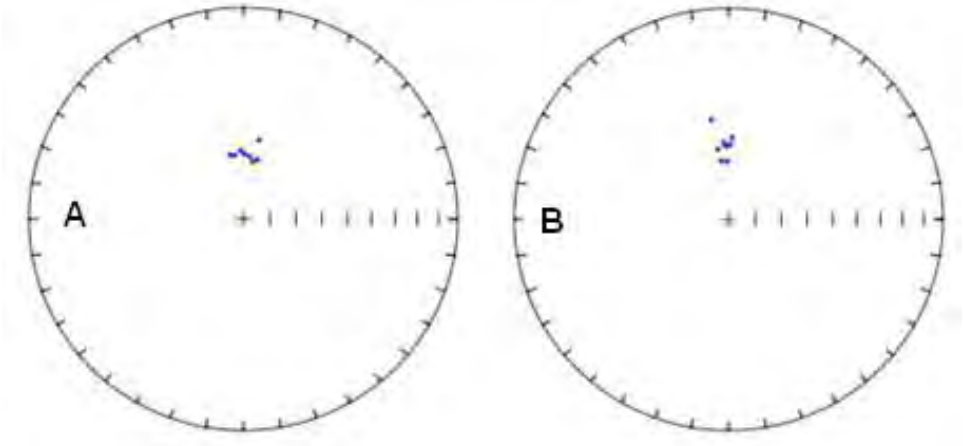

Figure 62. Direction of Magnetic Orientation Measured for Samples Collected from the Control Unit (A) and the Pilot Experiment Unit (B)

In addition, NRM normalized by susceptibility was compared; the results (Table 7) indicate that the samples from the two sites have very similar intensities. The overlap in distribution at 1 standard deviation suggests that the sites are not significantly different in normalized intensity.

Table 7. Natural Remanent Magnetism Normalized by Susceptibility for the Pilot and Control Units

Location	Norm. NRM	Location	Norm. NRM
Pilot-1	5.8E+04	CUI 1	4.7E+04
Pilot-2	3.0E+04	CUI 2	3.6E+04
Pilot-3	2.0E+04	CUI 3	3.6E+04
Pilot-4	5.3E+04	CUI 4	4.9E+04
Pilot-5	2.1E+04	CUI 5	4.1E+04
Pilot-6	3.6E+04	CUI 6	4.2E+04
Pilot-7	3.5E+04	CUI 7	4.3E+04
Pilot-8	4.4E+04	CUI 8	2.7E+04
MEAN	**3.7E+04**		**4.0E+04**
STD DEV	1.3E+04		6.5E+03

All of the samples had linear NRM vs. ARM relationships. The mean relative paleointensity for the control samples is 0.26 with a standard deviation of 0.04, and the mean relative paleointensity for the pilot samples is 0.29 with a standard deviation of 0.06. This indicates that the all of the samples were magnetized under very similar paleointensity conditions, and that the natural remanence for the two sites is essentially identical.

Taken as a whole, the conclusion is that both sites have very well-defined magnetizations, and that there are no significant differences between the magnetizations of the sediments of the control or pilot site both in terms of NRM intensity and directions. This is unexpected and could point to some secondary process (possibly the freeze-thaw cycle) that overprints any changes from sediment disturbance in a relatively short period of time. This could indicate there is a temporal limit to this type of investigation, helping to eliminate long-term soil processes as the cause of disturbance.

4.8.2 Anisotropy of Magnetic Susceptibility

The anisotropy of magnetic susceptibility was evaluated at the drive-over test site. Looking at the AMS orientations, the control site has AMS axes that are rather scattered, with k-min axes having a mean orientation that is approximately vertical. This would be very much in line with a natural sediment or soil (Figure 63). The tank-track site, however, has AMS axes that are very well clustered by comparison, and the k-min axis is offset from vertical. The other axes (k-int and k-max) are also clustered well, in contrast to the control site (Figure 63).

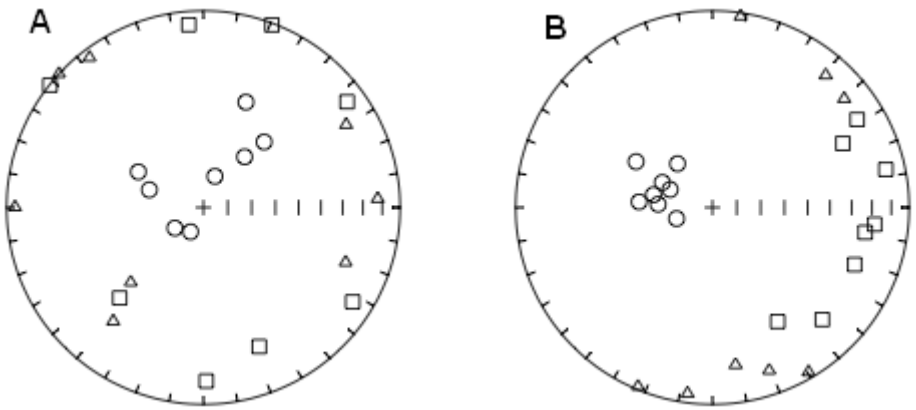

Figure 63. AMS Data for the Control (A) and Pilot (B) Locations

Looking at the AMS ellipsoid shapes, there is a very clear contrast. The control site samples, with two outliers, have low degrees of anisotropy, indicating a very weakly developed particle alignment. The tank-track samples are all much more highly anisotropic, with markedly oblate-shaped AMS fabrics (Figure 64). This is consistent with sediment compaction and consolidation.

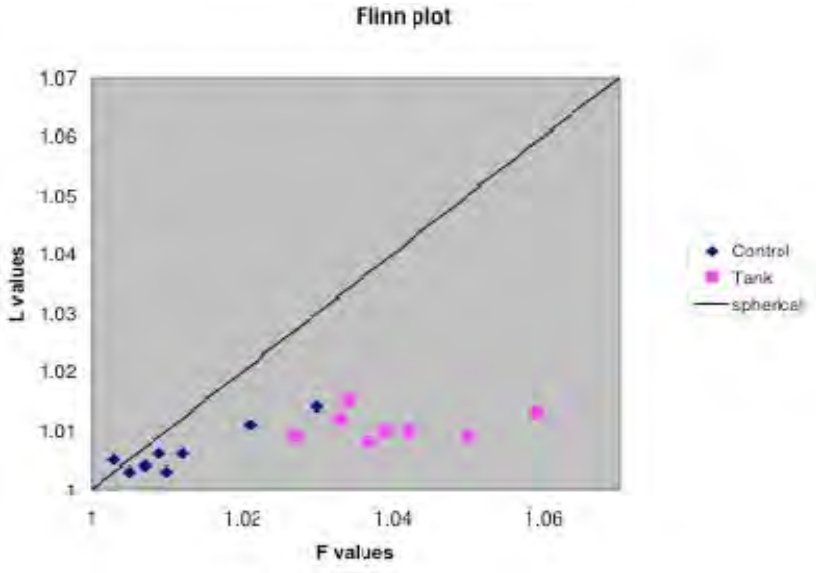

Figure 64. Flinn Plot Showing the Deviation from Spherical (Isotropic) with the Tank (Pilot) and Control Paleomagnetic Push Samples

It is also possible to extract some additional information from the AMS axes. In most sediment, the mineral alignment can provide information about the kinematics of the strain that produced the changes in alignment. The tank-track data suggest that the magnetic foliation is dipping towards the east; this imbrication suggests the tank was moving from east to west. Upon revisiting the sample orientations and drive-over map, it was confirmed that the tank was in fact moving toward the west. So not only was analysis of anisotropy of magnetic susceptibility able to identify soil impacted by vehicle movement, it was able provided an indication of which direction the vehicle was moving at the time of the impact.

5 Conclusions and Future Implementation

Overall, the objectives of this project were satisfied. Over the course of the project, the quantitative relationship between soil compaction and increasing magnetic susceptibility was verified, a geotechnical model of subsurface compaction under a vehicle rut was developed and evaluated, and various compaction and deformation measurement methods were developed and applied in both controlled and field settings. Taken together, the experiments conducted for this project provided a detailed evaluation of soil compaction that occurs under a vehicle rut. Here, we present a summary of the findings for all the experiments and a discussion of how these results are intertwined. Finally, we include a discussion of how the techniques and methods developed and applied by this research project could be used to reduce the time and cost necessary to conduct required site assessments of vehicle impacts on archaeological resources.

5.1 Summary of Results

The first experiment was a core compaction test that verified the relationship between bulk density and magnetic susceptibility. These results provided the basis for using magnetic susceptibility measurements to determine bulk density. They also provided confidence that a change in total magnetic field would occur when compaction occurred under a vehicle rut. The ability of the magnetometer to detect this change was verified by the proof-of-principle modeling exercise. This exercise demonstrated that the change in magnetic field caused by a vehicle rut would be much greater than the sensitivity of the magnetometer. The proof-of-principle testing implemented the geotechnical model to predict the amount and distribution of compaction that would occur under a vehicle rut. The development of the geotechnical model was important because it provided a tool for estimating the compaction profile under a rut based on standard civil engineering practices. Specifically, compaction was assumed to be proportional to stress curves under footings with static loading. The accuracy as well as shortcomings of the geotechnical model were demonstrated in later tests.

After completion of these initial exercises, hands-on testing began. The first series of tests involved the box tests; these experiments provided a detailed look at compaction within a controlled soil column of (nominally) uniform density and magnetic susceptibility. These experiments were used to refine the measurement techniques, to verify the geotechnical model, and to develop a better understanding of the depth and distance that a surface impact could propagate into to subsurface. Overall, the results of these experiments demonstrated that the cone penetrometer and down-hole volumetric magnetic susceptibility measurements could identify the depth and magnitude of compaction. Further, the results indicated that the geotechnical model also provided a good estimate of the compaction profile in homogeneous soil—both under and adjacent to the rut footprint.

After the success of the box tests, the same rut formation methodology and measurement techniques were applied in the field at the Yakima Training Center. These experiments indicated that the cone penetrometer and down-hole volumetric magnetic susceptibility measurement techniques were capable of identifying the depth and width of compaction under a rut. These techniques also proved capable of identifying changes in lithology. Unfortunately, these experiments also indicated that the geotechnical model was inaccurate in heterogeneous

sediment; the model did not have the functionality to account for the change in soil type limiting the depth of soil compaction. However, this functionality could likely be built in with future versions of the geotechnical model by incorporating a layered soil. Because the data showed that the compaction stopped at the depth where the geotechnical model predicted the compacted sediments to be lower in bulk density than the more compacted nature, a modification to the geotechnical model could include identifying the depth where compaction is limited, then recalculating the compaction profile to occur only over that finite depth interval. Finally, the results of the magnetometer measurements made as part of the field compaction experiments indicated that the change in the magnetic signature was easily identifiable.

Before magnetic modeling of the field compaction tests could begin, a remanence test had to be conducted. This test indicated that the soil at the Yakima Training Center had a strong remanence signature. This result was incorporated into the magnetic modeling of the field compaction tests. The modeling produced reasonable agreement with the measured magnetic signature of the rut, but it was done with a pre- and post-compaction measurement so that the magnetic signal resulting from compaction and rut formation were isolated. Real-world applications would not be able to conduct pre-compaction magnetic surveys.

Although the magnetic data collected as part of the drive-over tests were only evaluated at a cursory level due to time and budget constraints, the preliminary assessment is that the data were likely too noisy to be useful in determining the depth of compaction that resulted from vehicle rut formation. No estimate of the data quality with regard to quantifying impact on the replicated archaeological magnetic targets was made.

Although magnetometer surveys with subsequent modeling did not appear to be a viable option for identifying the depth of sediment compaction, analysis of the anisotropy of magnetic susceptibility did. The results of the pilot-scale tests indicated that AMS analysis of physical soil samples could readily identify soils that had been affected by a vehicle. Furthermore, the analysis was able to reveal which direction the vehicle was moving at the time of impact.

5.2 Future Application of Results

The overarching goal of this project was to develop and use methods to measure and assess the impacts of vehicles on buried archaeological deposits. Although this project was not able to apply any methods or tools to an actual archaeological assessment, the foundation has been laid for others to do so. The following is a discussion of how the methods used in this work might be implemented in a real-world setting to reduce the time and cost of conducting an archaeological assessment. This is presented as a theoretical site assessment where a military vehicle has driven over a known archaeological site.

An initial visit to the site would characterize the site for some key parameters; rut depth would be measured, soil samples from an undisturbed location would be collected for particle size distribution and bulk density analysis, and likely sites for future archaeological excavations would be selected. The results of these initial analyses would be used as input to the geotechnical model developed as part of this project. The results would provide an estimate of the depth and width of compaction. These estimates could be combined with records about the depth of cultural material at the site; if the predicted compaction is shallower than the shallowest

of known intact archaeological deposits, then a minimal field investigation would likely suffice to determine if there were any impacts on culturally sensitive materials. If the geotechnical model output indicates that compaction occurred at depths deeper than the cultural material, then a more rigorous site investigation will likely be warranted.

At this point, field activities would begin at the potentially impacted site. The geotechnical model would be used to guide the depth of investigation, and the comparison of the geotechnical model results with other archaeological records would be used to determine the number of excavations necessary. Prior to conducting any archaeological investigations, cone penetrometer, down-hole magnetic susceptibility, and bulk density measurements would be made to better quantify the depth of compaction and any lithologic changes over the interval of interest. These measurements would be made according to the methods presented in this report because they have, when used together, been demonstrated to be useful in delineating both lithologic changes and depth of compaction.

After the application of these minimally invasive characterization methods, archaeological excavation would begin. The excavation would be a 0.25-m^3 pit (Figure 65) excavated in 5-cm layers, with a portion of the pit under the rut footprint, and the rest outside of the rut footprint. Soil samples would be collected from the edges of the excavation unit and analyzed for AMR and AMS, as well as mass magnetic susceptibility. As indicated by the results in this report, AMS is capable of identifying changes in soil magnetic signature caused by vehicle impact, and AMR may yet prove similarly capable as well. Results of mass magnetic susceptibility measurements would be used to further identify lithologic changes that might limit compaction and enhance interpretation of the volumetric susceptibility measurements. Archaeological analysis would include lithic analysis, faunal analysis, organic matter float analysis, pottery analysis, phytolith analysis, and analysis of any other clast or material used in archaeological interpretation that could be physically altered by soil compaction.

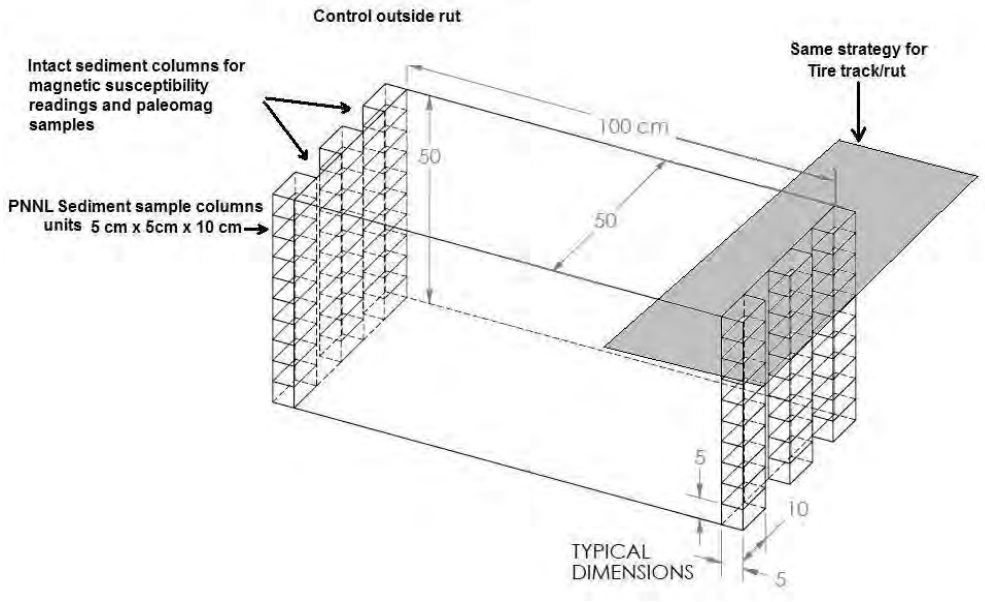

Figure 65. Schematic Detailing the Excavation Strategy for Field Assessments of Vehicle Impacts on Archaeological Resources

With this detailed characterization of the depth of vehicle impact, coupled with the archaeological findings of the excavation, a determination of adverse effect to archaeological resources could be made with relatively few excavations. Any differences in archaeological materials or sediment character would be compared with the results of the soil compaction evaluation (magnetic susceptibility, cone penetrometer, geotechnical model, AMS, AMR). This evaluation would provide information about the correlation between archaeological impacts and soil impacts. Future assessments could then use this correlation to make estimates about what type of archaeological information was likely to have been altered or destroyed by surface impacts.

The end result would be accomplishing required assessments of vehicle impacts on archaeological resources in less time and for less money. In addition, after a testing or training facility had conducted a number of these assessments while implementing the enhanced magnetic characterization techniques described in this report, sufficient data would likely exist to begin making predictions about what vehicle activities could result in an impact on archaeological resources. For example, if numerous site assessments indicated that when compaction depth did not exceed a depth of 50 cm there was no impact on archaeological materials, then the geotechnical model could be used to predict when compaction from vehicle activities would not exceed 50 cm. This would require the geotechnical model, or a modified version of it, to have been able to accurately predict the depth of compaction in previous assessments.

This project also lays a foundation for developing the capability to predict when activities would result in impacts on archaeological materials. In the peer-reviewed literature there are existing models that can predict rut depth for military vehicles under varying soil conditions (soil type, soil moisture, etc.). These models could be used to estimate vehicle rut depths. These data would serve as input to the geotechnical model, allowing site operations managers to make decisions about when it would or would not be acceptable to allow military vehicles to drive-over areas with known or suspected archaeological materials, and what type of archaeological materials would be impacted if it occurred.

6 References

Abbott JT and CD Frederick. 1990. "Proton Magnetometer Investigations of Burned Rock Middens in West-Central Texas: Clues to Formation Processes." *Journal of Archaeological Science* 17:535–545.

ASTM International. 2007. "Standard Test Methods for Laboratory Compaction Characteristics of Soil Using Standard Effort (12 400 ft-lbf/ft^3 (600 kN-m/m^3))." ASTM D 698-07, ASTM International, West Conshohocken, Pennsylvania.

Butler RF. 1992. *PALEOMAGNETISM: Magnetic Domains to Geologic Terranes.* Blackwell Scientific Publications, Oxford, UK.

Dalan RA. 2006. "Magnetic Susceptibility." In JK Johnson (ed), *Remote Sensing in Archaeology* (pp. 161–203). The University of Alabama Press, Tuscaloosa.

Dearing GA, RJL Dann, K Hay, JA Lees, PJ Loveland, BA Maher, and K O'Grady. 1996. "Frequency-dependent susceptibility measurements of environmental materials." *Geophysical Journal International* 224:228–240.

Foss C. 2003. Resolution of depth-extent in modelling magnetic anomalies over shallow sources in rugged terrain. Extended Abstract, ASEG 16th Geophysical Conference and Exhibition, Adelaide, Australia. Available online at http://web2.encom.com.au/pdfs/Resolution%20of%20depth%20extent.pdf

Foss C and B McKenzie. 2006. *Inversion of anomalies due to remanent magnetization – an example from the Black Hill Norite of South Australia.* AESC2006, Melbourne, Australia. Available online at http://web2.encom.com.au/pdfs/Inversion%20of%20anomalies%20due%20to%20remanent%20magnetization.pdf

Holtz RD and WD Kovacs. 1981. *An Introduction to Geotechnical Engineering*. Prentice-Hall, New Jersey.

Lagroix F and SK Banerjee. 2004. "The regional and temporal significance of primary aeolian magnetic fabrics preserved in Alaskan loess." *Earth and Planetary Science Letters* 225:379–395.

Little B, EM Seibert, J Townsend, JH Sprinkle Jr., and J Knoerl. 2000. "Guidelines for Evaluating and Documenting Archaeological Properties." National Register Bulletin (NRB36), U.S. Department of the Interior, National Park Service, Washington, D.C.

Maier G, R Scholger, and J Schön. 2006. "The influence of soil moisture on magnetic susceptibility measurements." *Journal of Applied Geophysics* 59:162–175.

Marwick B. 2005. "Element concentrations and magnetic susceptibility of anthrosols: Indicators of prehistoric human occupation in the inland Pilbara, Western Australia." *Journal of Archaeological Science* 32:1357–1368.

Mathé V, F Lévêque, P Mathé, C Chevallier, and Y Pons. 2006. "Soil anomaly mapping using a cesium magnetometer: Limits in the low magnetic amplitude case." *Journal of Applied Geophysics.* 58:202–217.

Mathé V and F Lévêque. 2003. "High resolution magnetic survey for soil monitoring: detection of drainage and soil tillage effects." *Earth and Planetary Science Letters* 212:241–251.

McPherron SJP, HL Dibble, and P Goldberg. 2005. "Z." *Geoarchaeology* 20:243–262.

NAVFAC. 1986. *Soils And Foundations Design Manuals*. Naval Facilities Engineering Command, Alexandria, Virginia. Available online at http://web.mst.edu/~rogersda/umrcourses/ge441/dm7_01.pdf

Nickens PR. 1991. "The destruction of archaeological sites and data." In Smith GS and JE Ehrenhard (eds.), *Protecting the Past* (pp. 73-81), CRC Press, Boca Raton, Florida.

Parkes PA. 1986. *Current Scientific Techniques in Archaeology*. St. Martin's Press, New York.

Somers LE, ML Hargrave, and JE Simms. 2003. *Geophysical Surveys in Archaeology: Guidance for Surveyors and Sponsors*. SR-03-21, Geotechnical and Structures Laboratory, Vicksburg, Mississippi. Available online at http://www.cecer.army.mil/techreports/hargrave_atags/hargrave_atags.pdf

Tauxe L, T Pick, and YS Kok. 1995. "Relative paleointensity in sediments: A pseudo-Thellier approach." *Geophysical Research Letters* 22:2885–2888.

Tauxe L. 1998. *Paleomagnetic Principles and Practice*. Dordrecht, Kluwer Academic Publishers, Norwell, Maine.

Tauxe L, JL Steindorf, and A Harris. 2006. Depositional remnant magnetization: Toward an improved theoretical and experimental foundation. *Earth and Planetary Science Letters* 244:515–529.

Appendix A

Magnetic Terms and Description

Appendix A

Magnetic Terms and Descriptions

Particle size, location, and disturbance are important to these processes as well. In the case of magnetite-bearing sediments, anisotropy of magnetic remanence (AMS) is dominated by multidomain grains (> 110 microns) while single-domain (< 0.2 microns) and pseudosingle-domain grains (0.2–110 microns) are the paleomagnetic recorders.

All sedimentary and soil environments have a number of natural processes that create a directional natural remanent magnetism (NRM).

Detrital remanent magnetism: This requires enough moisture for rotation of the magnetic particles in the sediment matrix to align with the present geomagnetic field. This type of remanent magnetism is locked in by the dewatering of the sediment matrix.

Chemical remanent magnetism: This type of remanent magnetism occurs when iron oxides change from one form to another or are created biogenically. Usually it is associated with the crystallization of the new iron oxide crystals. There is short-term (young iron oxides) and long-term (iron oxides that have already been through much weathering) chemical remanent magnetism.

Viscous remanent magnetism: This type of remanent magnetism is the result of stationary iron oxide crystals that are exposed to weak magnetic fields (such as the geomagnetic field) over long periods of time.

Direction of AMS is the result of physical depositional and post-depositional processes (including detrital remanent orientation). Natural processes such as wind, tide, and current directions can create a primary AMS, while processes such as freeze-thaw, pedogenesis, and bioturbation can create a secondary overprint.

Mass magnetic susceptibility: The magnetic susceptibility of the individual soil particles. This value is independent of the bulk density and is strictly a function of the mineralogy of the soil particles.

Volumetric magnetic susceptibility: The magnetic susceptibility of a volume of soil. This value is a function of the bulk density (see Eq. 1). If more particles are squeezed into a unit volume, then the total magnetic susceptibility of that volume increases because there are more magnetically susceptible particle within the volume.

Appendix B

Raw Data Tables

Appendix B

Raw Data Tables

Section 4.1 – Core Compaction Test

Wet Bulk Density (g/cc)	Soil column Length (in)	Measured Vol. Sus. (CGS)	Calculated Vol. Sus. (CGS)	% diff
2.51	11.25	413	436.17	5.5%
2.69	10.5	465	467.33	0.5%
2.86	9.875	486	496.91	2.2%
3.05	9.25	522.1	530.48	1.6%
3.13	9	538.6	545.22	1.2%
2.51	11.25	396.7	436.17	9.5%
2.69	10.5	452.1	467.33	3.3%
2.86	9.875	484	496.91	2.6%
3.05	9.25	517	530.48	2.6%
3.13	9	539	545.22	1.1%
2.51	11.25	412	436.17	5.7%
2.69	10.5	465	467.33	0.5%
2.86	9.875	484.5	496.91	2.5%
3.05	9.25	522.5	530.48	1.5%
3.13	9	540	545.22	1.0%
2.51	11.25	396.6	436.17	9.5%
2.69	10.5	452.6	467.33	3.2%
2.86	9.875	484.4	496.91	2.5%
3.05	9.25	518.6	530.48	2.3%
3.13	9	538	545.22	1.3%
2.51	11.25	413	436.17	5.5%
2.69	10.5	464.5	467.33	0.6%
2.86	9.875	485.5	496.91	2.3%
3.05	9.25	522	530.48	1.6%
3.13	9	540.6	545.22	0.9%
2.51	11.25	397	436.17	9.4%
2.69	10.5	451.6	467.33	3.4%
2.86	9.875	484	496.91	2.6%
3.05	9.25	517.6	530.48	2.5%
3.13	9	538	545.22	1.3%
2.51	11.25	413	436.17	5.5%
2.69	10.5	464.6	467.33	0.6%
2.86	9.875	485	496.91	2.4%
3.05	9.25	522.1	530.48	1.6%
3.13	9	538.6	545.22	1.2%
2.51	11.25	397.4	436.17	9.3%
2.69	10.5	453	467.33	3.1%
2.86	9.875	484	496.91	2.6%
3.05	9.25	510	530.48	3.9%

Wet Bulk Density (g/cc)	Soil column Length (in)	Measured Vol. Sus. (CGS)	Calculated Vol. Sus. (CGS)	% diff
3.13	9	538	545.22	1.3%
2.51	11.25	411.5	436.17	5.8%
2.69	10.5	464.1	467.33	0.7%
2.86	9.875	485	496.91	2.4%
3.05	9.25	522.5	530.48	1.5%
3.13	9	539.6	545.22	1.0%
2.51	11.25	398	436.17	9.2%
2.69	10.5	453.5	467.33	3.0%
2.86	9.875	483	496.91	2.8%
3.05	9.25	516.5	530.48	2.7%
3.13	9	537	545.22	1.5%

Section 4.4.1 – Box Test 1

Soil Moisture and Bulk Density Raw Data Box Test 1

Location	Tare wt (g)	wet wt + Container (g)	dry wt + Container (g)	Soil Moisture %	Volume (cm^3)	Mass Samp. wet (g)	Mass Samp. dry (g)	Depth to Center (cm)	Bulk Density (g/cc)
4" pipe (3.875"ID) undisturbed	68.74	337.95	315.71	9.0%	2319.32	3341.1	3065.14	15.24	1.32
Clear PVC (3.5"ID) undisturbed	41.54	235.8	219.23	9.3%	1340.13	2008.3	1837.15	41.28	1.37
compaction footprint 3/4" pvc	68.87	220.28	207.3	9.4%	68.60	151.41	138.43	18.42	2.02
compaction footprint 3/4" pvc	68.54	216.32	202.93	10.0%	91.02	147.78	134.39	37.62	1.48
compaction footprint 3/4" pvc	68.72	172.94	163.46	10.0%	67.28	104.22	94.74	56.67	1.41
compaction footprint 3/4" pvc	41.55	162.32	151.8	9.5%	75.98	120.77	110.25	73.91	1.45
east hole 3/4"pvc	68.45	162.78	155.25	8.7%	68.60	94.33	86.8	8.26	1.27
east hole 3/4"pvc	41.55	137.39	129.17	9.4%	59.36	95.84	87.62	23.65	1.48
east hole 3/4"pvc	68.42	183.89	173.89	9.5%	72.55	115.47	105.47	39.53	1.45
east hole 3/4"pvc	68.72	150.62	143.63	9.3%	58.04	81.9	74.91	55.25	1.29
east hole 3/4"pvc	68.89	187.9	177.58	9.5%	84.42	119.01	108.69	72.39	1.29

Raw Down-Hole Volumetric Magnetic Susceptibility Measurements Box Test 1

Compaction Footprint			
x (cm)	y (cm)	z (cm)	Mag. Sus. (SI) $x10^{-5}$
45.7	36	20	257.3
45.7	36	22	275.7
45.7	36	24	285.0
45.7	36	26	286.7
45.7	36	28	281.3
45.7	36	30	281.7
45.7	36	32	278.3
45.7	36	34	278.0
45.7	36	36	272.0
45.7	36	38	253.7
45.7	36	40	247.7
45.7	36	42	252.0
45.7	36	44	258.7
45.7	36	46	259.7
45.7	36	48	256.0
45.7	36	50	247.0
45.7	36	52	241.3
45.7	36	54	237.7
45.7	36	56	230.7
45.7	36	58	227.7
45.7	36	60	232.7
45.7	36	62	247.0
45.7	36	64	248.0
45.7	36	66	248.7
45.7	36	68	246.0
45.7	36	70	241.0
45.7	36	72	236.3
45.7	36	74	231.3
45.7	36	76	228.3
45.7	36	78	228.7

West Hole (post compaction)			
x (cm)	y (cm)	z (cm)	Mag. Sus. (SI) $x10^{-5}$
83	46	6	162.5
83	46	8	138.0
83	46	10	160.5
83	46	12	182.0
83	46	14	201.0
83	46	16	213.5
83	46	18	234.5
83	46	20	260.5
83	46	22	272.5
83	46	24	266.5
83	46	26	263.0
83	46	28	257.5
83	46	30	247.5
83	46	32	242.0
83	46	34	237.0
83	46	36	251.5
83	46	38	249.0
83	46	40	254.5
83	46	42	251.0
83	46	44	243.5
83	46	46	252.5
83	46	48	239.5
83	46	50	238.0
83	46	52	236.5
83	46	54	236.5
83	46	56	225.5
83	46	58	229.0
83	46	60	230.0
83	46	62	222.5
83	46	64	223.0
83	46	66	216.5
83	46	68	211.5
83	46	70	206.0
83	46	72	198.5
83	46	74	194.0
83	46	76	197.0

East Hole (post compaction)			
x (cm)	y (cm)	z (cm)	Mag. Sus. (SI) $x10^{-5}$
5	30	6	198.7
5	30	8	184.3
5	30	10	180.0
5	30	12	173.7
5	30	14	198.7
5	30	16	221.3
5	30	18	222.3
5	30	20	236.3
5	30	22	268.7
5	30	24	276.0
5	30	26	271.0
5	30	28	272.3
5	30	30	275.3
5	30	32	267.0
5	30	34	258.3
5	30	36	253.0
5	30	38	255.0
5	30	40	257.3
5	30	42	251.3
5	30	44	251.3
5	30	46	257.7
5	30	48	265.0
5	30	50	254.7
5	30	52	252.3
5	30	54	246.3
5	30	56	232.3
5	30	58	231.3
5	30	60	243.0
5	30	62	245.7
5	30	64	245.0
5	30	66	237.0
5	30	68	235.7
5	30	70	232.3
5	30	72	233.3
5	30	74	229.7
5	30	76	230.7
5	30	78	227.0

Raw Cone Penetrometer Results Box Test 1. Units are pounds of resistance per square inch.

Position		z (cm)->																		
x (cm)	y (cm)	0.0	2.5	5.1	7.6	10.2	12.7	15.2	17.8	20.3	22.9	25.4	27.9	30.5	33.0	35.6	38.1	40.6	43.2	45.7
40.6	81.3	36	158	219	193	188	214	239	219	382	443	382	341	310	300	422	433	392	351	331
40.6	73.7	56	87	143	173	183	224	275	310	555	575	504	422	377	341	336	412	494	433	392
50.8	81.3	87	188	219	193	178	183	178	178	489	499	366	300	275	285	478	448	377		
50.8	73.7	143	148	199	214	229	244	239	351	641	636	504	453	372	346	351	545	519		
81.3	45.7	76	127	148	168	168	173	244	244	260	412	514	468	382	285	285	326	331	295	290
71.1	45.7	15	46	97	127	137	163	224	275	585	540	478	417	377	351	361	412	443	387	346
10.1	45.7	61	163	209	199	193	193	209	183											
20.3	45.7	87	137	183	188	188	214	239	234	545	494	392	366	331	336	346	428	397	351	346
81.3	10.1	87	143	178	183	183	199	229	193	219	438	463	377	321	265	234	285	280	249	229
10.1	81.3	127	168	199	183	183	224	214	188	402	540	428	346	341	392	463				
50.8	25.4	41	46	81	143	193	275	331	326	438	585	646	555	443	397	382	382	524	514	
40.6	25.4		20	41	137	265	433	529	519	611	743	672	555	478	433	397	382	468	478	417
61	45.7		5	20	76	178	402	229	570	677	835	697	555	448	412	377	351	412	499	402
30.5	45.7	20	36	66	143	239	346	478	494	545	809	524	713	585	504	448	443	672		
40.6	50.8					97	341	590	789	748	830	631	825	692	580	529	468	377		
50.8	50.8					41	193	468	585	641	626	672	738	860	692	534	478			
50.8	45.7					15	122	341	743	804	657	534	723	682	580	540	489	478		
40.6	45.7					31	46	148	540	825	957	621	814	646	708	636	550	534	519	534

Geotechnical Model Output Box Test 1

b =	25	cm			
max den	2.00				
in situ den	1.4				
delta (del)	0.6				
rut depth	10	cm			
	Square Surface Contact				
adjusted z	**z**	**Den (ctr)**	**Den (b/2)**	**Den (b)**	
11.3	1.3	2.00	2.00	1.40	
12.8	1.6	2.00	1.97	1.40	
13.3	2.1	2.00	1.93	1.40	
13.8	2.5	2.00	1.90	1.40	
14.4	3.1	1.99	1.86	1.40	
15.4	4.2	1.99	1.83	1.40	
16.3	5.0	1.98	1.79	1.41	
17.5	6.3	1.96	1.76	1.41	
18.2	6.9	1.95	1.74	1.41	
19.1	7.8	1.93	1.71	1.41	
20.2	8.9	1.90	1.69	1.42	
21.7	10.4	1.87	1.66	1.42	
23.8	12.5	1.82	1.64	1.42	
25.1	13.9	1.79	1.62	1.43	
26.9	15.6	1.75	1.60	1.43	
29.1	17.9	1.71	1.59	1.44	
32.1	20.8	1.66	1.57	1.44	
36.3	25.0	1.60	1.55	1.45	
42.5	31.3	1.54	1.51	1.45	
52.9	41.7	1.49	1.49	1.45	
73.8	62.5	1.44	1.44	1.43	
136.3	125.0	1.41	1.41	1.41	

Section 4.4.2 – Box Test 2

Soil Moisture and Bulk Density Box Test 2

Location	Tare wt (g)	wet wt + Container (g)	dry wt + Container (g)	Soil Moisture %	Volume (cm^3)	Mass Samp. wet (g)	Mass Samp. dry (g)	Depth to Center (cm)	Bulk Denisty (g/cc)
east hole (EH)	44.52	138.99	127.74	13.5%	69.91	94.47	83.22	8.41	1.19
east hole (EH)	44.27	153.57	139.89	14.3%	73.87	109.3	95.62	25.72	1.29
east hole (EH)	44.04	155.81	141.4	14.8%	83.11	111.77	97.36	44.61	1.17
east hole (EH)	44.23	169.71	152.73	15.6%	88.38	125.48	108.5	65.25	1.23
west hole (WH)	44.51	143.27	131.44	13.6%	63.32	98.76	86.93	7.62	1.37
west hole (WH)	44.71	146.75	133.86	14.5%	63.32	102.04	89.15	22.86	1.41
west hole (WH)	44.68	126.94	116.15	15.1%	64.64	82.26	71.47	38.26	1.11
west hole (WH)	44.63	130.33	118.63	15.8%	62.00	85.7	74	53.50	1.19
west hole (WH)	44.48	188.53	168.58	16.1%	94.98	144.05	124.1	72.39	1.31
EH2 Post Compaction	44.76	133.59	123.29	13.1%	63.32	88.83	78.53	7.62	1.24
EH2 Post Compaction	68.9	175.64	162.45	14.1%	63.32	106.74	93.55	22.86	1.48
EH2 Post Compaction	68.55	160.84	148.69	15.2%	63.32	92.29	80.14	53.34	1.27
EH2 Post Compaction	68.74	189.8	173.45	15.6%	84.42	121.06	104.71	71.12	1.24
compaction (C)	44.51	96.87	90.51	13.8%	23.74	52.36	46	18.10	1.94
compaction (C)	44.52	123.45	113.26	14.8%	39.57	78.93	68.74	25.72	1.74
compaction (C)	44.74	146.42	132.73	15.6%	63.32	101.68	87.99	38.10	1.39
compaction (C)	44.72	146.34	132.12	16.3%	63.32	101.62	87.4	53.34	1.38
compaction (C)	68.76	184.29	167.86	16.6%	63.32	115.53	99.1	68.58	1.57

Raw Down-Hole Magnetic Susceptibility Measurements Box Test 2

Compaction Footprint			
x (cm)	y (cm)	z (cm)	Mag. Sus. (SI) $x10^{-5}$
45.7	33.02	18	227
45.7	33.02	20	233
45.7	33.02	22	304
45.7	33.02	24	299
45.7	33.02	26	291
45.7	33.02	28	287
45.7	33.02	30	280
45.7	33.02	32	272
45.7	33.02	34	270
45.7	33.02	36	290
45.7	33.02	38	297
45.7	33.02	40	285
45.7	33.02	42	280
45.7	33.02	44	278
45.7	33.02	46	267
45.7	33.02	48	266
45.7	33.02	50	275
45.7	33.02	52	264
45.7	33.02	54	272
45.7	33.02	56	272
45.7	33.02	58	264
45.7	33.02	60	267
45.7	33.02	62	281
45.7	33.02	64	293
45.7	33.02	66	299
45.7	33.02	68	284
45.7	33.02	70	282
45.7	33.02	72	285
45.7	33.02	74	283
45.7	33.02	76	282
45.7	33.02	78	291

West Hole			
x (cm)	y (cm)	z (cm)	Mag. Sus. (SI) $x10^{-5}$
73.66	46.99	4	240
73.66	46.99	6	240
73.66	46.99	8	239
73.66	46.99	10	245
73.66	46.99	12	251
73.66	46.99	14	254
73.66	46.99	16	252
73.66	46.99	18	240
73.66	46.99	20	245
73.66	46.99	22	256
73.66	46.99	24	250
73.66	46.99	26	245
73.66	46.99	28	249
73.66	46.99	30	254
73.66	46.99	32	264
73.66	46.99	34	254
73.66	46.99	36	243
73.66	46.99	38	247
73.66	46.99	40	244
73.66	46.99	42	244
73.66	46.99	44	223
73.66	46.99	46	229
73.66	46.99	48	224
73.66	46.99	50	228
73.66	46.99	52	231
73.66	46.99	54	230
73.66	46.99	56	243
73.66	46.99	58	240
73.66	46.99	60	252
73.66	46.99	62	253
73.66	46.99	64	255
73.66	46.99	66	272
73.66	46.99	68	292
73.66	46.99	70	281
73.66	46.99	72	276
73.66	46.99	74	271
73.66	46.99	76	273
73.66	46.99	78	274

East Hole			
x (cm)	y (cm)	z (cm)	Mag. Sus. (SI) $x10^{-5}$
13.3	34.3	4	198
13.3	34.3	6	210
13.3	34.3	8	209
13.3	34.3	10	208
13.3	34.3	12	228
13.3	34.3	14	235
13.3	34.3	16	228
13.3	34.3	18	215
13.3	34.3	20	197
13.3	34.3	22	213
13.3	34.3	24	209
13.3	34.3	26	201
13.3	34.3	28	196
13.3	34.3	30	192
13.3	34.3	32	216
13.3	34.3	34	212
13.3	34.3	36	211
13.3	34.3	38	209
13.3	34.3	40	194
13.3	34.3	42	196
13.3	34.3	44	196
13.3	34.3	46	192
13.3	34.3	48	197
13.3	34.3	50	193
13.3	34.3	52	199
13.3	34.3	54	197
13.3	34.3	56	206
13.3	34.3	58	203
13.3	34.3	60	198
13.3	34.3	62	201
13.3	34.3	64	226
13.3	34.3	66	227
13.3	34.3	68	238
13.3	34.3	70	245
13.3	34.3	72	250
13.3	34.3	74	248
13.3	34.3	76	258
13.3	34.3	78	255

Geotechnical Model Output Box Test 2

b =	30	cm		
max den	1.90			
in situ den	1.25			
delta (del)	0.65			
rut depth	14.8	cm		
	Square Surface Contact			
adjusted z	**z**	**Den (ctr)**	**Den (b/2)**	**Den (b)**
16.3	1.5	1.90	1.90	1.25
18.2	1.9	1.90	1.86	1.25
18.8	2.5	1.90	1.83	1.25
19.3	3.0	1.90	1.79	1.25
20.1	3.8	1.89	1.75	1.25
21.3	5.0	1.88	1.71	1.25
22.3	6.0	1.87	1.68	1.26
23.8	7.5	1.85	1.64	1.26
24.6	8.3	1.84	1.61	1.26
25.7	9.4	1.82	1.59	1.26
27.0	10.7	1.80	1.56	1.27
28.8	12.5	1.76	1.54	1.27
31.3	15.0	1.71	1.51	1.28
33.0	16.7	1.67	1.49	1.28
35.1	18.8	1.63	1.47	1.29
37.7	21.4	1.58	1.45	1.29
41.3	25.0	1.53	1.43	1.30
46.3	30.0	1.47	1.41	1.30
53.8	37.5	1.41	1.37	1.30
66.3	50.0	1.35	1.35	1.30
91.3	75.0	1.30	1.30	1.29
166.3	150.0	1.26	1.26	1.26

Raw Cone Penetrometer Data Box Test 2

		z (cm) ==>																	
x (cm)	y (cm)	0.0	2.5	5.1	7.6	10.2	12.7	15.2	17.8	20.3	22.9	25.4	27.9	30.5	33.0	35.6	38.1	40.6	43.2	45.7
32.385	78.1	61	87	81	76	71	92	92	92	87	87	81	76	76	81	76	76	97	117	122
38.735	78.1	41	76	76	71	61	66	81	97	87	92	97	87	76	76	81	76	71	76	87
45.72	78.1	56	76	76	71	66	76	81	76	76	117	112	97	81	81	76	76	76	76	81
55.88	78.1	46	87	76	71	81	92	92	87	107	112	92	87	81	81	87	81	87	87	92
67.31	78.1	97	127	107	87	92	112	107	97	112	127	107	76	66	71	81	76	56	61	92
73.66	78.1	56	107	122	112	107	127	132	112	97	87	87	81	71	76	66	76	71	107	81
18.415	68.58	31	76	76	76	76	81	87	107	107	97	92	81	71	71	66	66	61	66	66
73.66	68.58	112	132	127	92	117	81	112	112	97	97	97	87	81	87	76	81	76	81	117
19.05	54.61				66	66	66	81	92	87	81	127	122	117	112	107	97	92	81	87
73.66	54.61				87	76	81	112	122	127	122	97	97	92	97	87	81			
19.05	30.48				81	87	92	76	71	122	112	97	97	87	87	87	81	81	76	81
73.66	30.48	25	137	122	112	97	112	122	127	127	122	117	117	107	97	92	81	87	92	112
77.47	30.48				117	107	97	107	112	97	87	112	143	137	143	92	97	92	97	122
26.67	73.66	56	76	81	81	81	97	97	92	137	127	127	117	107	97	97	97	87	97	117
45.72	73.66	61	92	87	76	81	112	117	107	117	107	107	97	97	92	87	81	81	87	92
55.88	73.66	41	76	76	81	81	107	107	112	107	107	97	97	92	92	81	81	87	81	81

Deflection of Purple Dyed Layers Box Test 2

x (cm)	y (cm)	z pre comp (cm)	Deflection	z post comp (cm)
0	45.72	10.2	0	10.2
12.7	45.72	10.2	0	10.2
19.1	45.72	10.2	0	10.2
25.5	45.72	10.2	1.9	12.1
31.8	45.72	10.2	11.4	21.6
38.2	45.72	10.2	12	22.2
43.22	45.72	10.2	12.7	22.9
48.3	45.72	10.2	12.7	22.9
54.7	45.72	10.2	12.7	22.9
61	45.72	10.2	10.8	21
67.5	45.72	10.2	0	10.2
73.7	45.72	10.2	0	10.2
91.4	45.72	10.2	0	10.2
0	45.72	20.3	0	20.3
12.7	45.72	20.3	0	20.3
19.1	45.72	20.3	1.3	21.6
25.5	45.72	20.3	4.4	24.7
31.8	45.72	20.3	6.8	27.1
38.2	45.72	20.3	8.3	28.6
43.22	45.72	20.3	9.5	29.8
48.3	45.72	20.3	8.9	29.4
54.7	45.72	20.3	7.6	27.9
61	45.72	20.3	5.7	26
67.5	45.72	20.3	2.5	22.8
73.7	45.72	20.3	0	20.3
91.4	45.72	20.3	0	20.3
0	45.72	40.6	0	40.6
12.7	45.72	40.6	0	40.6
19.1	45.72	40.6	0.6	41.2
25.5	45.72	40.6	1.5	42.1
31.8	45.72	40.6	2.5	43.1
38.2	45.72	40.6	3.2	43.8
43.22	45.72	40.6	3.8	44.4
48.3	45.72	40.6	3.8	44.4
54.7	45.72	40.6	3.6	44.2
61	45.72	40.6	2.5	43.1
67.5	45.72	40.6	1.3	41.9
73.7	45.72	40.6	0	40.6
91.4	45.72	40.6	0	40.6

x (cm)	y (cm)	z pre comp (cm)	Deflection	z post comp (cm)
0	45.72	61	0	61
12.7	45.72	61	0.5	61.5
19.1	45.72	61	1	62
25.5	45.72	61	1.2	62.2
31.8	45.72	61	1.3	62.3
38.2	45.72	61	1.5	62.5
43.22	45.72	61	1.8	62.8
48.3	45.72	61	1.5	62.5
54.7	45.72	61	1.3	62.3
61	45.72	61	1	62
67.5	45.72	61	0.6	61.6
73.7	45.72	61	0	61
91.4	45.72	61	0	61

Section 4.4.3 – Box Test 3

Raw Down-Hole Magnetic Susceptibility Measurements Box Test 3

Compaction Footprint			
x (cm)	y (cm)	z (cm)	Mag. Sus. (SI) $x10^{-5}$
51	36	26	252
51	36	28	283
51	36	30	293
51	36	32	297
51	36	34	294
51	36	36	283
51	36	38	290
51	36	40	299
51	36	42	283
51	36	44	269
51	36	46	258
51	36	48	277
51	36	50	285
51	36	52	260
51	36	54	258
51	36	56	284
51	36	58	267
51	36	60	257
51	36	62	263
51	36	64	269
51	36	66	276
51	36	68	254
51	36	70	273
51	36	72	273
51	36	74	264
51	36	76	254
51	36	78	251
51	36	80	253

West Hole			
x (cm)	y (cm)	z (cm)	Mag. Sus. (SI) $x10^{-5}$
71	46	8	165
71	46	10	187
71	46	12	213
71	46	14	216
71	46	16	241
71	46	18	254
71	46	20	262
71	46	22	235
71	46	24	231
71	46	26	247
71	46	28	263
71	46	30	266
71	46	32	266
71	46	34	266
71	46	36	265
71	46	38	263
71	46	40	259
71	46	42	256
71	46	44	263
71	46	46	270
71	46	48	264
71	46	50	258
71	46	52	251
71	46	54	249
71	46	56	246
71	46	58	235
71	46	60	245
71	46	62	251
71	46	64	273
71	46	66	276
71	46	68	276
71	46	70	266
71	46	72	270
71	46	74	272
71	46	76	266
71	46	78	264
71	46	80	289
71	46	81	279

East Hole			
x (cm)	y (cm)	z (cm)	Mag. Sus. (SI) $x10^{-5}$
12	27	4	177
12	27	6	177
12	27	8	180
12	27	10	189
12	27	12	183
12	27	14	182
12	27	16	180
12	27	18	183
12	27	20	191
12	27	22	197
12	27	24	226
12	27	26	230
12	27	28	223
12	27	30	238
12	27	32	243
12	27	34	246
12	27	36	236
12	27	38	231
12	27	40	244
12	27	42	253
12	27	44	248
12	27	46	245
12	27	48	250
12	27	50	239
12	27	52	238
12	27	54	229
12	27	56	214
12	27	58	224
12	27	60	231
12	27	62	230
12	27	64	251
12	27	66	256
12	27	68	257
12	27	70	256
12	27	72	250
12	27	74	239
12	27	76	241
12	27	78	236
12	27	80	228

Geotechnical Model Output Box Test 3

b =	30	cm						
max den	2.00							
in situ den	1.4							
delta (del)	0.6							
rut depth	20	cm						
	Square Surface Contact				**Infinite Strip Surface Contact**			
adjusted z	**z**	**Den (ctr)**	**Den (b/2)**	**Den (b)**	**z**	**Den (ctr)**	**Den (b/2)**	**Den (b)**
21.5	1.5	2.00	2.00	1.40	0.3	2.00	2.00	1.40
23.4	1.9	2.00	1.97	1.40	3.0	2.00	1.98	1.41
24.0	2.5	2.00	1.93	1.40	3.3	2.00	1.95	1.41
24.5	3.0	2.00	1.90	1.40	3.8	2.00	1.93	1.41
25.3	3.8	1.99	1.86	1.40	4.3	1.99	1.90	1.41
26.5	5.0	1.99	1.83	1.40	4.6	1.99	1.88	1.41
27.5	6.0	1.98	1.79	1.41	5.0	1.99	1.86	1.42
29.0	7.5	1.96	1.76	1.41	5.5	1.99	1.83	1.42
29.8	8.3	1.95	1.74	1.41	6.0	1.99	1.81	1.42
30.9	9.4	1.93	1.71	1.41	6.7	1.98	1.78	1.42
32.2	10.7	1.90	1.69	1.42	7.5	1.98	1.76	1.42
34.0	12.5	1.87	1.66	1.42	8.6	1.97	1.75	1.43
36.5	15.0	1.82	1.64	1.42	10.0	1.95	1.73	1.44
38.2	16.7	1.79	1.62	1.43	12.0	1.93	1.72	1.45
40.3	18.8	1.75	1.60	1.43	15.0	1.89	1.70	1.46
42.9	21.4	1.71	1.59	1.44	20.0	1.83	1.68	1.48
46.5	25.0	1.66	1.57	1.44	25.0	1.77	1.66	1.50
51.5	30.0	1.60	1.55	1.45	30.0	1.73	1.64	1.52
59.0	37.5	1.54	1.51	1.45	37.5	1.68	1.63	1.53
71.5	50.0	1.49	1.49	1.45	60.0	1.58	1.57	1.52
96.5	75.0	1.44	1.44	1.43	150.0	1.48	1.48	1.47
171.5	150.0	1.41	1.41	1.41	300.0	1.44	1.44	1.44

Raw Cone Penetrometer Data Box Test 3

		z (cm) ==>																	
x (cm)	y (cm)	2.5	5.1	7.6	10.2	12.7	15.2	17.8	20.3	22.9	25.4	27.9	30.5	33.0	35.6	38.1	40.6	43.2	45.7
13.5	33	5	5	10	36	41	71	61	66	61	56	56	61						
19	33	46	46	46	61	81	87	81	92	97	92	87	122	122	107	92	117	117	97
73	34	46	71	81	87	92	97	92	92	117	117	97	92	97	117	112	97	97	97
78.5	35	15	56	56	71	71	71	76	76	87	81	76	76	107	112	97	107	97	97
17.5	39	25	25	71	92	87	87	92	92	92	122	117	112	97	112	112	97	97	97
26	32	10	20	66	117	127	137	163	168	163	143	137	148	137	122	107	122	112	92
24	40	36	81	117	158	168	168	163	158	158	148	168	148	127	122	132	122	107	97
37	39								361	484	453	382	331	270	234	214	188	163	137
48	41								326	463	489	433	453	397	310	265	224	193	163
36	32								199	382	366	331	295	270	239	214	193	188	168
46.5	33								0	127	366	438	412	377	341	285	249	234	199
56	31								97	285	392	351	326	300	270	239	219	214	199

Deflection of Purple Dyed Layers Box Test 3

x (cm)	y (cm)	z pre comp (cm)	Deflection	z post comp (cm)
6	45.72	10	0	10
16	45.72	10	0.5	10.5
26	45.72	10	4	14
27	45.72	10	9	19
28	45.72	10	11.5	21.5
36	45.72	10	14	24
46	45.72	10	14	24
56	45.72	10	15.5	25.5
58	45.72	10	15	25
59	45.72	10	14	24
61	45.72	10	10	20
66	45.72	10	1.5	11.5
76	45.72	10	0	10
86	45.72	10	0	10
6	45.72	20	0	20
16	45.72	20	0.5	20.5
26	45.72	20	6	26
30	45.72	20	8	28
36	45.72	20	9	29
46	45.72	20	9.3	29.3
56	45.72	20	9.5	29.5
60	45.72	20	7	27
66	45.72	20	2	22
76	45.72	20	0	20
86	45.72	20	0	20
6	45.72	30	-0.79	29.21
12.7	45.72	30	-0.79	29.21
17.78	45.72	30	-0.155	29.845
22.86	45.72	30	0.48	30.48
27.94	45.72	30	1.75	31.75
33.02	45.72	30	3.655	33.655
38.1	45.72	30	4.925	34.925
43.18	45.72	30	5.56	35.56
48.26	45.72	30	5.56	35.56
53.34	45.72	30	5.56	35.56
58.42	45.72	30	4.925	34.925
63.5	45.72	30	3.655	33.655
68.58	45.72	30	1.115	31.115
73.66	45.72	30	-0.155	29.845
78.74	45.72	30	-0.155	29.845
83.82	45.72	30	-0.79	29.21
86	45.72	30	-0.79	29.21

x (cm)	y (cm)	z pre comp (cm)	Deflection	z post comp (cm)
6	45.72	39.37	0	39.37
7.62	45.72	39.37	0	39.37
12.7	45.72	39.37	0.635	40.005
17.78	45.72	39.37	0.635	40.005
22.86	45.72	39.37	1.27	40.64
27.94	45.72	39.37	1.905	41.275
33.02	45.72	39.37	2.54	41.91
38.1	45.72	39.37	3.175	42.545
43.18	45.72	39.37	3.81	43.18
48.26	45.72	39.37	3.81	43.18
53.34	45.72	39.37	3.81	43.18
63.5	45.72	39.37	2.44	41.81
73.66	45.72	39.37	1.27	40.64
78.74	45.72	39.37	0.635	40.005
83.82	45.72	39.37	0	39.37
86	45.72	39.37	0	39.37
6	45.72	60	0	60
16	45.72	60	0	60
26	45.72	60	0	60
36	45.72	60	0	60
46	45.72	60	0	60
56	45.72	60	0	60
66	45.72	60	0	60
76	45.72	60	0	60
86	45.72	60	0	60

Section 4.5.1 – Manual Compaction Test 1

Soil Moisture and Bulk Density Manual Compaction Test 1

Location	Tare wt (g)	wet wt + Container (g)	dry wt + Container (g)	Soil Moisture %	Volume (cm^3)	Mass Samp. wet (g)	Mass Samp. dry (g)	Depth (cm)	Bulk Density (g/cm^3)
east hole	44.61	129.11	114.87	20.3%	63.32	84.5	70.26	7.62	1.11
east hole	44.52	137.64	124.65	16.2%	63.32	93.12	80.13	22.86	1.27
east hole	44.24	120.28	110.78	14.3%	63.32	76.04	66.54	38.10	1.05
east hole	44.27	171.81	158.46	11.7%	63.32	127.54	114.19	53.34	1.80
compaction	44.73	165.16	148.19	16.4%	63.32	120.43	103.46	7.62	1.63
compaction	44.61	119.42	109.93	14.5%	55.40	74.81	65.32	21.91	1.18
compaction	44.52	159.95	151.22	8.2%	71.23	115.43	106.7	37.15	1.50
compaction	44.63	141.38	136.05	5.8%	63.32	96.75	91.42	53.34	1.44

Magnetic Susceptibility and Estimated Bulk Density Manual Compaction Test 1

Compaction Footprint				
x (cm)	y (cm)	z (cm)	Mag. Sus. (SI) $x10^{-5}$	Estimated Bulk Density (g/cm^3)
42	42	22	687	1.79
42	42	24	621	1.62
42	42	26	592	1.55
42	42	28	566	1.48
42	42	30	541	1.41
42	42	32	534	1.39
42	42	34	528	1.38
42	42	36	516	1.35
42	42	38	466	1.22
42	42	40	393	1.21
42	42	42	320	1.19
42	42	44	283	1.18
42	42	46	281	1.32
42	42	48	269	1.40
42	42	50	274	1.56
42	42	52	260	1.53
42	42	54	242	1.45
42	42	56	218	1.34
42	42	58	198	1.24
42	42	60	203	1.31
42	42	62	207	1.37
42	42	64	245	1.66
42	42	66	216	1.50
42	42	68	169	1.20

West Hole				
x (cm)	y (cm)	z (cm)	Mag. Sus. (SI) $x10^{-5}$	Estimated Bulk Density (g/cm^3)
87	45.7	8	486	1.27
87	45.7	10	451	1.18
87	45.7	12	431	1.13
87	45.7	14	403	1.05
87	45.7	16	381	1.00
87	45.7	18	391	1.02
87	45.7	20	385	1.01
87	45.7	22	435	1.14
87	45.7	24	487	1.27
87	45.7	26	511	1.33
87	45.7	28	517	1.35
87	45.7	30	518	1.35
87	45.7	32	509	1.33
87	45.7	34	471	1.23
87	45.7	36	333	1.18
87	45.7	38	335	1.12
87	45.7	40	351	1.15
87	45.7	42	311	1.12
87	45.7	44	266	1.18
87	45.7	46	248	1.17
87	45.7	48	253	1.26
87	45.7	50	231	1.60
87	45.7	52	230	1.60
87	45.7	54	215	1.49
87	45.7	56	206	1.43
87	45.7	58	207	1.44

East Hole				
x (cm)	y (cm)	z (cm)	Mag. Sus. (SI) $x10^{-5}$	Estimated Bulk Density (g/cm^3)
0	45.7	8		
0	45.7	10	478	1.13
0	45.7	12	476	1.24
0	45.7	14	481	1.26
0	45.7	16	462	1.21
0	45.7	18	473	1.23
0	45.7	20	456	1.19
0	45.7	22	472	1.23
0	45.7	24	477	1.25
0	45.7	26	489	1.28
0	45.7	28	503	1.31
0	45.7	30	502	1.31
0	45.7	32	484	1.26
0	45.7	34	485	1.27
0	45.7	36	461	1.20
0	45.7	38	428	1.12
0	45.7	40	396	1.11
0	45.7	42	384	1.10
0	45.7	44	365	1.26
0	45.7	46	364	1.39
0	45.7	48	339	1.48
0	45.7	50	306	1.61
0	45.7	52	259	1.52
0	45.7	54	231	1.47
0	45.7	56	263	1.63
0	45.7	58	248	1.65
0	45.7	60	231	1.60
0	45.7	62	220	1.53
0	45.7	64	227	1.58

Raw Cone Penetrometer Data Manual Compaction Test 1

		z (cm) ==>																	
x (cm)	y (cm)	2.5	5.1	7.6	10.2	12.7	15.2	17.8	20.3	22.9	25.4	27.9	30.5	33.0	35.6	38.1	40.6	43.2	45.7
86.5	45.7	10	163	173	188	178	168	173	168	173	178	188	199	214	214	224	234	234	239
78.5	45.7	163	178	219	219	193	173	173	173	178	183	183	183	188	193	209	193	199	214
71.5	45.7	148	163	168	173	188	188	219	224	219	219	219	199	193	188	193	193	199	219
61.5	53	76	76	112	183	422	443	448	453	428	412	377	336	316	285	280	270	260	249
42	36						10	290	575	672	723	738	652	550	499	489	478	468	621
42	56						117	422	529	529	794	682	708	473	443	377	331	316	336
23.5	45.7	41	61	117	224	504	534	519	524	494	443	382	336	300	326	463	529	555	
8.5	45.7	127	178	214	193	188	183	188	183	173	163	158	158	158	163	163	193	295	346
42	26.7	66	148	163	209	270	346	351	346	361	351	361	341	321	336	570	646	662	
42	6.7	36	137	178	199	209	193	209	214	193	183	209	209	219	199	183	188	214	275

Section 4.5.2 – Manual Compaction Test 2

Soil Moisture And Bulk Density Data

Location	tare wt (g)	wet wt + Container (g)	dry wt + Container (g)	Soil Moisture %	Volume (cm^3)	Mass Samp. wet (g)	Mass Samp. dry (g)	Depth (cm)	Bulk Density (g/cm^3)
east hole	44.52	143.72	130.27	15.7%	63.32	99.2	85.75	7.5	1.35
east hole	44.24	128.59	117.94	14.5%	63.32	84.35	73.7	22.8	1.16
east hole	44.71	131.7	119.6	16.2%	63.32	86.99	74.89	38.0	1.18
east hole	44.64	124.5	118.97	7.4%	63.32	79.86	74.33	53.3	1.17
compaction	44.26	163.19	146.99	15.8%	63.32	118.93	102.73	22.6	1.62
compaction	44.75	142.03	131.33	12.4%	63.32	97.28	86.58	37.8	1.37

Magnetic Susceptibility and Estimated Bulk Density Manual Compaction Test 2

Compaction Footprint				
x (cm)	y (cm)	z (cm)	Mag. Sus. (SI) $x10^{-5}$	Estimated Bulk Density (g/cm^3)
110	125	18.90	379	1.08
110	125	20.90	479	1.37
110	125	22.90	715	2.04
110	125	24.90	739	2.11
110	125	26.90	737	2.11
110	125	28.90	692	1.98
110	125	30.90	559	1.60
110	125	32.90	428	1.22
110	125	34.90	334	0.95
110	125	36.90	291	0.77
110	125	38.90	255	0.73
110	125	40.90	219	0.67
110	125	42.90	209	0.68
110	125	44.90	211	0.74
110	125	46.90	206	0.77
110	125	48.90	224	0.90
110	125	50.90	214	0.92
110	125	52.90	184	0.84
110	125	54.90	160	0.78
110	125	56.90	138	0.72
110	125	58.90	123	0.69
110	125	60.90	115	0.69
110	125	62.90	114	0.73
110	125	64.90	130	0.90
110	125	66.90	133	0.98
110	125	68.90	117	0.92
110	125	70.90	112	0.95
110	125	72.90	158	1.43
110	125	74.90	149	1.44
110	125	76.90	112	1.16

West Hole				
x (cm)	y (cm)	z (cm)	Mag. Sus. (SI) $x10^{-5}$	Estimated Bulk Density (g/cm^3)
70	134	10.71	269	0.85
70	134	12.71	321	1.00
70	134	14.71	313	0.95
70	134	16.71	324	0.95
70	134	18.71	325	0.93
70	134	20.71	356	1.02
70	134	22.71	349	1.00
70	134	24.71	357	1.02
70	134	26.71	357	1.11
70	134	28.71	372	1.24
70	134	30.71	352	1.26
70	134	32.71	339	1.30
70	134	34.71	291	1.19
70	134	36.71	262	1.15
70	134	38.71	239	1.12
70	134	40.71	214	1.07
70	134	42.71	210	1.13
70	134	44.71	187	1.08
70	134	46.71	208	1.28
70	134	48.71	224	1.48
70	134	50.71	147	1.04
70	134	52.71	106	0.80
70	134	54.71	162	1.31
70	134	56.71	221	1.91
70	134	58.71	193	1.79
70	134	60.71	135	1.34
70	134	62.71	145	1.54
70	134	64.71	128	1.45
70	134	66.71	120	1.46
70	134	68.71	112	1.46
70	134	70.71	110	1.53
70	134	72.71	114	1.70
70	134	74.71	131	2.09

East Hole				
x (cm)	y (cm)	z (cm)	Mag. Sus. (SI) $x10^{-5}$	Estimated Bulk Density (g/cm^3)
162	122	3	333	1.09
162	122	5	366	1.22
162	122	7	379	1.24
162	122	9	363	1.17
162	122	11	400	1.27
162	122	13	439	1.37
162	122	15	462	1.40
162	122	17	471	1.39
162	122	19	468	1.34
162	122	21	455	1.21
162	122	23	457	1.30
162	122	25	457	1.39
162	122	27	400	1.30
162	122	29	339	1.18
162	122	31	316	1.18
162	122	33	256	1.02
162	122	35	243	1.04
162	122	37	247	1.13
162	122	39	238	1.17
162	122	41	220	1.15
162	122	43	201	1.13
162	122	45	187	1.12
162	122	47	180	1.16
162	122	49	171	1.18
162	122	51	156	1.15
162	122	53	148	1.17
162	122	55	125	1.06
162	122	57	115	1.04
162	122	59	119	1.15
162	122	61	125	1.29
162	122	63	146	1.62
162	122	65	102	1.13
162	122	67	101	1.12
162	122	69	128	1.42
162	122	71	156	1.73
162	122	73	170	1.89

Cone Penetrometer Results Manual Compaction Test 2

		z (cm) ==>																	
x (cm)	y (cm)	2.5	5.1	7.6	10.2	12.7	15.2	17.8	20.3	22.9	25.4	27.9	30.5	33.0	35.6	38.1	40.6	43.2	45.7
69.8	135.6	112	188	183	158	127	112	107	97	107	122	117	132	143	127	137	280	428	641
79.9	128.0	143	219	214	178	163	143												
79.9	122.5	71	132	158	143	132	127	127	122	122	132	137	143	122	137	260	331	351	428
98.1	126.2				56	310	331	366	555	575	484	422	372	331	331	438	453		
116.7	119.5					15	275	478	463	550	728	646	545	484	433	412	448	534	
118.6	128.3				158	336	341	366	443	565	519	422	392	382	361	234	163		
129.2	125.6	10	41	46	87	219	290	351											
141.4	123.4	107	168	224	244	300	310	310	295	285	275	260	260	224	219	244	570	463	692
156.8	123.1	112	168	199	199	244	270	270	229	214	219	219	209	209	199	193	209	402	672
170.7	121.9	148	209	249	316	366	351	321	280	260	224	239	229	229	224	219	224	244	249

Section 4.5.3 – Manual Compaction Test 3

Soil Moisture and Bulk Density

Location	Tare wt (g)	wet wt + Container (g)	dry wt + Container (g)	Soil Moisture %	Volume (cm^3)	Mass Samp. wet (g)	Mass Samp. dry (g)	Depth (cm)	Bulk Density (g/cm^3)
east hole	44.75	110.72	101.53	16%	63.32	65.97	56.78	7.62	0.90
east hole	44.51	115.15	106.1	15%	63.32	70.64	61.59	22.86	0.97
east hole	44.25	118.91	110.39	13%	63.32	74.66	66.14	38.10	1.04
east hole	44.52	116.66	111.98	7%	63.32	72.14	67.46	53.34	1.07
compaction	44.28	168.49	151.52	16%	63.32	124.21	107.24	24.12	1.69
compaction	44.72	159.03	144.06	15%	63.32	114.31	99.34	39.36	1.57
compaction	44.6	134.13	124.13	13%	63.32	89.53	79.53	54.60	1.26
compaction	44.61	128.95	123.34	7%	63.32	84.34	78.73	69.84	1.24

Magnetic Susceptibility and Estimated Bulk Density Manual Compaction Test 3

Compaction Footprint				
x (cm)	y (cm)	z (cm)	Mag. Sus. (SI) $x10^{-5}$	Estimated Bulk Density (g/cm^3)
93	128	23.3	324	0.85
93	128	25.3	429	1.14
93	128	27.3	547	1.47
93	128	29.3	626	1.71
93	128	31.3	645	1.79
93	128	33.3	670	1.88
93	128	35.3	659	1.89
93	128	37.3	618	1.80
93	128	39.3	565	1.68
93	128	41.3	511	1.56
93	128	43.3	480	1.50
93	128	45.3	420	1.35
93	128	47.3	382	1.26
93	128	49.3	355	1.21
93	128	51.3	336	1.18
93	128	53.3	324	1.18
93	128	55.3	315	1.20
93	128	57.3	303	1.20
93	128	59.3	290	1.21
93	128	61.3	275	1.20
93	128	63.3	244	1.13
93	128	65.3	239	1.17
93	128	67.3	219	1.15
93	128	69.3	220	1.24
93	128	71.3	237	1.19
93	128	73.3	246	1.23
93	128	75.3	247	1.24
93	128	77.3	238	1.19
93	128	79.3	261	1.31
93	128	81.3	317	1.59
93	128	83.3	332	1.66
93	128	85.3	314	1.57
93	128	87.3	242	1.21
93	128	89.3	247	1.24
93	128	91.3	224	1.12

West Hole				
x (cm)	y (cm)	z (cm)	Mag. Sus. (SI) $x10^{-5}$	Estimated Bulk Density (g/cm^3)
36	128	0.0	280	0.70
36	128	1.9	303	0.76
36	128	3.9	304	0.76
36	128	5.9	336	0.85
36	128	7.9	345	0.87
36	128	9.9	334	0.85
36	128	11.9	342	0.87
36	128	13.9	363	0.93
36	128	15.9	340	0.88
36	128	17.9	327	0.85
36	128	19.9	354	0.93
36	128	21.9	373	1.00
36	128	23.9	388	1.05
36	128	25.9	395	1.08
36	128	27.9	402	1.12
36	128	29.9	399	1.13
36	128	31.9	392	1.13
36	128	33.9	401	1.18
36	128	35.9	407	1.22
36	128	37.9	421	1.29
36	128	39.9	411	1.30
36	128	41.9	375	1.22
36	128	43.9	336	1.12
36	128	45.9	319	1.10
36	128	47.9	293	1.05
36	128	49.9	271	1.00
36	128	51.9	261	1.01
36	128	53.9	252	1.02
36	128	55.9	251	1.06
36	128	57.9	222	0.99
36	128	59.9	203	0.96
36	128	61.9	192	0.96
36	128	63.9	188	1.01
36	128	65.9	183	1.06
36	128	67.9	180	1.00
36	128	69.9	177	0.98
36	128	71.9	185	1.03
36	128	73.9	226	1.13
36	128	75.9	234	1.17
36	128	77.9	248	1.24
36	128	79.9	275	1.38
36	128	81.9	302	1.51
36	128	83.9	317	1.59

East Hole				
x (cm)	y (cm)	z (cm)	Mag. Sus. (SI) $x10^{-5}$	Estimated Bulk Density (g/cm^3)
159	132	7.4	238	0.60
159	132	9.4	339	0.85
159	132	11.4	360	0.90
159	132	13.4	365	0.91
159	132	15.4	358	0.90
159	132	17.4	359	0.90
159	132	19.4	357	0.92
159	132	21.4	352	0.92
159	132	23.4	360	0.95
159	132	25.4	373	0.99
159	132	27.4	380	1.02
159	132	29.4	377	1.03
159	132	31.4	383	1.06
159	132	33.4	399	1.12
159	132	35.4	384	1.10
159	132	37.4	369	1.08
159	132	39.4	387	1.16
159	132	41.4	391	1.19
159	132	43.4	400	1.25
159	132	45.4	409	1.32
159	132	47.4	410	1.36
159	132	49.4	401	1.37
159	132	51.4	374	1.32
159	132	53.4	363	1.33
159	132	55.4	327	1.25
159	132	57.4	236	1.18
159	132	59.4	144	0.72
159	132	61.4	144	0.72
159	132	63.4	134	0.67
159	132	65.4	154	0.77
159	132	67.4	156	0.78
159	132	69.4	266	1.33
159	132	71.4	305	1.53

Cone Penetrometer Data Manual Compaction Test 3

		z (cm) ==>																	
x (cm)	y (cm)	2.5	5.1	7.6	10.2	12.7	15.2	17.8	20.3	22.9	25.4	27.9	30.5	33.0	35.6	38.1	40.6	43.2	45.7
148.4	127.7	244	326	260	199	178	148	132	137	137	148	158	143	143	168	173	168	163	173
139.6	129.5	229	209	244	219	178	137	127	127	117	117	112	112	112	122	127	143	163	173
125.7	129.1	132	163	148	168	224	199	178	173	168	173	178	183	188	188	188	193	209	234
121.3	132.3	132	158	148	143	143	143	148	199	260	265	260	260	260	249	239	229	229	244
116.2	127.4	87	81	81	87	112	143	310	387	463	514	519	494	448	433	412	392	382	361
69.1	124.3	127	168	163	183	209	199	188	188	183	183	183	173	168	173	188	188	173	178
62.5	126.8	239	209	219	219	229	219	193	173	168	158	148	148	158	163	168	168	163	173
46.3	124.8	158	122	193	244	219	183	158	143	137	127	127	132	137	132	143	143	137	143
36.0	135.0		183	193	183	173	148	143	132	132	143	148	143	148	168	173	168	158	163
105.8	141.6								351	377	753	763	646	621	570	494	448	428	402
95.7	133.2								280	534	570	646	784	708	631	540	473	433	387
85.5	134.3								422	657	662	728	652	662	570	499	468	412	366

Section 4.6 – Magnetometer Readings

Manual Compaction Test 1

		Pre-Compaction		Post-Compaction	
X	Y	TOP_RDG	BOTTOM_RDG	TOP_RDG	BOTTOM_RDG
46.3	93.7	54437.92	54462.38	54438.67	54464.04
46.3	91.2	54437.95	54462.23	54438.68	54464
46.3	88.6	54437.86	54461.85	54438.74	54463.8
46.3	86.1	54437.88	54461.61	54438.66	54463.7
46.3	83.6	54437.97	54461.39	54438.73	54463.7
46.3	81.0	54438	54461.2	54438.79	54463.67
46.3	78.5	54437.99	54460.9	54438.75	54463.36
46.3	75.9	54438.07	54460.81	54438.75	54463.05
46.3	73.4	54438.07	54460.41	54438.78	54462.75
46.3	70.9	54438.21	54460.19	54438.58	54462.4
46.3	68.3	54438.21	54460.01	54438.65	54462.08
46.3	65.8	54438.26	54459.71	54438.68	54461.66
46.3	63.2	54438.14	54459.4	54438.56	54460.82
46.3	60.7	54438.55	54459.44	54438.56	54460.23
46.3	58.2	54438.34	54458.81	54438.69	54459.63
46.3	55.6	54438.55	54458.75	54438.62	54458.87
46.3	53.1	54438.5	54458.35	54438.5	54457.44
46.3	50.5	54438.71	54458.36	54438.81	54457.53
46.3	48.0	54438.65	54458.09	54438.82	54456.46
46.3	45.5	54438.69	54457.67	54438.74	54455.57
46.3	42.9	54438.57	54457.13	54438.78	54454.79
46.3	40.4	54438.7	54457.14	54438.94	54454.56
46.3	37.8	54438.75	54456.83	54438.97	54454.07
46.3	35.3	54438.81	54456.53	54438.69	54453.41
46.3	32.8	54438.85	54456.4	54438.69	54452.88
46.3	30.2	54438.86	54456.15	54438.91	54453.22
46.3	27.7	54438.76	54455.75	54438.88	54453.09
46.3	25.1	54438.7	54455.31	54438.98	54453.34
46.3	22.6	54438.54	54454.71	54439.03	54453.11
46.3	20.1	54438.53	54454.21	54438.98	54453.26
46.3	17.5	54438.5	54453.75	54438.88	54453.13
46.3	15.0	54438.52	54453.39	54438.86	54453.22
46.3	12.4	54438.63	54452.94	54438.72	54453.19
46.3	9.9	54438.6	54452.6	54438.95	54453.29
46.3	7.4	54438.49	54452.06	54438.93	54453.38
46.3	4.8	54438.45	54451.74	54439.08	54453.29
46.3	2.3	54438.48	54451.51	54438.66	54452.81
42.5	2.3	54437.98	54450.23	54438.4	54451.82
42.5	4.8	54437.92	54450.48	54438.4	54451.77
42.5	7.4	54437.84	54450.85	54438.46	54451.76
42.5	9.9	54437.96	54451.34	54438.45	54451.56
42.5	12.4	54437.93	54451.61	54438.5	54451.59
42.5	15.0	54438.01	54452.14	54438.72	54451.74

		Pre-Compaction		Post-Compaction	
X	Y	TOP_RDG	BOTTOM_RDG	TOP_RDG	BOTTOM_RDG
42.5	17.5	54437.92	54452.56	54438.58	54451.53
42.5	20.1	54438.1	54453.27	54438.62	54451.62
42.5	22.6	54438.16	54453.66	54438.89	54452.28
42.5	25.1	54438.25	54454.07	54438.91	54452.01
42.5	27.7	54438.33	54454.38	54438.81	54451.73
42.5	30.2	54438.47	54454.87	54438.85	54451.43
42.5	32.8	54438.22	54454.8	54438.82	54451.56
42.5	35.3	54438.08	54455.08	54438.72	54451.63
42.5	37.8	54438.15	54455.33	54438.63	54451.76
42.5	40.4	54437.78	54455.13	54438.75	54452.74
42.5	42.9	54437.9	54455.69	54438.64	54452.91
42.5	45.5	54437.7	54455.85	54438.61	54453.53
42.5	48.0	54437.65	54456.02	54438.51	54454.1
42.5	50.5	54437.91	54456.49	54438.45	54455.03
42.5	53.1	54437.59	54456.56	54438.43	54456.02
42.5	55.6	54437.62	54456.88	54438.32	54456.8
42.5	58.2	54437.64	54457.27	54438.19	54457.62
42.5	60.7	54437.78	54457.62	54438.3	54458.55
42.5	63.2	54437.94	54458.17	54438.32	54459.21
42.5	65.8	54437.83	54458.48	54438.2	54459.94
42.5	68.3	54437.77	54458.71	54438.19	54460.38
42.5	70.9	54437.77	54458.98	54438.31	54460.96
42.5	73.4	54437.76	54459.39	54438.5	54461.82
42.5	75.9	54437.9	54459.91	54438.44	54461.96
42.5	78.5	54437.83	54460.03	54438.38	54462.02
42.5	81.0	54437.89	54460.64	54438.42	54462.43
42.5	83.6	54437.95	54460.94	54438.55	54462.59
42.5	86.1	54437.89	54461.1	54438.44	54462.66
42.5	88.6	54437.87	54461.24	54438.42	54462.68
42.5	91.2	54437.54	54461.14	54438.19	54462.53
42.5	93.7	54437.6	54461.46	54438.05	54462.52
38.7	93.7	54436.65	54459.85	54437.62	54461.27
38.7	91.2	54436.63	54459.52	54437.49	54461.13
38.7	88.6	54436.65	54459.24	54437.62	54461.14
38.7	86.1	54436.6	54459.02	54437.68	54461.1
38.7	83.6	54436.68	54458.88	54437.41	54460.74
38.7	81.0	54436.66	54458.64	54437.31	54460.57
38.7	78.5	54436.74	54458.4	54437.41	54460.54
38.7	75.9	54436.95	54458.21	54437.32	54460.3
38.7	73.4	54437.22	54458.3	54437.22	54459.69
38.7	70.9	54437.31	54457.88	54437.23	54459.33
38.7	68.3	54437.28	54457.6	54437.22	54458.85
38.7	65.8	54437.25	54457.15	54437.17	54457.99
38.7	63.2	54437.46	54457.07	54437.39	54457.74
38.7	60.7	54437.44	54456.74	54437.41	54456.94
38.7	58.2	54437.43	54456.29	54437.52	54456.19
38.7	55.6	54437.47	54456	54437.61	54455.43

		Pre-Compaction		Post-Compaction	
X	Y	TOP_RDG	BOTTOM_RDG	TOP_RDG	BOTTOM_RDG
38.7	53.1	54437.47	54455.69	54437.71	54454.67
38.7	50.5	54437.42	54455.28	54437.93	54453.86
38.7	48.0	54437.39	54455	54437.77	54452.83
38.7	45.5	54437.64	54454.78	54437.92	54452.01
38.7	42.9	54437.68	54454.6	54437.69	54451.14
38.7	40.4	54437.72	54454.44	54437.71	54450.48
38.7	37.8	54437.53	54453.87	54437.76	54450.12
38.7	35.3	54437.52	54453.55	54437.7	54449.81
38.7	32.8	54437.51	54453.29	54437.9	54449.69
38.7	30.2	54437.64	54453.17	54438.13	54449.94
38.7	27.7	54437.5	54452.67	54438.4	54450.19
38.7	25.1	54437.49	54452.46	54438.43	54450.33
38.7	22.6	54437.52	54452.07	54438.33	54450.33
38.7	20.1	54437.59	54451.86	54438.38	54450.49
38.7	17.5	54437.67	54451.48	54438.16	54450.49
38.7	15.0	54437.92	54451.09	54438.25	54450.82
38.7	12.4	54438.06	54450.87	54438.21	54450.69
38.7	9.9	54437.87	54450.4	54438.16	54450.75
38.7	7.4	54437.86	54449.92	54438.14	54450.66
38.7	4.8	54437.58	54449.03	54438.17	54450.8
38.7	2.3	54437.68	54449.13	54438.24	54450.75

Manual Compaction Test 2

		Pre-Compaction		Post-Compaction	
X (cm)	Y (cm)	TOP_RDG	BOTTOM_RDG	TOP_RDG	BOTTOM_RDG
110.06	158.04	54407.9	54440.8	54410.2	54445.32
109.86	155.50	54407.67	54439.8	54410.03	54444.53
109.65	152.96	54407.13	54438.4	54409.83	54443.69
109.44	150.41	54407	54437.5	54409.44	54442.68
109.24	147.87	54406.76	54436.78	54409.21	54441.76
109.03	145.33	54406.68	54435.98	54409.34	54441.31
108.83	142.79	54406.55	54435.38	54408.59	54439.72
108.62	140.24	54406.12	54434.36	54408.42	54438.78
108.41	137.70	54405.63	54433.45	54408.05	54437.6
108.21	135.16	54405.52	54432.91	54407.99	54436.58
108.00	132.62	54405.3	54432.2	54407.46	54434.76
107.79	130.07	54404.95	54431.53	54407.22	54433.14
107.59	127.53	54404.68	54430.89	54406.92	54431.59
107.38	124.99	54404.5	54430.44	54406.73	54429.98
107.17	122.45	54404.05	54430.01	54406.47	54428.15
106.97	119.90	54404.26	54429.97	54406.22	54426.51
106.76	117.36	54404.22	54429.93	54406.14	54424.94
106.55	114.82	54403.42	54429.39	54405.97	54423.19
106.35	112.28	54403.43	54429.46	54405.14	54421.2
106.14	109.73	54403.27	54429.48	54404.95	54419.99

		Pre-Compaction		Post-Compaction	
X (cm)	Y (cm)	TOP_RDG	BOTTOM_RDG	TOP_RDG	BOTTOM_RDG
105.93	107.19	54402.81	54429.11	54404.97	54419.03
105.73	104.65	54402.56	54428.78	54404.72	54418.16
105.52	102.11	54402.27	54428.72	54404.13	54417.35
105.31	99.56	54401.88	54428.36	54403.81	54416.91
105.11	97.02	54401.77	54428.08	54403.57	54416.68
104.90	94.48	54401.07	54427.42	54402.96	54416.78
104.70	91.94	54400.85	54427.06	54403.27	54417.48
104.49	89.39	54400.78	54427.03	54402.69	54417.82
104.28	86.85	54400.66	54426.79	54402.56	54418.64
104.08	84.31	54400.05	54425.64	54402.51	54419.2
103.87	81.77	54399.68	54425.29	54402.09	54420.03
103.66	79.22	54399.67	54424.92	54402.09	54420.7
103.46	76.68	54399.31	54424.34	54401.96	54421.19
103.25	74.14	54399.14	54423.75	54401.49	54421.33
103.04	71.60	54398.52	54422.3	54401.25	54421.35
102.84	69.05	54398.3	54421.47	54400.94	54421.49
102.63	66.51	54398.14	54420.79	54400.74	54421.49
98.90	66.76	54398.73	54422.55	54401.52	54423.34
99.10	69.31	54398.93	54423.57	54401.7	54423.04
99.29	71.85	54398.99	54423.98	54401.91	54423.05
99.49	74.40	54398.89	54424.66	54402.25	54423.17
99.69	76.94	54399.23	54425.25	54402.51	54422.85
99.89	79.49	54399.44	54425.9	54402.74	54422.35
100.09	82.03	54399.85	54426.3	54402.86	54421.51
100.29	84.58	54399.91	54426.63	54402.99	54420.83
100.49	87.12	54400.18	54426.88	54403.08	54420.3
100.69	89.67	54400.79	54427.72	54403.14	54419.6
100.89	92.21	54400.8	54427.86	54403.78	54418.88
101.09	94.76	54401.4	54428.68	54404.05	54418.72
101.28	97.30	54401.73	54429.04	54404.36	54418.51
101.48	99.85	54401.96	54429.12	54404.49	54418.59
101.68	102.39	54401.68	54428.66	54404.56	54418.87
101.88	104.94	54401.92	54428.94	54404.84	54419.47
102.08	107.48	54402.25	54429	54405.01	54419.95
102.28	110.03	54402.49	54429.09	54405.31	54421.24
102.48	112.57	54402.79	54429.22	54405.73	54423.04
102.68	115.12	54402.97	54429.25	54405.85	54424.05
102.88	117.66	54403.14	54429.24	54405.94	54425.56
103.08	120.21	54403.12	54429.39	54406.16	54427.19
103.27	122.75	54403.75	54430.08	54406.33	54428.79
103.47	125.30	54403.87	54430.32	54406.72	54430.86
103.67	127.84	54404.12	54430.77	54406.94	54432.48
103.87	130.39	54404.51	54431.55	54407.16	54433.92
104.07	132.93	54404.66	54432.1	54407.39	54435.33
104.27	135.48	54404.88	54432.67	54407.71	54436.78
104.47	138.02	54405.09	54433.29	54407.82	54437.77
104.67	140.57	54405.48	54434.35	54408.19	54439

		Pre-Compaction		Post-Compaction	
X (cm)	Y (cm)	TOP_RDG	BOTTOM_RDG	TOP_RDG	BOTTOM_RDG
104.87	143.11	54405.67	54435.06	54408.56	54440.01
105.07	145.66	54405.76	54435.76	54408.71	54441
105.26	148.20	54406	54436.61	54409.41	54442.49
105.46	150.75	54406	54437.17	54409.31	54443.03
105.66	153.29	54406.49	54438.57	54409.61	54443.94
105.86	155.84	54406.6	54439.38	54409.78	54444.73
106.06	158.38	54406.99	54440.48	54410.03	54445.59
102.07	158.77	54406.77	54440.59	54410.29	54445.96
101.88	156.22	54406.75	54439.93	54410.07	54445.09
101.69	153.67	54406.58	54439.05	54409.92	54444.3
101.49	151.12	54406.32	54438.13	54409.72	54443.6
101.30	148.57	54406.16	54437.27	54409.63	54442.85
101.11	146.02	54405.89	54436.44	54409.19	54441.62
100.92	143.47	54405.48	54435.56	54408.94	54440.76
100.73	140.92	54405.28	54434.81	54408.89	54439.86
100.53	138.37	54405.36	54434.31	54408.32	54438.34
100.34	135.83	54404.83	54433.33	54408.21	54437.45
100.15	133.28	54404.69	54432.73	54408.16	54436.01
99.96	130.73	54404.33	54432.09	54407.73	54434.66
99.77	128.18	54404.2	54431.58	54407.46	54433.06
99.57	125.63	54403.67	54430.94	54407.31	54431.69
99.38	123.08	54403.44	54430.47	54406.97	54430.13
99.19	120.53	54403.2	54430.22	54406.77	54428.67
99.00	117.98	54403.06	54429.98	54406.2	54426.72
98.81	115.43	54402.84	54429.83	54405.99	54425.11
98.61	112.88	54402.26	54429.41	54405.96	54423.98
98.42	110.33	54401.97	54429.34	54405.69	54422.81
98.23	107.79	54401.76	54429.14	54405.03	54421.64
98.04	105.24	54401.39	54428.9	54404.92	54420.78
97.85	102.69	54401.23	54428.88	54404.78	54420.54
97.65	100.14	54400.99	54428.93	54404.55	54420.18
97.46	97.59	54400.7	54428.76	54404.19	54420.44
97.27	95.04	54400.24	54428.37	54403.89	54420.43
97.08	92.49	54400.36	54428.46	54403.49	54420.56
96.89	89.94	54400.13	54428.16	54403.47	54421.41
96.69	87.39	54399.81	54427.72	54403.16	54421.76
96.50	84.84	54399.65	54427.42	54403.2	54422.63
96.31	82.29	54399.24	54426.76	54402.72	54423.18
96.12	79.75	54398.83	54426.04	54402.64	54423.61
95.93	77.20	54398.45	54425.29	54402.34	54423.89
95.73	74.65	54398.63	54424.97	54401.88	54424.13
95.54	72.10	54398.16	54424.04	54401.76	54424.31
95.35	69.55	54397.8	54423.09	54401.86	54424.43
95.16	67.00	54394.86	54419.81	54398.97	54421.61

Manual Compaction Test 3

		Pre-Compaction		Post-Compaction	
X	Y	TOP_RDG	BOTTOM_RDG	TOP_RDG	BOTTOM_RDG
96.32	171.45	54423.76	54439.79	54421.24	54438.28
96.30	168.83	54424.22	54440.07	54421.88	54438.76
96.28	166.21	54424.43	54440.45	54422.13	54439.19
96.26	163.58	54425	54440.81	54422.63	54439.63
96.24	160.96	54425.47	54441.21	54422.85	54439.95
96.22	158.34	54425.83	54441.49	54423.06	54440.24
96.21	155.71	54425.91	54441.64	54423.4	54440.53
96.19	153.09	54426.27	54442.09	54423.78	54440.74
96.17	150.47	54427.3	54442.81	54424.44	54440.88
96.15	147.84	54428.34	54443.64	54424.73	54440.92
96.13	145.22	54428.68	54444.09	54424.72	54440.79
96.11	142.60	54428.81	54444.3	54425.29	54440.56
96.09	139.98	54429	54444.48	54425.73	54440.24
96.07	137.35	54429.75	54445.01	54425.93	54439.92
96.06	134.73	54429.98	54445.48	54426.5	54439.52
96.04	132.11	54430.06	54445.81	54426.83	54439.04
96.02	129.48	54430.19	54446.09	54426.86	54438.57
96.00	126.86	54430.28	54446.65	54427.38	54438.15
95.98	124.24	54430.6	54447.38	54428.08	54437.67
95.96	121.61	54430.9	54448.19	54428.29	54437.43
95.94	118.99	54431.58	54449.15	54428.72	54437.35
95.93	116.37	54431.58	54449.78	54429.02	54437.51
95.91	113.75	54431.95	54450.8	54429.28	54437.7
95.89	111.12	54432.34	54451.88	54429.65	54438.18
95.87	108.50	54432.67	54453.14	54429.95	54438.94
95.85	105.88	54433.04	54454.18	54430.34	54440.13
95.83	103.25	54433.6	54455.35	54430.65	54441.52
95.81	100.63	54433.78	54456.36	54431.07	54443.32
95.80	98.01	54434.03	54457.38	54431.69	54444.92
95.78	95.38	54434.84	54458.72	54431.98	54446.6
95.76	92.76	54434.9	54459.52	54432.32	54448.49
95.74	90.14	54435.3	54460.56	54432.6	54450.47
95.72	87.52	54435.41	54461.4	54432.38	54451.87
95.70	84.89	54435.88	54462.4	54432.47	54453.58
95.68	82.27	54436.07	54463.06	54433.53	54456.06
95.66	79.65	54436.31	54463.9	54433.63	54457.77
95.65	77.02	54436.64	54464.9	54433.94	54459.32
92.17	78.59	54437.77	54466.01	54434.29	54459.98
92.20	81.18	54437.51	54465.3	54434.47	54458.79
92.22	83.78	54436.91	54464.09	54434.25	54457.22
92.25	86.37	54436.14	54462.78	54433.53	54455.19
92.27	88.96	54435.18	54461.2	54433.16	54452.72
92.30	91.56	54434.92	54460.26	54432.84	54450.84
92.32	94.15	54434.27	54459.1	54432.71	54449.25
92.35	96.74	54433.97	54457.99	54432.13	54446.92

		Pre-Compaction		Post-Compaction	
X	Y	TOP_RDG	BOTTOM_RDG	TOP_RDG	BOTTOM_RDG
92.37	99.33	54433.45	54456.78	54432.1	54445.52
92.40	101.93	54433.11	54455.68	54431.86	54443.87
92.42	104.52	54432.75	54454.56	54431.55	54442.28
92.45	107.11	54432.12	54453.14	54431.53	54441.29
92.47	109.71	54431.79	54452.08	54431.24	54440.27
92.50	112.30	54431.55	54450.99	54430.72	54439.53
92.52	114.89	54431.06	54449.86	54430.42	54438.81
92.55	117.49	54430.61	54448.73	54429.96	54438.49
92.57	120.08	54430.22	54447.72	54429.82	54438.63
92.60	122.67	54429.66	54446.61	54429.55	54438.77
92.62	125.26	54429.21	54445.71	54429.3	54439.14
92.65	127.86	54428.89	54444.85	54428.65	54439.7
92.67	130.45	54428.3	54444.02	54428.35	54440.02
92.70	133.04	54427.67	54443.3	54428.49	54440.66
92.72	135.64	54426.78	54442.39	54428.07	54441.1
92.75	138.23	54426.52	54441.87	54427.62	54441.63
92.77	140.82	54426.21	54441.37	54427.18	54441.75
92.80	143.42	54425.59	54440.74	54427.07	54442.23
92.82	146.01	54425.41	54440.37	54426.8	54442.51
92.85	148.60	54424.97	54440.03	54426.25	54442.48
92.87	151.19	54424.37	54439.75	54425.86	54442.43
92.90	153.79	54424.12	54439.63	54425.33	54442.36
92.92	156.38	54424.28	54439.72	54425.06	54442.18
92.95	158.97	54424.47	54439.97	54424.92	54441.95
92.97	161.57	54424.05	54439.8	54424.78	54441.64
93.00	164.16	54424.08	54439.72	54424.75	54441.35
93.02	166.75	54423.98	54439.7	54423.94	54440.85
93.05	169.35	54423.96	54439.83	54423.3	54440.37
93.07	171.94	54424.03	54439.94	54423.13	54440.06
89.82	172.73	54426.04	54441.68	54424.31	54440.7
89.79	170.16	54426.56	54442.16	54424.35	54440.98
89.76	167.58	54426.36	54441.88	54424.63	54441.36
89.73	165.01	54425.75	54441.16	54424.88	54441.57
89.70	162.44	54425.65	54441.01	54425.29	54441.86
89.67	159.87	54426.2	54441.32	54425.59	54442.16
89.64	157.30	54426.47	54441.53	54425.72	54442.38
89.60	154.73	54426.61	54441.65	54426.14	54442.68
89.57	152.16	54427.13	54442.02	54426.39	54442.65
89.54	149.59	54427.66	54442.52	54426.64	54442.67
89.51	147.01	54428.14	54442.96	54427.37	54442.61
89.48	144.44	54428.66	54443.57	54427.24	54442.25
89.45	141.87	54429.34	54444.18	54427.47	54442.09
89.42	139.30	54430.06	54444.99	54427.89	54441.82
89.39	136.73	54430.35	54445.44	54428.2	54441.39
89.35	134.16	54430.33	54445.7	54428.62	54441
89.32	131.59	54430.41	54445.99	54428.86	54440.62
89.29	129.01	54430.71	54446.56	54429.44	54440.19

		Pre-Compaction		Post-Compaction	
X	Y	TOP_RDG	BOTTOM_RDG	TOP_RDG	BOTTOM_RDG
89.26	126.44	54430.54	54446.88	54429.59	54439.85
89.23	123.87	54430.71	54447.54	54430.04	54439.64
89.20	121.30	54430.84	54448.3	54430.38	54439.63
89.17	118.73	54431.41	54449.43	54430.74	54439.71
89.14	116.16	54431.62	54450.47	54431.13	54440.24
89.10	113.59	54431.78	54451.49	54431.29	54440.68
89.07	111.02	54432.33	54452.87	54431.95	54441.79
89.04	108.44	54432.89	54454.06	54432.05	54442.58
89.01	105.87	54433.13	54455.11	54432.38	54443.8
88.98	103.30	54433.59	54456.25	54432.61	54445.14
88.95	100.73	54433.91	54457.39	54433.45	54447.21
88.92	98.16	54434.43	54458.62	54433.38	54448.74
88.88	95.59	54435.14	54459.87	54433.62	54450.3
88.85	93.02	54435.42	54460.91	54434.01	54452.42
88.82	90.45	54435.65	54461.66	54434.43	54454.28
88.79	87.87	54435.91	54462.64	54434.72	54456.3
88.76	85.30	54436.08	54463.32	54435.32	54458.22
88.73	82.73	54437	54464.73	54435.57	54459.87
88.70	80.16	54435.05	54463.16	54432.67	54458.24